New Encapsulated bis Cyclometalated Ir(III) Complexes with Potent Anticancer PDT Activity

Cristina Bermejo-Casadesús,[1,⊥] Carlos Gonzalo-Navarro,[2,⊥] Juan Angel Organero,[3] Ana María Rodríguez,[4] Lucía Santos,[5] Elisenda Zafon,[1] Joao Carlos Lima,[6] Artur J. Moro,[6] Mònica Iglesias,[7] Pedro Tavares,[8,9] Daniel Martínez,[2] Blanca R. Manzano,*[,2] Anna Massaguer,*[,1] Gema Durá*[,2]

[1] Universitat de Girona, Departament de Biologia, Facultat de Ciències, Maria Aurelia Capmany 40, 17003 Girona, Spain.

[2] Universidad de Castilla-La Mancha, Departamento de Química Inorgánica, Orgánica y Bioquímica- IRICA, Facultad de Ciencias y Tecnologías Químicas, Avda. Camilo José Cela, 10, 13071 Ciudad Real, Spain.

[3] Universidad de Castilla-La Mancha, Departamento de Química Física, Facultad de Ciencias Ambientales y Bioquímicas and INAMOL, 45071 Toledo, Spain.

[4] Universidad de Castilla-La Mancha, Departamento de Química Inorgánica, Orgánica y Bioquímica- IRICA, Escuela Técnica Superior de Ingenieros Industriales, Avda. Camilo José Cela, 3, 13071 Ciudad Real, Spain.

[5] Universidad de Castilla-La Mancha, Departamento de Química Física, Facultad de Ciencias y Tecnologías Químicas, Avda. Camilo José Cela, s/n, 13071 Ciudad Real, Spain.

[6] Universidade NOVA de Lisboa, LAQV-REQUIMTE, Departamento de Química, Faculdade de Ciências e Tecnologia, 2829-516 Caparica, Portugal.

[7] Universitat de Girona, Departament de Química, Facultat de Ciències, Maria Aurelia Capmany 40, 17003 Girona, Spain.

[8] Associate Laboratory i4HB - Institute for Health and Bioeconomy, NOVA School of Science and Technology, Universidade NOVA de Lisboa, 2829-516 Caparica, Portugal.

[9] UCIBIO – Applied Molecular Biosciences Unit, Department of Chemistry, NOVA School of Science and Technology, Universidade NOVA de Lisboa, 2829-
516 Caparica, Portugal

[⊥] Both authors have contributed equally to the work.

Emails: gema.dura@uclm.es; anna.massaguer@udg.edu; blanca.manzano@uclm.es

Electronic Supplementary Information

Table of Contents

Experimental Section

Materials. $IrCl_3 \cdot xH_2O$ was purchased from Johnson Matthey and used as received. The proligand H-pbpz was prepared by reaction of benzo[*h*]quinoline-5,6-dione with *o*-phenylenediamine according to the literature methods.[1] Benzo[*h*]quinoline-5,6-dione was prepared as reported.[1] The reagents benzo[*h*]quinoline, iodopentoxide and 2,3-diaminonaphthalene were purchased from Alfa Aesar, *o*-phenylendiamine from Sigma-Aldrich, silver trifluoromethanesulfonate ($AgOSO_2CF_3$) and ammonium hexafluorophosphate (NH_4PF_6) from Acros. The BOC-aminoethyl methacrylate monomer was prepared as reported.[2] Poly(ethyleneglycol) methyl ether methacrylate, 2-aminoethyl methacrylate and 2-carboxyethyl acrylate were purchased from Sigma-Aldrich, 2-cyano-2-propyl dodecyl trithiocarbonate and trioxane from TCI, di-*tert*-butyl decarbonate from ThermoScientific, (1-ethyl-3-(3-dimethylaminopropyl)carbodiimide) hydrochloride (EDC·HCl) and azobisisobutyronitrile from Glentham and trifluoroacetic acid from Acros. All of them were used without further purification. Deuterated solvents were purchased from Eurisotop. Conventional solvents such as diethyl ether (Fisher Scientific), acetone (Fisher Scientific), dimethyl sulfoxide (Scharlau), *N*,*N*-dimethylformamide (Acros), ethanol (Scharlau), methanol (Scharlau), dichloromethane (Scharlau), diglyme (Acros), 2-methoxyethanol (Fisher Chemical), 1,4-dioxane (ThermoScientific), water (Honeywell) or acetic acid (Scharlau) were degassed and in some cases distilled prior to use.

Experimental Details. All synthetic manipulations were performed under an inert, oxygen-free, dry nitrogen atmosphere using standard Schlenk techniques. All metal complexes were synthesized in dark conditions and protected from light using aluminium foil throughout each step of synthesis, isolation and characterization. Solvents were dried and distilled under nitrogen atmosphere begore use. Elemental analyses were performed on a FlashEA112 microanalyzer (ThermoFinnigan). ESI+ MS (mass spectrometry) data were recorded on a Thermo MAT95XP mass spectrometer using N,N-dimethylformamide (DMF) as the sample solvent. UV-vis absorption spectra were recorded on a Secomam Uvikon XS spectrophotometer using the LabPower Junior program. Luminescence excitation and emission spectra were recorded on a PTI Quanta Master TM spectrofluorometer from Photon Technology International (PTI) equipped with a 75 W Xenon short arc lamp and a model 814PTM detection system. Multinuclear NMR (nuclear magnetic resonance) spectra were recorded at 298 K on a Varian Unity Inova 400 or on a Varian Inova 500 spectrometer. Chemical shift values (δ) are reported in ppm (parts per million) and coupling constants (J) in Hertz. The splitting of proton resonances is defined as follows: s = singlet, d = doublet, t = triplet, q = quadruplet, m = multiplet, bs = broad singlet. 2D-NMR spectra such as ^{1}H–^{1}H gCOSY, ^{1}H–^{13}C gHSQC and ^{1}H–^{13}C gHMBC were recorded using standard pulse–pulse sequences. ^{1}H NMR chemical shifts were internally referenced to (CHD_2)(CD_3)SO (2.50 ppm) for DMSO-d_6 via the residual proton solvent resonances. The probe temperature (±1 K) was controlled by a standard unit calibrated with a methanol reference. All NMR data processing was performed using MestReNova version 12.0.0.

Unless otherwise stated, reagents and solvents were reagent quality and commercially available. Flash chromatography was carried out using neutral alumina (Acros, Brockmann I, 60A, 40-300 µM). Microwave irradiations were performed in a Discover® (CEM) focused microwave reactor. Dialysis purification of polymers was performed using molecular porous membrane tubing with a 3.5 kDa MWCO (Molecular Weight Cut Off). The purity of final compounds was determined by reversed-phase high performance liquid chromatography (HPLC) analyses on a LiquidPurple ODS C18 column (250 × 4.6 mm, 5 µm, flow rate: 1 mL min^{-1}) using linear gradients of 0.05% trifluoroacetic acid in Milli-Q H_2O (A) and 0.05% trifluoroacetic acid in MeCN (B) and coupled to a UV-vis detector. The HPLC column was maintained at 25 °C. The detection wavelength was 260 nm. All final compounds were >95% pure by this method.

Methods and Instrumentation

X-ray Crystallographic Structure Determination. For X-ray structure analyses the crystal of compounds **1**, **2** and **4** were mounted at the end of a glass fiber with Paratone-N oil and transferred to a Bruker X8 APEX II CCD diffractometer using graphite-monochromated MoKα radiation (λ = 0.71073 Å). Data were integrated and corrected for Lorentz polarization effects using SAINT[3] and were corrected for absorption effects using SADABS.[4] Space group assignments were based upon systematic absences, *E* statistics, and successful refinement of the structures. Structures were solved by direct methods with the aid of successive difference Fourier maps and were refined against all data using the SHELXTL software package.[5]

For compound **1**, it was necessary to measure several crystals due to the loss of crystallinity observed during data acquisition, even at low temperature. For the best selected crystal, the data obtained allowed the structure to be solved unambiguously. The crystal shows three molecules in the asymmetric unit and different solvent molecules. One of these molecules and a PF_6^- anion show disorder, so during refinement it was necessary to apply several constraints for the solvent molecules and the disordered atoms. Several crystallizations have been carried out under different conditions for compound **2** and only very small-sized crystals have been obtained. Despite the low resolution and low diffraction intensity, the data obtained have allowed us to identify the formation of compound **2**.

Suitable single crystals for the X-ray diffraction study were obtained in the following way. **1**: by slow diffusion of an acetone/pentane mixture into a solution of **1** in DCM. [**2**][OSO_2CF_3]: by slow diffusion of pentane into a solution of **2** with sodium trifluoromethanesulfonate in acetone. **4**: by slow diffusion of pentane into a solution of **D2** in DMSO/acetone mixture.

Analysis of π-π stacking by ^{1}H NMR spectroscopy. Solutions of complexes **1** and **3** at different concentrations in DMSO-d_6 ranging from 0.1 mM to 5 mM were analysed by ^{1}H NMR spectroscopy. Due to the higher solubility of complex **1**, a higher concentration (10 mM) was also studied.

Photostability studies in DMSO-d_6 (NMR spectroscopy). Solutions of complexes **1** and **3** at 2 mM in DMSO-d_6 were studied by ^{1}H NMR spectroscopy at different times until 48 hours in dark conditions and 8 h under blue light irradiation (470 nm, 51.4 mW cm^{-2}) to evaluate their stability.

Photostability studies in DMEM. The stability of the complexes in biological media were studied by UV-vis spectroscopy. Complexes **1** and **3** were dissolved in DMSO at 1.0×10^{-3} M and then diluted to 1.0×10^{-5} M with Dulbecco's modified Eagle's medium (DMEM) without phenol red (Corning). The solutions were studied in the dark and under blue light irradiation (470 nm, 51.4 mW cm^{-2}).

Dynamic Light Scattering (DLS). The hydrodynamic diameter of the particles of complexes **1** and **3** at 1.0×10^{-4} M in water (10% DMSO) at 25 °C was studied before and after 1 h of blue light irradiation (470 nm, 51.4 mW cm^{-2}) using a Dynamic Light Scattering (DLS, ZetaPlus, Brookhaven, Holtsville, NY) instrument operating at a 90 scattering angle with a 635 nm (35 mW) diode laser source. The path length of the cuvette was 1 cm.

Photophysical properties. For photophysical measurements, all solvents used were spectroscopic grade. UV-vis absorption spectra were recorded on a Secomam Uvikon XS spectrophotometer at room temperature using the LabPower Junior program. Quartz cuvettes with 1 cm optical path length were used for the measurements. Molar absorption coefficients (ε) were determined by direct application of the Beer-Lambert

law, using solutions of the compounds with concentrations ranging from 10^{-6} to 10^{-5} M. In the case of nanoparticles, solutions of 0.25 mg/mL were used.

Photoluminescence excitation and emission spectra were recorded on a PTI Quanta Master TM spectrofluorometer from Photon Technology International (PTI) equipped with a Xenon short arc lamp (75 W) and an 814PTM detector. Hellma quartz cuvettes with 1 cm optical path length were used. Felix32 software was used to collect and process luminescence data.

Solutions of all complexes in acetonitrile and water (1% DMSO) at 1.0×10^{-5} M were prepared. For optical measurements in degassed acetonitrile, the compounds were dissolved in a glove-box under a nitrogen atmosphere and the solutions were kept under inert atmosphere in closed cuvettes equipped with Teflon septum screw caps. All optical measurements were recorded at room temperature. The emission quantum yields (ϕ_{em}) were measured by comparative method using $[(ppy)_2Ir(bpy)]PF_6$ as reference (ϕ_{em} = 0.0707 in acetonitrile).[6] The emission spectra of optically-matched solutions of the compounds in degassed acetonitrile were recorded. The absorbance of the compounds and the reference solutions was set below 0.1 at the excitation wavelength to avoid the inner filter effect. The ϕ_{em} were calculated according to equation 1:

$$\phi_{em,s} = \phi_{em,ref} \times \left(\frac{Area_{em,s}}{Area_{em,ref}}\right) \times \left(\frac{A_{ref}}{A_s}\right) \times \left(\frac{\eta_s^2}{\eta_{ref}^2}\right) \quad \text{(Equation 1)}$$

where the subindexes s and ref correspond to the complex and the reference, respectively, $Area_{em}$ represents the area under the curve of the emission spectrum, A is the absorbance at the excitation wavelength and η is the refractive index of the solvent. To evaluate the effect of O_2 on the emission properties, the acetonitrile solutions were bubbled for 60 seconds.

Transient Absorption (TAS) measurements. Transient absorption spectra were measured using a transient absorption setup composed of a LKS 60 ns laser photolysis spectrometer from Applied Photophysics, with a Brilliant Q-Switch Nd:YAG laser from Quantel, using the third harmonics (λ_{ex} = 355 nm, laser pulse half-width equal to 4 ns). Measurements were repeated in degassed and aerated samples. Absorbance was adjusted to 0.2. For the measurements in water, the solutions of **1** were prepared by adding a small aliquot of a stock solution of **1** in DMSO ($[\mathbf{1}]_{stock}$ = 9.5 x 10^{-4} M) to water, to reach an absorption of *circa* 0.2-0.3 at the laser excitation wavelength (355 nm). The final concentration of **1** was around 15 µM (~1% DMSO in water).

$^1O_2$ quantum yield determination. Singlet oxygen ($^1O_2$) generation was studied for **1** and **3** using the 9,10-anthracenediyl-bis(methylene)dimalonic acid (ABDA) assay according to a relative procedure adapted from the literature.[7] ABDA was selected as $^1O_2$ scavenger due to its fast reaction with this molecule and high selectivity. Fresh stock air-equilibrated solutions of photosensitizers **1** and **3** (5.00×10^{-5} M) in water (5% DMSO) and ABDA (Sigma Aldrich, 6.00×10^{-4} M) in H_2O:DMSO (40:60) were prepared. In a quartz cell, 0.50 mL of ABDA solution and 0.12-0.20 mL of PS solution were mixed with water to obtain a final solution (3 mL) of ABDA in water (10% DMSO). The starting absorbance of ABDA in water (10% DMSO) was adjusted around 1.2 (1.00×10^{-4} M). The absorbance of the photosensitizers was adjusted around 0.016 at 470 nm. Then, the evolution was monitored by UV-vis spectroscopy in dark and under blue light irradiation (470 nm, 51.4 mW cm^{-2}) for 30 s irradiation intervals during a total exposure period of 4 min. The consumption of ABDA was measured by monitoring its absorbance intensity decrease at 400 nm with irradiation time. $^1O_2$ generation quantum yield (ϕ_Δ) was calculated from equation 2 using $[Ru(bpy)_3]^{2+}$ as reference:

$$\phi_{\Delta,s} = \phi_{\Delta,ref} \cdot \frac{S_s}{S_{ref}} \cdot \frac{F_{ref}}{F_s} \quad \text{(Equation 2)}$$

where s and ref subindex correspond to the complex and the reference, ϕ_Δ is the $^1O_2$ generation quantum yield (0.18 for $[Ru(bpy)_3]Cl_2$ in water),[8] S is the slope of the plots of the -ln(normalized absorbance) of ABDA at 400 nm *vs.* the irradiation time, F is the correction factor of absorption, which is given by $F = 1 - 10^{-O.D.}$ (where O.D. is the optical density at 470 nm of solutions of the photosensitizers). The reproducibility of the results was confirmed by performing each experiment three times. The stability of ABDA probe was confirmed in dark conditions and under light irradiation.

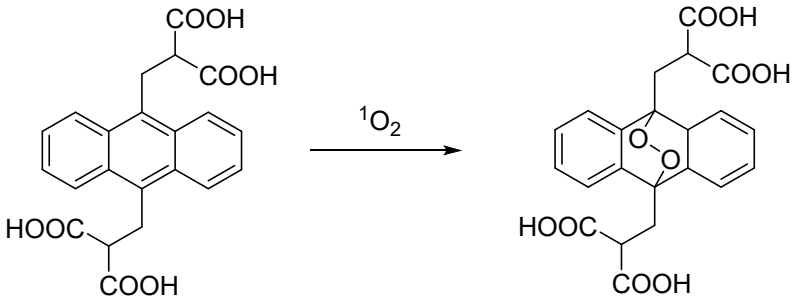

Superoxide anion radical ($O_2^{\bullet-}$) generation. Dihydrorhodamine 123 (DHR123) is used as the superoxide anion radical indicator.[9] Ir(III) complexes and $[Ru(bpy)_3]^{2+}$ were prepared as 10 μM in water (1 % DMSO) and DHR123 (TargetMol) was prepared as 30 μM in water (0.3 % DMSO). In a quartz cell, 300 μL of PS solution and 1,000 μL of DHR123 solution were mixed with 1,700 μL of water to obtain a final solution (3 mL) of DHR123 (10 μM) and PS (1 μM) in water (0.2 % DMSO). Then, the cuvette was exposed to blue light (470 nm, 51.4 mW cm^{-2}) for indicated times and the fluorescence spectra were immediately recorded. $[Ru(bpy)_3]^{2+}$ was used as reference. As control, DHR123 solution without PS was monitored under blue light irradiation. For superoxide anion radical quenching experiment, ascorbic acid (Tokyo Chemical Industry, TCI) was added to the above solution at 1 mM before light irradiation. For singlet oxygen quenching experiment, sodium azide (Fisher Scientific) was added to the above solution at 1 mM before light irradiation.

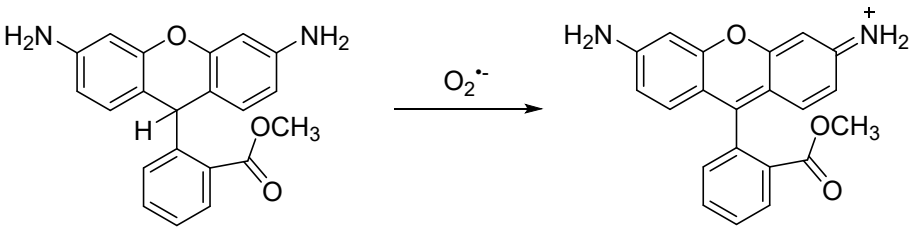

NADH oxidation. Fresh stock solutions of the complexes at 10 μM in water (1 % DMSO) and NADH at 300 μM in water were prepared. In a quartz cell, 300 μL of complex solution, 1 mL of NADH solution and 1.7 mL of water were mixed to prepare a final solution with 1.0 μM of complex and 100 μM of NADH (complex/NADH rate = 1/100) in water (0.1 % DMSO). The solutions were studied by recording UV-vis absorption spectra in dark conditions and under blue light irradiation (470 nm, 51.4 mW cm^{-2}) at room temperature for 10 minutes with time intervals of 30 seconds. The stability of the NADH at 100 μM in dark and under blue light irradiation was also confirmed (data not shown).

The photocatalytic rate of the photosensitizers was evaluated by monitoring its absorbance decrease at 340 nm, which correspond to NADH oxidation. The turnover numbers (TONs) of complexes were calculated by measuring the absorption difference at 340 nm after 5 minutes of reaction. TON was calculated from the difference in NADH concentration after 5 minutes divided by the concentration of photocatalyst (equation

3), where b is the optical path length (1 cm). The concentration of NADH was obtained using the extinction coefficient ε_{340} = 5751 M^{-1} cm^{-1}.[10,11]

$$\text{TON} = \frac{[\text{NADH consumed in 5 min}]}{[\text{Catalyst}]} = \frac{\dfrac{A_{0\text{ h}} - A_{5\text{ min}}}{b \cdot \varepsilon_{340\text{ nm}}}}{[\text{Catalyst}]} \qquad \text{(Equation 3)}$$

Photoactivation protocol in non-biological studies. Photoactivation in non-biological studies was carried out in a 16-compartment 'Medusa' photo-multireactor built by Microbeam, equipped with high-power LEDs (2.3 W, 700 mA, Luxeon Rebel, Philips Lumileds). The LEDs are situated below each compartment (Figure S86). Every reactor position is composed of 40 mL cylindrical glass flask provided by Scharlau. All reaction positions were irradiated from the bottom using monochromatic light provided by LEDs of blue light (470 ± 20 nm, 51.4 mW cm^{-2}). All reactions in the system could be stirred using an orbital stirrer, which was set at 50 rpm.

Lipophilicity. The partition coefficients of complexes **1** and **3** were determined by standard "shake flask" method as previously described.[11] Octanol-saturated water (OSW) and water-saturated octanol (WSO) were prepared using analytical grade 1-octanol and ultrapure water. The complexes were dissolved in WSO and molar extinction coefficient was determined. Then, 2 mL of 25 µg/mL of complex in WSO were shaken with 2 mL of OSW at 1500 rpm for 6 h at room temperature. The organic phases were collected by centrifugation (4,000 rpm, 10 min, r.t.). The absorbance of WSO phase before and after shaking was measured. The distribution coefficients (log $P_{o/w}$) of the complexes were obtained from the ratio of the complexes present in 1-octanol before and after shaking (equation 4). Each experiment was repeated three times.

$$\log P = \log \frac{C_{1-oct}}{C_{water}} = \log \frac{C_{1-oct}}{C_{total} - C_{1-oct}} = \log \frac{A_{1-oct}}{A_{total} - A_{1-oct}} \qquad \text{(Equation 4)}$$

where $A_{1\text{-oct}}$ corresponds to the absorbance of WSO phase and A_{total} the actual concentration of the WSO before shaking.

EPR experiments

Spectra were acquired at room temperature using a MiniScope MS 400 X-band EPR spectrometer (Magnettech, Germany), with samples loaded into 10 µL glass capillaries (Duran Ringcaps, Hirschmann, Germany). Acquisition parameters were as follows: single scan (60 s); gain, 200 (A) or 300 (B); modulation amplitude, 0.1 mT; microwave power, 4 mW (A) or 20 mW (B); microwave frequency, 9.44 GHz. Red lines below the spectra represent simulations obtained using EasySpin (easyspin.org) [12], assuming isotropic spin systems with the following parameters: (A) g = 2.0064, A_N = 1.57 mT; (B) g = 2.0061, A_H = 1.00 mT, A_N = 1.25 mT. Irradiation was performed *in situ* using a UV-LED spot light source of 365 nm ± 2 nm and 2000 mW/cm^2 (model LC-L1V5 equipped with a L14310-115 LED, Hamamatsu Photonics K.K., Hamamatsu City, Japan).

Synthesis of copolymers

*Synthesis of **P1b***. In a typical RAFT polymerization, the monomers PEGMA (polyethyleneglycol methyl ether methacrylate) (1 g, 40 eq), and BOC-aminoethyl methacrylate (0.5 g, 40 eq), the chain transfer agent 2-cyano-2-propyl dodecyl trithiocarbonate (20.18 mg, 1 eq) and azobisisobutyronitrile (AIBN) (1.6 mg, 0.5 eq) were dissolved in 1,4-dioxane (10 mL). The reaction mixture was degassed by three freeze-pump-thaw cycles, then the vessel was backfilled with N_2 and allowed to warm to room temperature. The reaction mixture was then placed in an oil bath at 70 ˚C, and the polymerization was quenched after 4 h by rapid freezing. The polymer was purified by dialysis with MeOH. The polymer **P1** was obtained as a pale-yellow oil after evaporation of the solvent. The conversion of the polymer was calculated via ^{1}H NMR following the decrease of the integrals

of the monomers signals relative to the signal corresponding to the trioxane (used as standard). Copolymer **P1** (1.07 g) was dissolved in CH_2Cl_2 (5 mL), trifluoroacetic acid (TFA) (5 mL) was added and then the reaction mixture was left to stir for 12 h. After this time the polymer was purified by dialysis with MeOH. The polymer **P1b** was obtained as a pale-yellow oil after evaporation of the solvent.

*Synthesis of **P2***. In a typical RAFT polymerization, the monomers PEGMA (2 g, 40 eq), and 2-carboxyethyl acrylate (432 mg, 80 eq), the chain transfer agent 2-cyano-2-propyl dodecyl trithiocarbonate (40.36 mg, 1 eq) and AIBN (3.2 mg, 0.5 eq) were dissolved in 1,4-dioxane (10 mL). The reaction mixture was degassed by three freeze-pump-thaw cycles, then the vessel was backfilled with N_2 and allowed to warm to room temperature. The reaction mixture was then placed in an oil bath at 70 ˚C, and the polymerization was quenched after 4 h by rapid freezing. The polymer was purified by dialysis with MeOH. The polymer **P2** was obtained as a pale-yellow oil after evaporation of the solvent. The conversion of the polymer was calculated via ^{1}H NMR following the decrease of the integrals of the monomers signals relative to the signal corresponding to the trioxane (used as standard).

Synthesis of polymeric nanoparticles

Equimolar dilute solutions of copolymers were mixed in water (1.5 mL, 20 mg/mL), and the corresponding amount of EDC (1-ethyl-3-(3-dimethylaminopropyl)carbodiimide) (0.5 mL, 5%) was added dropwise. The solution was left 12 h stirring at room temperature. After this time, the solution was purified by dialysis in water using a molecular porous membrane tubing with a 3.5 kDa MWCO (Molecular Weight Cut Off) and then, lyophilised to obtain a solid.

A similar procedure was performed to obtain nanoparticles with the Ir complexes **1** and **3** encapsulated. The copolymers were mixed in water, complexes in 0.25 mL of DMF were added and the corresponding amount of EDC was added dropwise.

DLS. The hydrodynamic diameter of the nanoparticles was measured in H_2O at 25 °C at 0.1 mg/mL using a Dynamic Light Scattering (DLS, ZetaPlus, Brookhaven, Holtsville, NY) instrument operating at a 90 scattering angle with a 635 nm (35 mW) diode laser source. The path length of the cuvette was 1 cm.

SEM. **NP1** and **NP3** were analysed using a GeminiSEM 500 High Resolution Scanning Electron Microscope (HRSEM) from ZEISS brand (Oberkochen, Germany). Nanoparticles solutions in water were dried before analysis.

Cell lines

The A549 lung adenocarcinoma, HeLa cervical carcinoma, MCF-7 breast cancer, BxPC3 pancreatic adenocarcinoma human cell lines as well as the MRC-5 lung fibroblast were obtained from the American Type Culture Collection (ATCC). Cells were cultured in Dulbecco's modified Eagle's medium (DMEM) (Corning) supplemented with 10% fetal bovine serum (FBS) (Gibco-BRL), 1% L-glutamine (Corning), and 1% penicillin-streptomycin (Corning) at 37 °C in a Heracell 150 incubator (Thermofisher Scientific) with a humidified atmosphere with 5% CO_2. Cells cultures were maintained by successive trypsinization and seeding. The MYCOPLASMA Gel Form kit (*Biotools*) was used regularly to control mycoplasma contamination.

Dilution of the complexes and nanoparticles

Complexes **1** and **3** were dissolved in sterile dimethyl sulfoxide (DMSO) to a concentration of 5 mM and subsequently diluted with Milli-Q water to obtain 1 mM stock solutions (20% DMSO, v/v). Nanoparticles **NP1** and **NP3** were diluted in sterile Milli-Q water to a concentration of 1 mg/mL. This NP concentration contains 23.319 µM of complex **1** in the case of **NP1** and 27.560 µM of complex **3** for **NP3**, as determined by analysis of the iridium content using an Agilent 7500c ICP-mass spectrometer (Technical Research Services of the

University of Girona). Aliquots of stock solutions were stored at –20 °C. Prior to each treatment, stock solutions were further diluted in cell culture media and used at concentrations ranging from 0 to 50 μM.

Cytotoxicity assays

The cytotoxic activity of the complexes was determined by MTT assays. Cells were seeded in 96-well plates at different densities depending on the cell line (2,500 A549 cells/well, 1,500 HeLa cells/well, 3,500 MCF7 cells/well, 3,500 BxPC3 cells/well, or 5,000 MRC-5 cells/well) and allowed to attach overnight. Cells were incubated by triplicate with solutions of the complexes or NPs ranging from 0.0001 to 50 μM for 4 h to allow their internalization, and plates were kept in the dark or irradiated for 1 h with blue light (460 nm), green light (515 nm) or red light (635 nm) using a light-emitting diode (LED) system (Lux Light), that provided a total light dose of 24.1 J cm^{-2}. After 48 h of treatment, the medium was removed, cells were washed with phosphate buffered saline (PBS), and incubated for 2 h with 100 μL of fresh culture medium containing 10 μL of MTT solution (0.5 mg/mL) (Sigma-Aldrich). Subsequently, the medium was discarded and 100 μL of DMSO (Sigma-Aldrich) was added to each well to dissolve the purple formazan crystals. Absorbance was measured at a wavelength of 570 nm using a Multiscan Plate Reader (Synergy 4, Biotek, Winooski, USA). For each compound, the concentration that inhibited cell viability by 50% (IC_{50}) was established using the Gen5 Data Analysis Software (BioTeck). The phototoxicity index (PI = $IC_{50,dark}/IC_{50,light}$) of each compound was determined. At least three independent experiments were performed for each complex and for each cell line.

Hemolysis assay

The hemolytic activity of the complexes was determined using commercial porcine blood, anticoagulated with sodium polyphosphate (Friusa, Spain). The blood was centrifuged to remove the plasma and washed three times with PBS. The blood cells were obtained and diluted with PBS to a final concentration of 5%. Equal volumes of the blood cells and the complexes at different concentrations were mixed and then kept in the dark or exposed to blue light for 1 h at 37 °C with agitation at 220 rpm in an orbital shaker. The negative control was prepared by mixing the blood cells with PBS. The positive control was prepared with Tween 0.2% in PBS to induce complete release of hemoglobin from RBC. After the treatments, the samples were centrifuged, and the supernatant was collected to measure hemoglobin release. 80 μL of each supernatant and 80 μL of water were added to a 96-well plate, and the absorbance of each well was measured using a Synergy 4 plate reader (Biotek) at 540 nm. The percentage of hemolysis was calculated using equation 5, where Ax = absorption of the sample; An = absorption of the negative control; Ap = absorption of positive control).

$$H\ (\%) = 100\ x \frac{(Ax - An)}{(Ap - An)} \quad \text{(Equation 5)}$$

Clonogenic assays

HeLa cells were seeded in 12-well plates at a density of 100,000 cells per well and incubated overnight. Subsequently, cells were treated with the complexes at the corresponding $IC_{50,light}$, for 4 h. Cells exposed to cisplatin (Accord Healthcare) at 5 uM were included as positive control and untreated cells as a negative control. Next, cells were kept in the dark or irradiated with blue light for 1 h (total dose: 24.1 J cm^{-2}). After removal of the treatments and washing with PBS, cells were harvested by trypsinization and counted using a Novocyte flow cytometer (Agilent Technologies). One thousand cells from each sample were seeded in 5 cm culture dishes and incubated for 10 days to allow the formation of colonies of at least 50 cells. The colonies were then fixed and stained with 1% methylene blue in 70% ethanol and counted using the Alpha Innotech Imaging System (Alpha Innotech) and the Fiji ImageJ software. The experiments were conducted in triplicate.

ROS production

HeLa and A549 cells were seeded in 12 well-plates at a density of 100,000 cells per well and incubated overnight. Cells were then incubated with the complexes at the corresponding $IC_{50,light}$ for 4 h to facilitate their internalization. Treatments were then removed, and the cells were washed with PBS. The 2',7'-dichlorodihydrofluorescein diacetate probe (H_2DCFDA) (Sigma-Aldrich) was added to each well at a concentration of 10 µM. Subsequently, cells were irradiated with blue light (24.1 J cm^{-2}) or maintained in the dark for 1 h. Cells were collected by trypsinization, and the median fluorescence emission of 10,000 cells was measured with a Novocyte flow cytometer (Agilent Technologies) equipped with the NovoExpress software. The fluorescence fold increase versus untreated control cells was determined. Three independent experiments were conducted for each complex and cell line. The same protocol was followed to evaluate the superoxide production. In this case, samples were stained using the ROS-ID® Superoxide detection kit (Enzo life sciences), according to the manufacturer instructions.

To evaluate the influence of ROS on the photocytotoxic effect of the complexes, HeLa cells were incubated with complexes **1** or **3** at their respective $IC_{50,light}$ for 4 hours, followed by irradiation with blue light (460 nm) for 1h in the absence or presence of selective ROS scavengers: 1% DMSO (Panreac) for $^{\bullet}OH$, 5 mM sodium azide (Sigma Aldrich) for $^1O_2$ or 5 mM tiron (4,5-dihydroxy-1,3-benzenedisulfonic acid) for $O_2^{\bullet-}$. Cell viability was assessed using MTT assays after 48 hours of treatment. The percentage of viable cells was determined in comparison to cells exposed to medium alone or supplemented with the respective ROS scavenger. Each condition was tested by triplicate in three independent experiments.

Mitochondrial damage

Evaluation of mitochondrial membrane potential. HeLa cells were seeded in 12-well plates at a density of 100,000 cells per well. Cells were treated with complexes **1** and **3** the corresponding $IC_{50,light}$ for 4 h, followed by either blue light irradiation or maintenance in the dark for one additional hour. Next, treatments were removed, cells were washed with PBS and harvested by trypsinization. Changes in the mitochondrial membrane potential were immediately measured using the JC-1 (5,5',6,6'-tetrachloro-1,1',3,3'-tetraethylbenzimidazolocarbo-cyanine iodide) MMP detection Kit (Biotium), according to the manufacturer's instructions. For each treatment, the median fluorescence of 10,000 cells was analysed with a Novocyte flow cytometer. Red fluorescence emission from JC-1 aggregates in healthy mitochondria was detected at 590 nm (FL2), while green fluorescence emission from JC-1 monomers, indicative of mitochondrial depolarization, was detected at 529 nm (FL1).

Microscopy experiments. HeLa cells were seeded on glass-bottom chambers slides (Ibidi) at a density of 50,000 cells per well and allowed to attach overnight. Cells were then treated with the complexes at the corresponding $IC_{50,light}$ for 4 h and kept in the dark or irradiated with blue light for 1 h. Untreated cells were used as the negative controls. Upon the treatment, cells were washed three times with PBS and the mitochondria were stained with MitoTracker™ Red CMXRos (Molecular Probes) diluted at 200 nM in phenol red-free DMEM for 30 minutes at 37°C. Cell nuclei were stained with Hoechst 33342 (Invitrogen) diluted at 1:4000. Subsequently, the cells were washed three times with PBS and fresh phenol red-free DMEM was added to the chambers. Mitochondrial damage was immediately evaluated by confocal microscopy using a Nikon A1R confocal microscope. Cell nuclei were visualized in blue (excitation/emission: 350/461 nm), and mitochondria were visualized in red (excitation/emission: 579/599 nm). Images were analyzed using the NIS-Elements AR (Nikon, Japan) and Fiji/ImageJ softwares.

Apoptosis assay

HeLa cells were seeded in 12-well plates at a density of 100,000 cells per well and incubated overnight. Cells were incubated with the complexes at the corresponding $IC_{50,light}$ and $IC_{50,light}$×5 for 4 h and then irradiated

with blue light for 1h. Untreated cells were included as a control. Cells were immediately harvested by trypsinization and stained with annexin V-FITC and propidium iodide using a Vybrant® Apoptosis Assay Kit (Molecular Probes), according to the manufacturer's instructions. Fluorescence emission was analysed using a Novocyte Flow Cytometer (Agilent Technologies). Annexin-FITC staining was detected at a wavelength of 520 nm (FL1) and propidium iodide was detected at 617 nm (FL2). 10,000 cells per sample were measured, and the percentages of live, early apoptotic, late apoptotic, and necrotic cell populations were determined. The experiment was conducted in triplicate.

Wound healing assay

A549 cells were seeded in 6-well plates at a density of 750,000 cells per well. Once grown in confluent monolayers, cells were treated with the complexes at the corresponding $IC_{50,light}$ for 4 h and then kept in the dark or irradiated with blue light for 1 h. Subsequently, treatments were removed, and the cells were washed twice with PBS. Subsequently, a pipette tip was employed to create a cross-shaped wound by scratching the cell monolayer. The cells were washed twice with PBS, and DMEM supplemented with 0.5% FBS, 1% L-glutamine, and 1% penicillin-streptomycin was added to the wells. This concentration of FBS was selected to avoid cellular division. Untreated cells were used as negative control. Photographs of the cross wound were taken at 0 h and 24 h using an Olympus CKX41 microscope with LCmicro software (Olympus). The MRI Wound Healing Tool macro of Image J was utilized for the analysis of cell migration. Three independent experiments were conducted for each compound.

Cytotoxic activity in 3D-cultures

A549 spheroids were generated in 96-well plates coated with a thin solidified layer of Geltrex™ reduced growth factor basement membrane matrix (Gibco). 1,500 cells were seeded per well in culture medium supplemented with 2% Geltrex and allowed to grow for six days to generate MCS, which were subsequently treated with complexes **1** and **3** and **NP1** and **NP3** at concentrations ranging from 0.01 to 50 µM in dark or irradiated conditions. For photoactivated treatments, plates were exposed to blue light for 1 h upon a 4 h incubation with the complexes and NP. Non-treated spheroids were used as the control. After 48 h, the treatments were removed, cells were washed with PBS, and cell viability was determined by adding 100 µL of medium and 100 µL of CellTiter-Glo 3D reagent (Promega) to each well. Following the manufacturer's protocol, cells were kept in agitation for 5 min and incubated for 25 min at room temperature. Then, the luminescence was determined using a Multiscan Plate Reader (Synergy 4, Biotek, Winooski, USA). The IC_{50} values were calculated with the Gen5 Data Analysis Software (BioTeck) for two independent experiments, each with duplicate samples. In addition, images of MCSs exposed for 48 h to each treatment were captured using an Olympus CKX41 microscope.

To further validate the results in a larger-scale 3D model, A549 cells were seeded at a density of 4,000 cells per well in 96-well round-bottom plates with an ultra-low attachment surface (TC-Plate 96 Well, BIOFLOAT, Sarstedt). After 5 days of incubation, spheroid formation was confirmed and baseline images (t = 0 h) were acquired using an Olympus CKX41 microscope. Spheroids were then treated in duplicate with complexes **1** and **3** and nanoparticles **NP1** and **NP3**, at the corresponding $IC_{50,light}$ determined from the Geltrex-based 3D model, and at five times the $IC_{50,light}$. Following a 4-hour incubation period, spheroids were irradiated with blue light for 1 hour. Final images (t = 48 h) were captured 43 hours post-irradiation, and changes in spheroid size and morphology were analyzed.

Cellular Uptake

HeLa and A549 cell lines were seeded at a concentration of 2 million cells per well in 6-well plates. After 24 h, cells were incubated with the complexes and NPs at 5uM for 4 h. Untreated cells were used as a control. Upon the treatment, the medium was removed, cells were harvested by trypsinization and washed 3 times with PBS. The number of cells in each sample was counted using a Novocyte flow cytometer (Agilent Technologies) and next samples were centrifuged to obtain the cell pellet. The iridium content in each sample was subsequently measured using an Agilent 7500c ICP-mass spectrometer (Technical Research Services of the University of Girona). Previously, the cell pellets were dissolved in 400 µL of 69% v/v concentrated nitric acid and heated at 60 °C overnight. The digested samples were then allowed to cool and diluted up to 5 mL with Milli-Q water. Before each quantification, standards were freshly prepared in Milli-Q water containing the same proportion of HNO_3 (8%). The amount of metal determined in each sample was normalized to the cell number. Three independent samples were analyzed for each complex.

To elucidate the internalization mechanism of complex **1** and **NP1**, their cellular uptake was assessed by flow cytometry at both 37 °C (physiological temperature) and 4 °C (metabolism inhibitory temperature). A549 and HeLa cells were seeded in 12-well plates at a density of 100,000 cells per well and treated for 4 h with complex **1** at 5 µM, **NP1** at 50 µg/mL (1.17 µM), or medium alone as the control. Incubations were performed at 37 °C or 4 °C (on ice). Cells were then washed with PBS, trypsinized, and the fluorescence emission at 675 nm was measured using a Novocyte flow cytometer. The mean fluorescence intensity of each sample was normalized to that of the untreated control. Three independent experiments were carried out per compound.

Subcellular distribution

Microscopy experiments. HeLa cells were seeded on glass-bottomed 8-well chamber slides (Ibidi) at a density of 50,000 cells per well and allowed to attach for 24 h. Cells were treated with complex **1** at 5 µM or **NP1** ($\lambda_{ex}/\lambda_{em}$: 440/596 nm) at 50 µg/mL in phenol red-free DMEM, or medium alone as a negative control. MitoView™ Green (Biotium) ($\lambda_{ex}/\lambda_{em}$: 490/523 nm) and LysoTracker™ Green DND-26 (ThermoFisher Scientific) ($\lambda_{ex}/\lambda_{em}$: 504/511 nm) were used at a concentration of 100 nM to stain mitochondria or lysosomes, respectively. Hoechst 33258 (Sigma) ($\lambda_{ex}/\lambda_{em}$: 352/454 nm) diluted at 1:4000 was used to identify the cell nucleus. After 1 h of incubation at 37°C, treatments were removed, cells were rinsed with cold PBS and images were captured using a Nikon A1R confocal microscope. Images were analysed using NIS-Elements AR software (Nikon, Japan) and ImageJ software using the following acquisition settings: Blue channel: $\lambda_{ex}/\lambda_{em}$: 400/450 nm, Green channel: $\lambda_{ex}/\lambda_{em}$: 488/525, and Red channel: $\lambda_{ex}/\lambda_{em}$: 488/595.

ICP-MS experiments. To further assess the subcellular distribution of the compounds, HeLa cells were seeded and treated with complex **1** or **NP1** (5 µM, 4 h) as previously described. Following trypsinization, mitochondria were isolated using the Mitochondria Isolation Kit for Cultured Cells (Thermo Fisher) according to the manufacturer's protocol. Protein content in both the mitochondrial and residual cytosolic fractions was quantified using the Pierce™ BCA Protein Assay Kit (Thermo Fisher). Iridium content in each fraction was then measured by ICP-MS, as detailed above. Iridium levels (µg) were normalized to total protein (mg) for each fraction. Three independent biological replicates were analyzed per treatment.

Statistics

Statistical analyses were performed using the GraphPad Prism software (GraphPad Software). Quantitative variables are expressed as mean or median and standard deviation (SD). Statistical differences were analysed using non-parametric test. Statistical significance was set at $P < 0.05$.

Atom Numbering

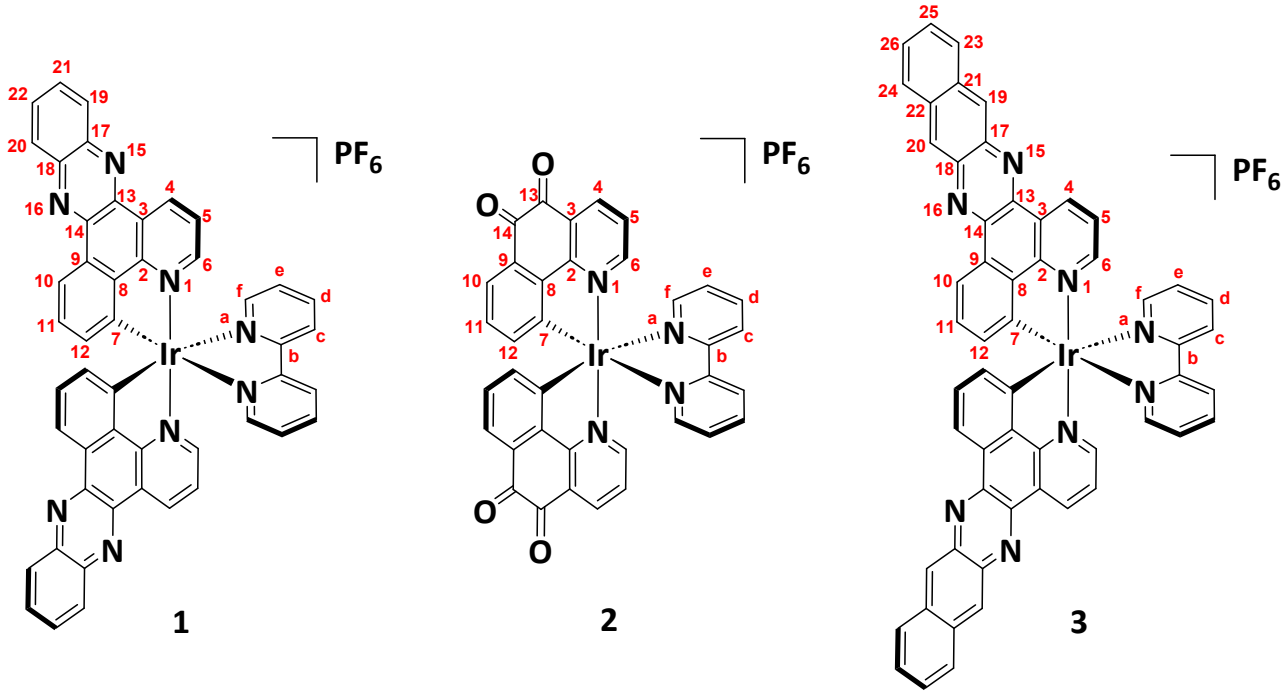

1 2 3

Synthesis of the complexes

[(pbpz)$_2$IrCl$_2$]$_2$, ***D1****.* A mixture of 4,9,14-triazadibenzo[*a*,*c*]anthracene (H-pbpz, 0.12 g, 0.41 mmol, 2.1 equiv.) and $IrCl_3 \cdot 3H_2O$ (0.068 g, 0.19 mmol, 1.0 equiv.) was charged under an inert atmosphere to a microwave vessel. A mixture of diglyme/H_2O (3:1) (4 mL) was added and the vessel was closed and irradiated at 220 °C for 10 min. The crude reaction was centrifugated (5 min, 5,000 rpm, 25 °C) and the supernatant liquid was removed. The brown solid was washed with acetone (2 × 8 mL) and diethyl ether (1 × 8 mL). The product was used without further purification.

[(bhqdo)$_2$IrCl$_2$]$_2$, ***D2****.* A mixture of benzo[*h*]quinoline-5,6-dione (bhqdo, 0.086 g, 0.41 mmol, 2.1 equiv.) and $IrCl_3 \cdot 3H_2O$ (0.068 g, 0.19 mmol, 1.0 equiv.) was charged under an inert atmosphere to a microwave vessel. A mixture of 2-methoxyethanol/H_2O (3:1) (4 mL) was added and the vessel was closed and irradiated at 150 °C for 10 min. After cooling to room temperature, water (1 mL) was added. Then, the crude reaction was centrifugated (5 min, 5,000 rpm, 25 °C) and the supernatant liquid was removed. The black solid was washed with acetone/diethyl ether (1:1) (3 × 8 mL). The product was used without further purification.

[(pbpz)$_2$Ir(bpy)]PF$_6$, ***1.*** In a 100 mL Schlenk flask, previously purged with nitrogen, a solution of $[(pbpz)_2IrCl_2]_2$ (**D1,** 0.25 g, 0.16 mmol, 1.0 equiv.), 2,2'-bipyridine (0.05 g, 0.31 mmol, 2.0 equiv.) and $AgOSO_2CF_3$ (0.08 g, 0.31 mmol, 2.0 equiv.) in degassed DCM/MeOH (2:1) (50 mL) was stirred under reflux for 24 h under a nitrogen atmosphere. The resulting precipitate (AgCl) was removed by filtration over Celite. To recover all the product, the residue was washed with degassed DCM (2 × 5 mL) until the filtrate was colourless. The resulting solution was stirred for 1 h with NH_4PF_6 (0.52 g, 3.2 mmol, 20.0 equiv.). Then, the solution was evaporated in vacuo until dryness. The product was purified by a flash chromatography with neutral Al_2O_3 as stationary phase and $CH_2Cl_2 \rightarrow CH_2Cl_2$:MeOH (98:2) as mobile phase. The fractions with the desired complex were evaporated in vacuo until dryness to give a yellow solid (0.0876 g, 0.083 mmol, 39 %). **^{1}H NMR (400 MHz, DMSO-*d*$_6$):** δ 9.49 (dd, ^3J = 8.2 Hz, ^4J = 1.3 Hz, 2H, H^4), 8.97 (d, ^3J = 8.3 Hz, 2H, H^c), 8.61 (dd, ^3J = 7.9 Hz, ^4J = 1.0 Hz, 2H, H^{10}), 8.42 – 8.35 (m, 4H, H^{19} and H^{20}), 8.30 (td, ^3J = 8.0 Hz, ^4J = 1.6 Hz, 2H, H^d), 8.24 (dd, ^3J = 5.6 Hz, ^4J = 1.4 Hz, 2H, H^6), 8.09 – 8.03 (m, 6H, H^f, H^{21} and H^{22}), 7.75 (dd, ^3J = 8.2, 5.5 Hz, 2H, H^5), 7.65 (ddd, ^3J =

7.7, 5.5 Hz, ^4J = 1.2 Hz, 2H, H^e), 7.35 (t, ^3J = 7.7 Hz, 2H, H^{11}), 6.64 (dd, ^3J = 7.4 Hz, ^4J = 1.0 Hz, 2H, H^{12}). **$^{13}C\{^1H\}$ NMR (126 MHz, DMSO-d_6):** δ 160.0 (C, C^2), 155.7 (C, C^b), 151.4 (CH, C^6), 150.7 (CH, C^f), 148.0 (C, C^7), 142.5 (C, C^{17} or C^{18}), 141.9 (C, C^{17} or C^{18}), 141.2 (C, C^8), 140.9 (C, C^{14}), 140.3 (CH, C^d), 140.0 (C, C^{13}), 135.1 (CH, C^4), 132.6 (CH, C^{12}), 131.6 (CH, C^{21} or C^{22}), 131.4 (CH, C^{21} or C^{22}), 131.1 (CH, C^{11}), 130.9 (C, C^9), 129.3 (CH, C^{19} or C^{20}), 129.2 (CH, C^{19} or C^{20}), 128.9 (CH, C^e), 126.1 (C, C^3), 125.2 (CH, C^c), 124.4 (CH, C^5), 118.3 (CH, C^{10}). **$^{19}F\{^1H\}$ NMR (471 MHz, DMSO-d_6):** δ -70.2 (d, J = 711.1 Hz). **Elemental Analysis** calculated for $C_{48}H_{28}N_8PF_6Ir\cdot(H_2O)$ (1071.99 g/mol): C 53.78, H 2.82, N 10.45; found: C 53.48, H 2.49, N 10.04. **MS (ESI+, DMF)**: m/z calculated for $[(pbpz)_2Ir(bpy)]^+$: 909.01, found: 909.21.

$[(bhqdo)_2Ir(bpy)]PF_6$, ***2****.* In a 100 mL Schlenk flask, a solution of $[(bhqdo)_2IrCl_2]_2$ (**D2**) (0.16 g, 0.13 mmol, 1.0 equiv.), 2,2'-bipyridine (bby, 0.04 g, 0.26 mmol, 2.0 equiv.) and $AgOSO_2CF_3$ (0.07 g, 0.26 mmol, 2.0 equiv.) in degassed DCM/MeOH (2:1) (60 mL) was stirred under reflux for 36 h. After cooling to room temperature, an excess of NH_4PF_6 (0.57 g, 3.52 mmol, 13.8 equiv.) was added to the solution and stirred at room temperature overnight. Then, the crude was concentrated in vacuo until dryness and purified by flash chromatography with neutral Al_2O_3 as stationary phase and $CH_2Cl_2 \rightarrow CH_2Cl_2$:MeOH (9:1) as mobile phase. The pure fractions were evaporated in vacuo until dryness. The product was washed with diethyl ether (3 × 10 mL) and pentane (5 × 10 mL) to obtain a reddish brown solid (0.18 g, 0.20 mmol, 78 %). **^1H NMR (400 MHz, DMSO-d_6):** δ 8.91 (d, ^3J = 8.3 Hz, 2H, H^c), 8.39-8.27 (m, 4H, H^d and H^d), 8.01 (d, ^3J = 5.6 Hz, 2H, H^f), 7.86 (d, ^3J = 5.9 Hz, 2H, H^6), 7.72 (d, ^3J = 6.6 Hz, 2H, H^e), 7.63 (d, ^3J = 6.9 Hz, 2H, H^{10}), 7.34 (t, ^3J = 6.9 Hz, 2H, H^5), 7.15 (t, ^3J = 7.6 Hz, 2H, H^{11}), 6.73 (d, ^3J = 7.7 Hz, 2H, H^{12}). **$^{13}C\{^1H\}$ NMR (101 MHz, DMSO-d_6):** δ 176.9 (C, C^{14}), 176.2 (C, C^{13}), 166.1 (C, C^2), 155.4 (C, C^b), 153.0 (CH, C^6), 150.8 (CH, C^f), 148.7 (C, C^7), 143.9 (C, C^8), 140.1 (CH, C^d or C^4), 137.9 (CH, C^{12}), 136.8 (CH, C^d or C^4), 131.9 (C, C^9), 131.0 (CH, C^{11}), 128.8 (CH, C^e), 128.2 (C, C^3), 125.1 (CH, C^c), 125.0 (CH, C^5), 122.3 (CH, C^{10}). **$^{19}F\{^1H\}$ NMR (471 MHz, DMSO-d_6):** δ -70.2 (d, J = 711.1 Hz). **Elemental Analysis** calculated for $C_{36}H_{20}F_6IrN_4O_4P$ (909.75 g/mol): C 47.53, H 2.22, N 6.16; found: C 47.34, H 2.09, N 6.04. **MS (ESI+, CH_2Cl_2)**: m/z calculated for $[(bhqdo)_2Ir(bpy)]^+$: 765.1108, found: 765.1120.

$[(pbpn)_2Ir(bpy)]PF_6$, ***3****.* In a 100 mL Schlenk flask, a solution of $[(bhqdo)_2Ir(bpy)]PF_6$ (**2**, 0.23 g, 0.25 mmol, 1.0 equiv.) and 2,3-diaminonaphtalene (0.10 g, 0.61 mmol, 2.4 equiv.) in EtOH (50 mL) was stirred under reflux for 5 h. A red precipitate was obtained. The resulting solution was removed by filtration over Celite. The product was washed with EtOH (3 × 20 mL), diethyl ether (3 × 20 mL) and pentane (3 × 20 mL) to give a red solid (0.14 g, 0.12 mmol, 42 %). **^1H NMR (500 MHz, DMSO-d_6):** δ 9.43 (d, ^3J = 8.1 Hz, 2H, H^4), 9.07 (s, 2H, H^{19} or H^{20}), 9.03 (s, 2H, H^{19} or H^{20}), 8.98 (d, ^3J = 8.4 Hz, 2H, H^c), 8.59 (d, ^3J = 7.8 Hz, 2H, H^{10}), 8.38 – 8.30 (m, 6H, H^d, H^{23} and H^{24}), 8.22 (d, ^3J = 5.2 Hz, 2H, H^6), 8.10 (d, ^3J = 5.2 Hz, 2H, H^f), 7.74 – 7.66 (m, 8H, H^e, H^5, H^{25} and H^{26}), 7.34 (t, ^3J = 7.7 Hz, 2H, H^{11}), 6.70 (d, ^3J = 7.4 Hz, 2H, H^{12}). **$^{13}C\{^1H\}$ NMR (126 MHz, DMSO-d_6):** δ 160.8 (C, C^2), 155.7 (CH, C^b), 151.5 (CH, C^6), 150.8 (CH, C^f), 148.3 (C, C^7), 143.4 (C, C^8), 141.6 (C, C^{13} or C^{14}), 141.0 (C, C^{13} or C^{14}), 140.0 (CH, C^d), 138.1 (C, C^{17} or C^{18}), 137.6 (CH, C^{17} or C^{18}), 135.0 (CH, C^4), 134.2 (C, C^{21} or C^{22}), 133.9 (C, C^{21} or C^{22}), 133.2 (CH, C^{12}), 131.5 (C, C^9), 131.0 (CH, C^{11}), 128.9 (CH, C^e), 128.5 (CH, C^{23} or C^{24}), 128.4 (CH, C^{23} or C^{24}), 127.5 (CH, C^{25} or C^{26}), 127.44 (CH, C^{19} or C^{20}), 127.42 (CH, C^{19} or C^{20}), 127.3 (CH, C^{25} or C^{26}), 126.5 (C, C^3), 125.2 (CH, C^c), 124.6 (CH, C^5), 118.6 (CH, C^{10}). **$^{19}F\{^1H\}$ NMR (471 MHz, DMSO-d_6):** δ -70.2 (d, J = 711.1 Hz). **Elemental Analysis** calculated for $C_{56}H_{32}F_6IrN_8P\cdot(H_2O)_{3.1}$ (1209.94 g/mol): C 55.59, H 3.18, N 9.26; found C 55.29, H 3.14, N 9.06. **MS (ESI+, DMF)**: m/z calculated for $[(pbpn)_2Ir(bpy)]^+$: 1009.13, found: 1009.24. m/z calculated for $[(pbpn)(bhq(NH_2)_2)Ir(bpy)]^+$: 887.02, found: 887.18.

NMR spectra of complexes

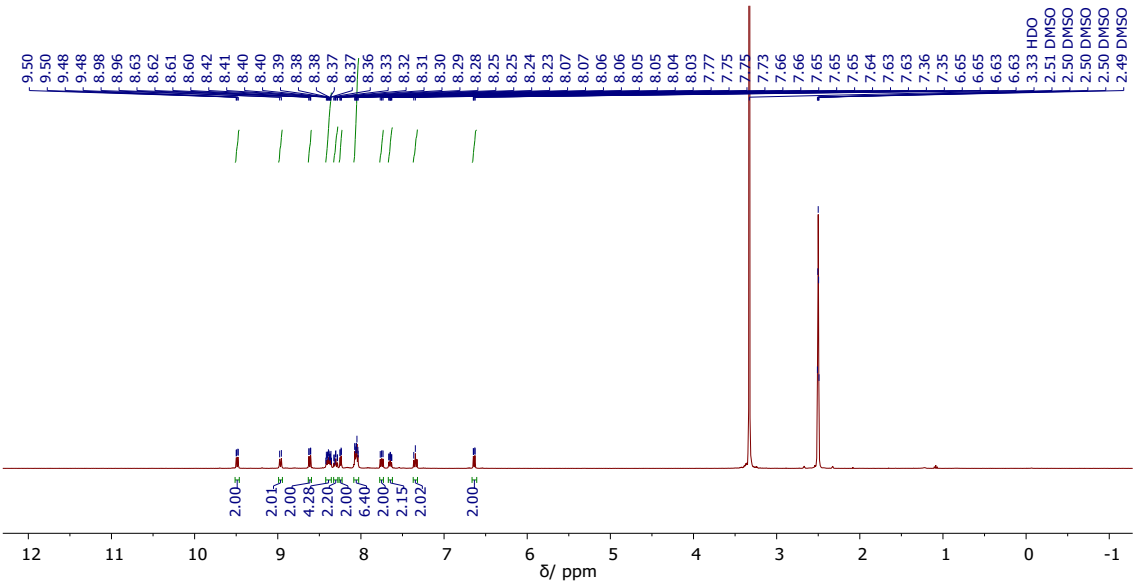

Figure S1. ^{1}H NMR (400 MHz, DMSO-d_6, 298 K) spectrum of **1**.

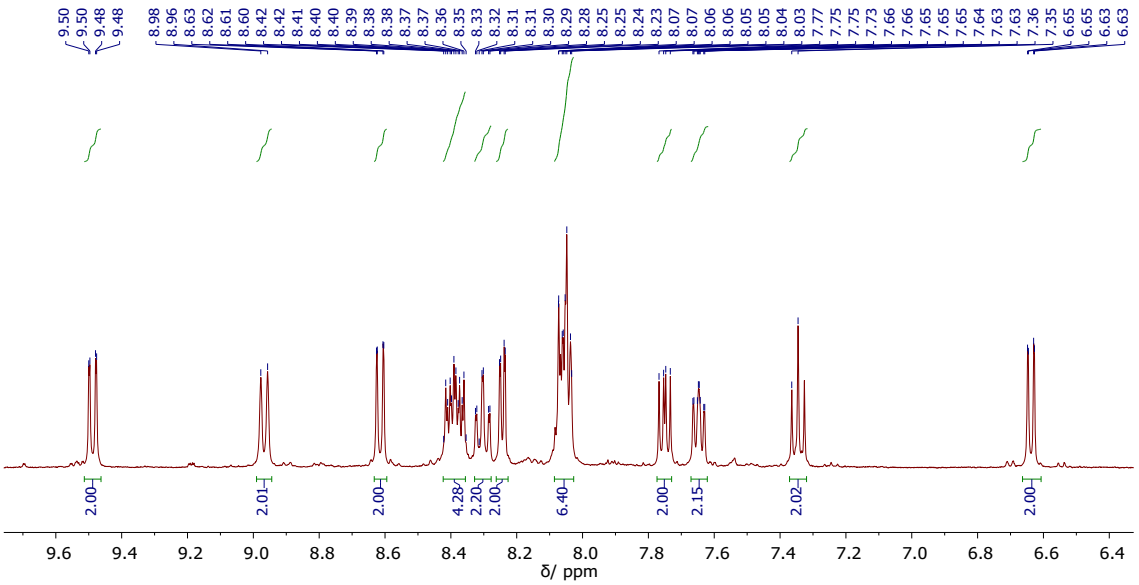

Figure S2. ^{1}H NMR (400 MHz, DMSO-d_6, 298 K) spectrum of **1** in the aromatic region.

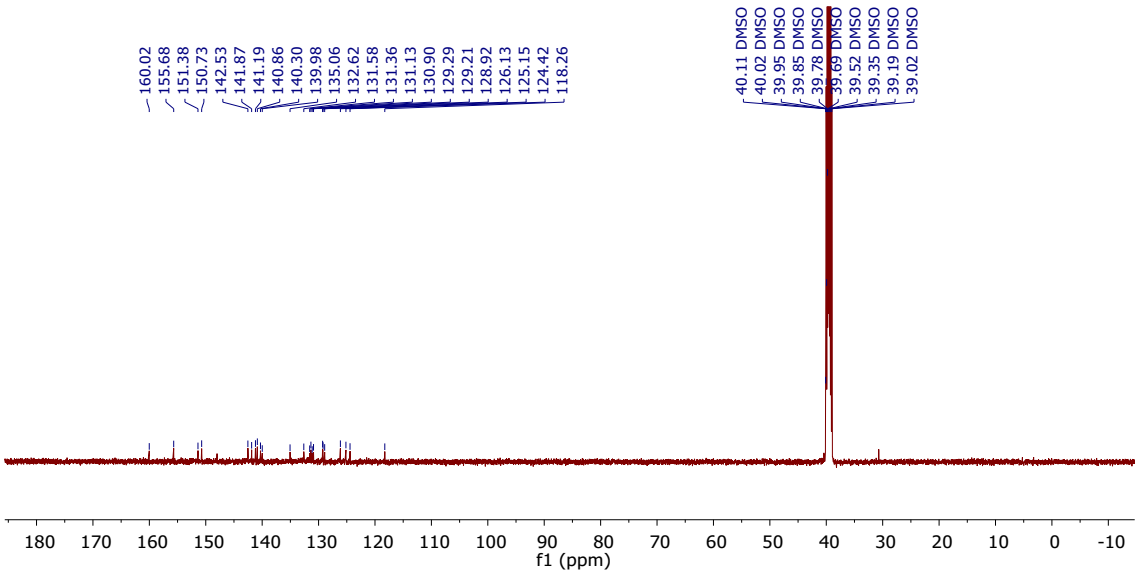

Figure S3. $^{13}C\{^{1}H\}$ NMR (126 MHz, DMSO-d_6, 298 K) spectrum of **1**.

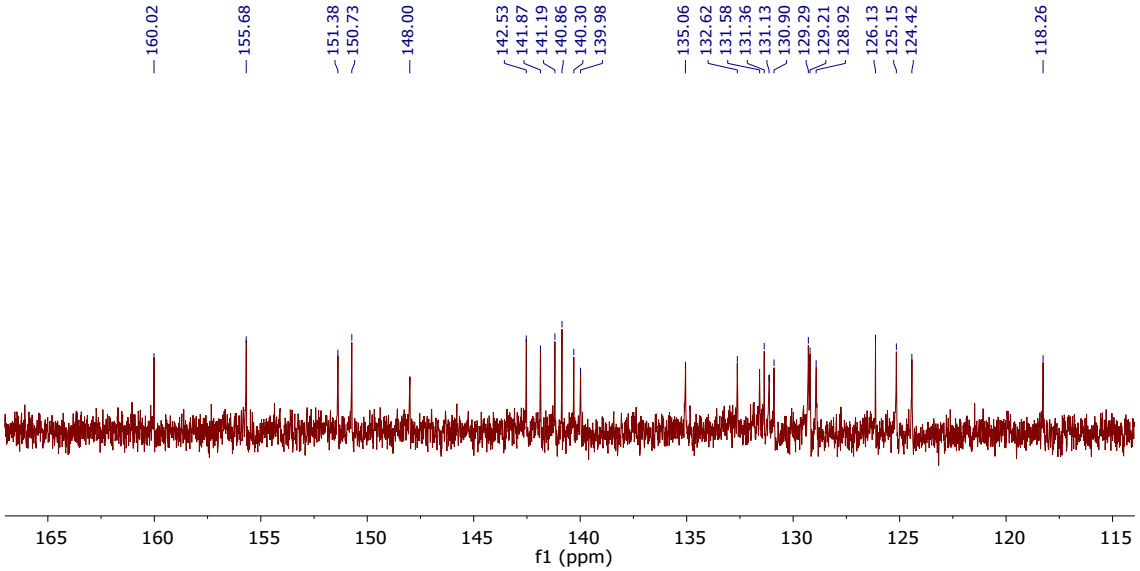

Figure S4. $^{13}C\{^{1}H\}$ NMR (126 MHz, DMSO-d_6, 298 K) spectrum of **1** in the aromatic region.

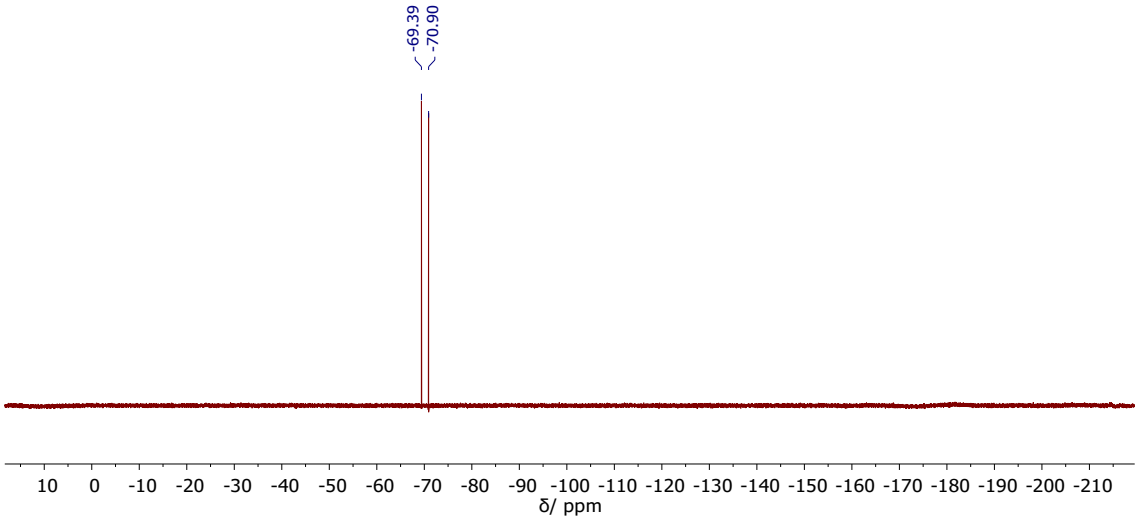

Figure S5. $^{19}F\{^{1}H\}$ NMR (471 MHz, DMSO-d_6, 298 K) spectrum of **1**.

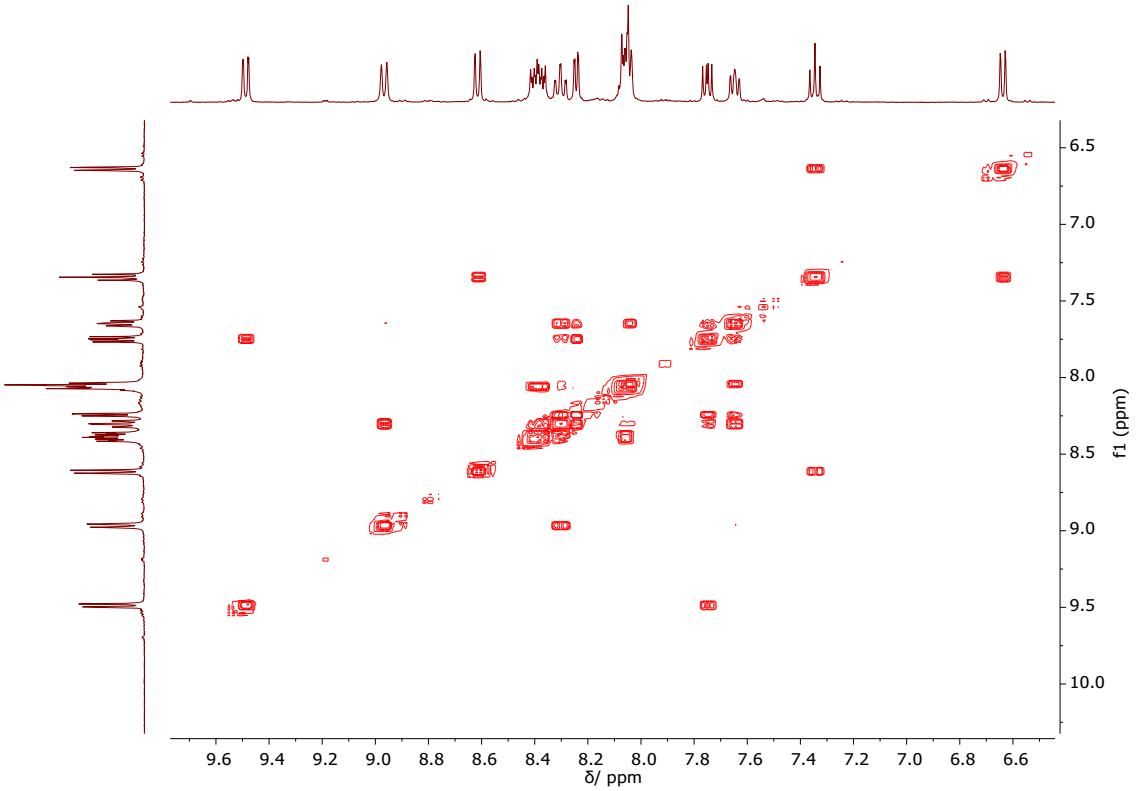

Figure S6. ^{1}H-^{1}H COSY (400 MHz, DMSO-d_6, 298 K) spectrum of **1** in the aromatic region.

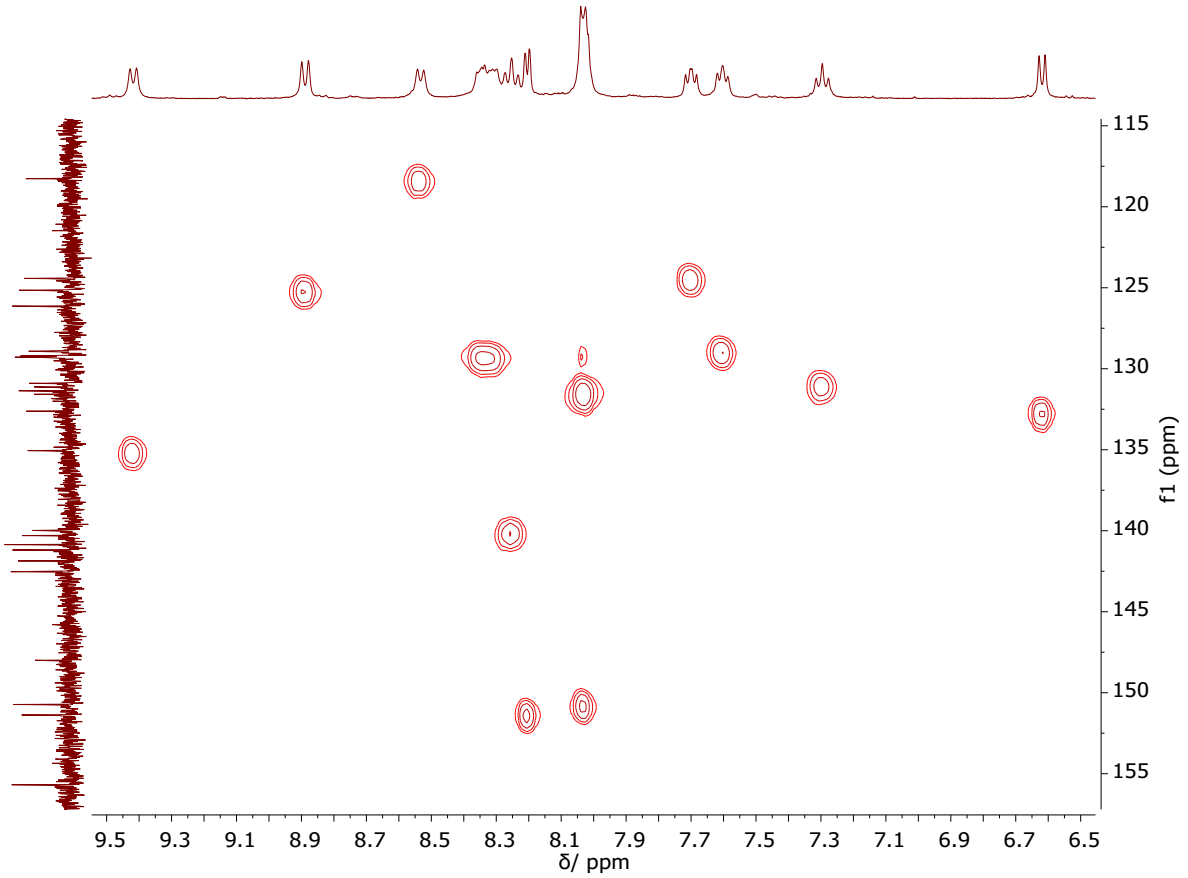

Figure S7. ^{1}H-^{13}C HSQC (DMSO-d_6, 298 K) spectrum of **1** in the aromatic region.

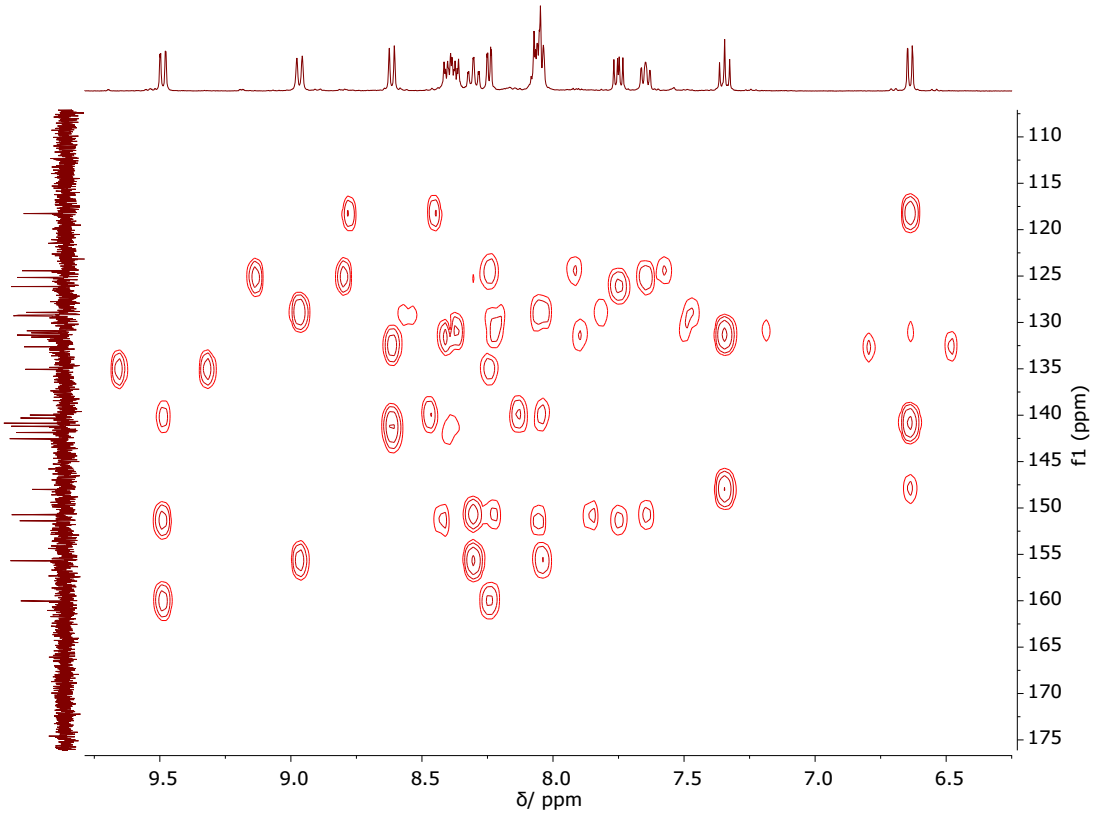

Figure S8. ^{1}H-^{13}C HMBC (DMSO-d_6, 298 K) spectrum of **1** in the aromatic region.

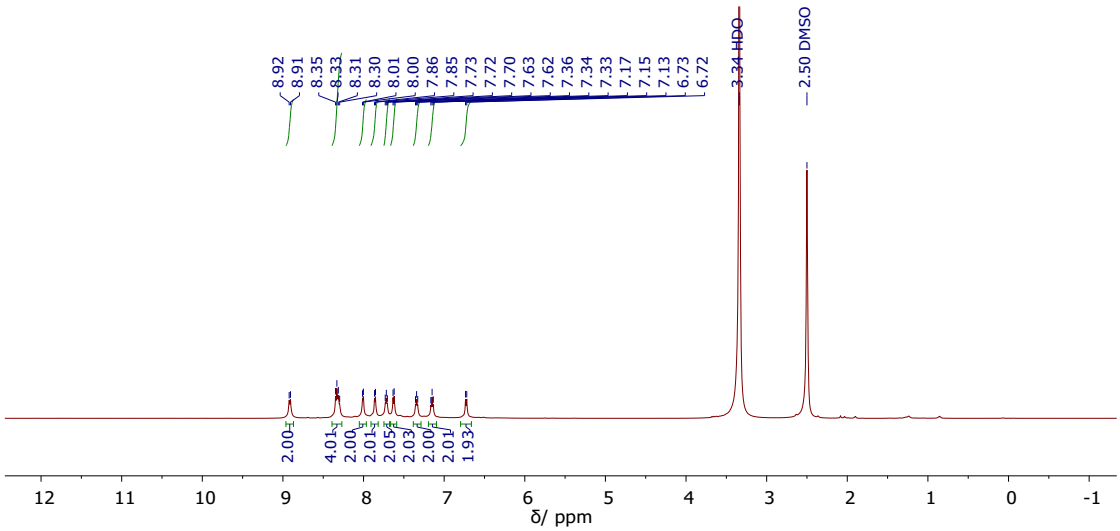

Figure S9. ^{1}H NMR (400 MHz, DMSO-d_6, 298 K) spectrum of **2**.

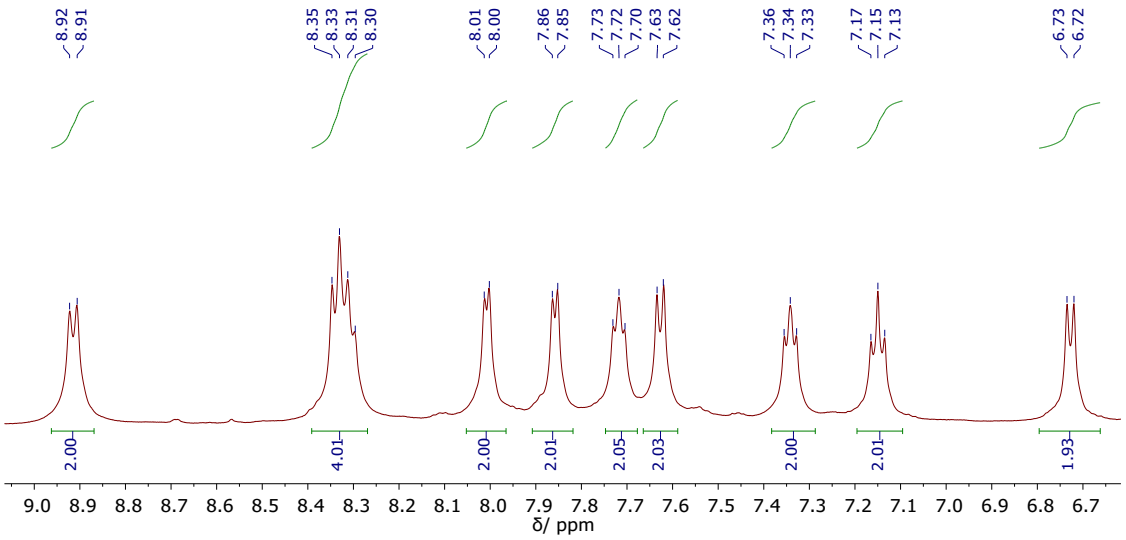

Figure S10. ^{1}H NMR (400 MHz, DMSO-d_6, 298 K) spectrum of **2** in the aromatic region.

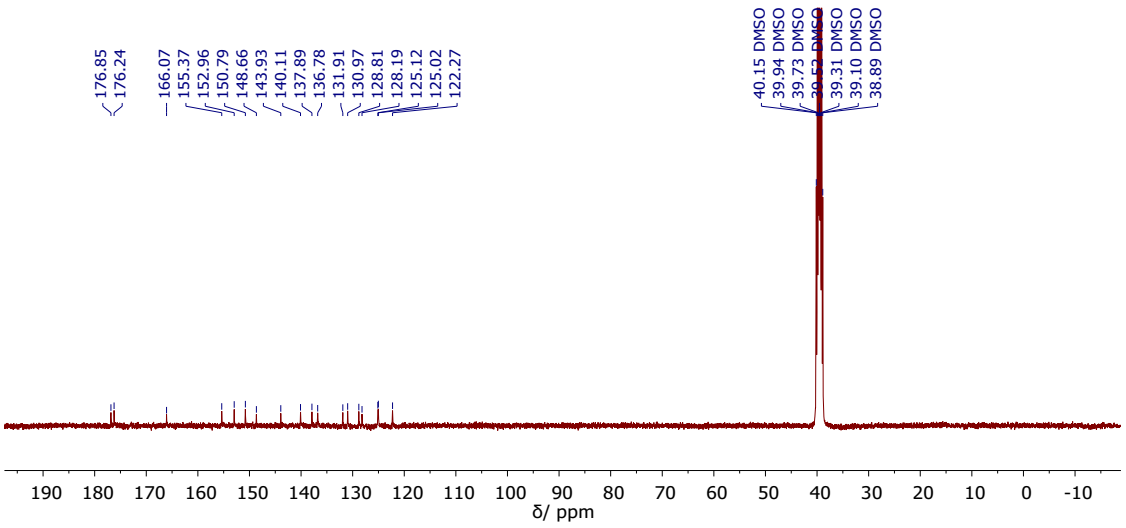

Figure S11. ^{13}C{^{1}H} NMR (126 MHz, DMSO-d_6, 298 K) spectrum of **2**.

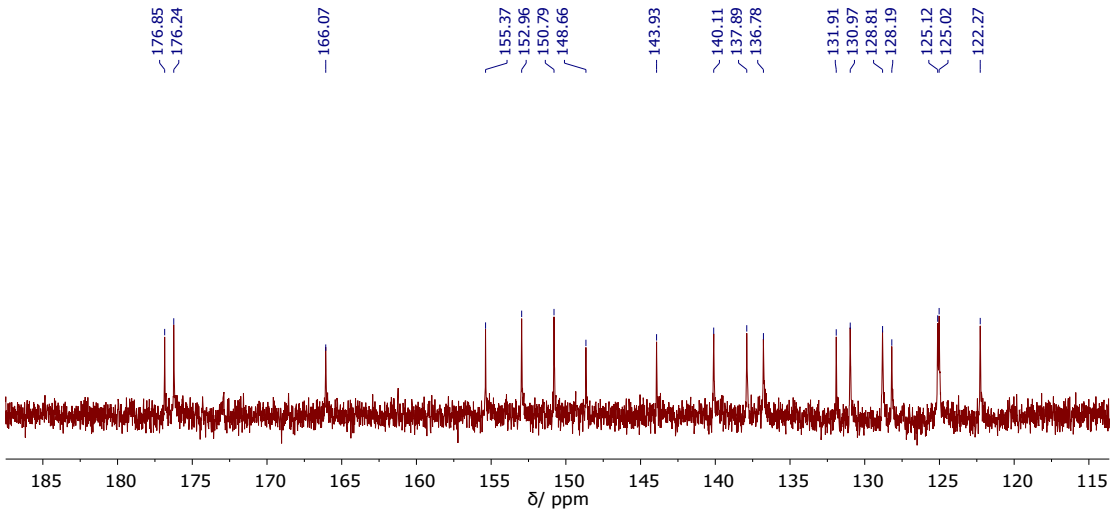

Figure S12. $^{13}C\{^{1}H\}$ NMR (126 MHz, DMSO-d_6, 298 K) spectrum of **2** in the aromatic region.

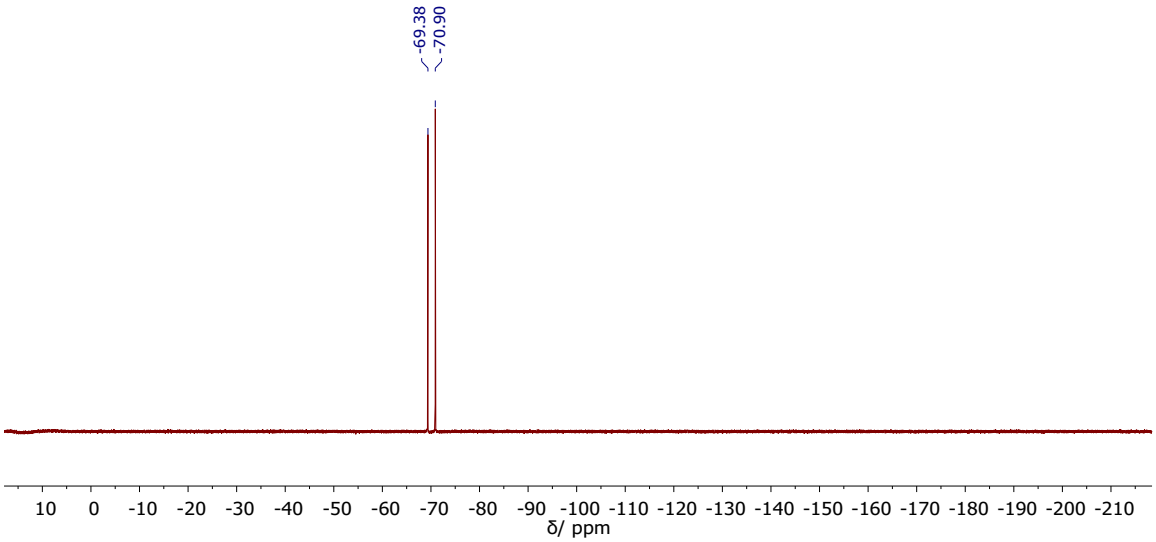

Figure S13. $^{19}F\{^{1}H\}$ NMR (471 MHz, DMSO-d_6, 298 K) spectrum of **2**.

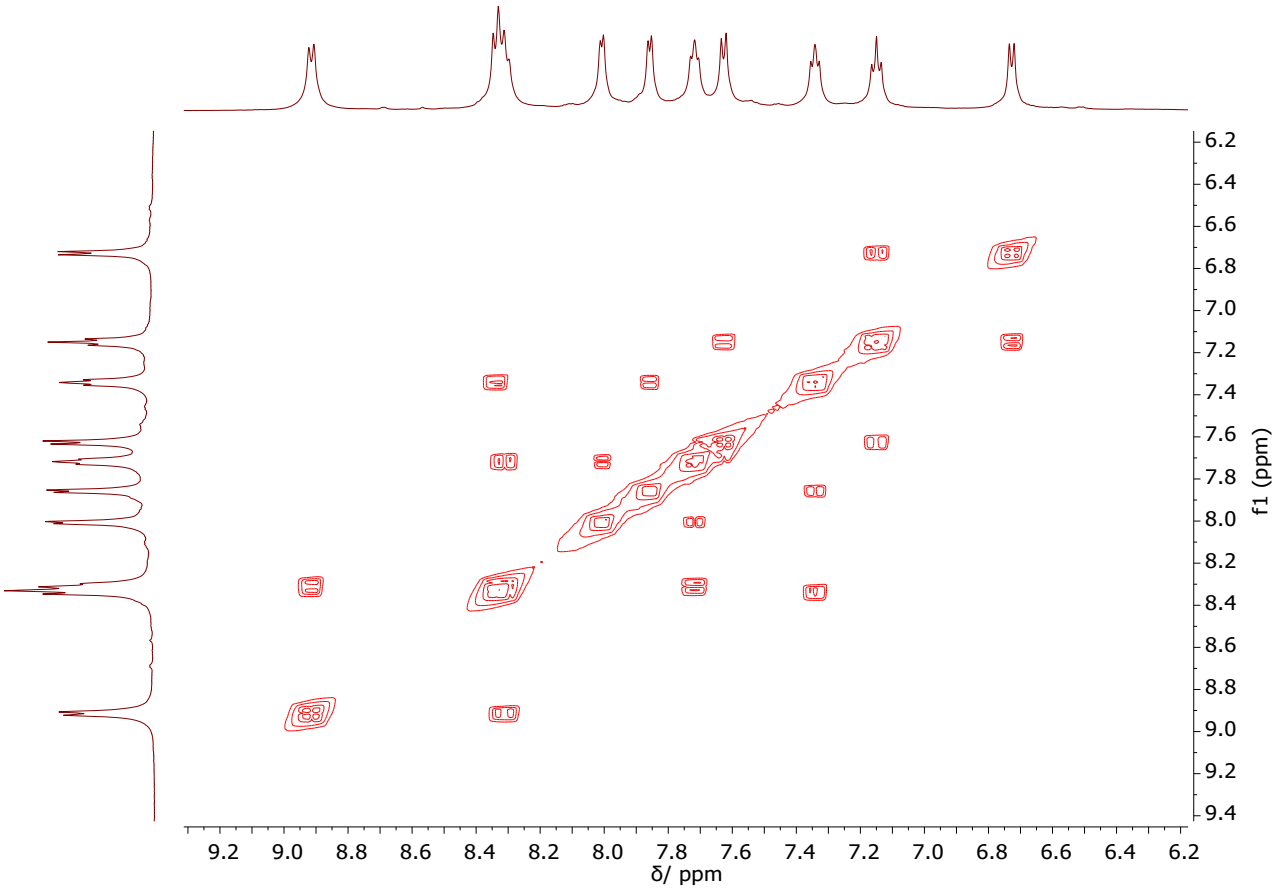

Figure S14. ^{1}H-^{1}H COSY (400 MHz, DMSO-d_6, 298 K) spectrum of **2** in the aromatic region.

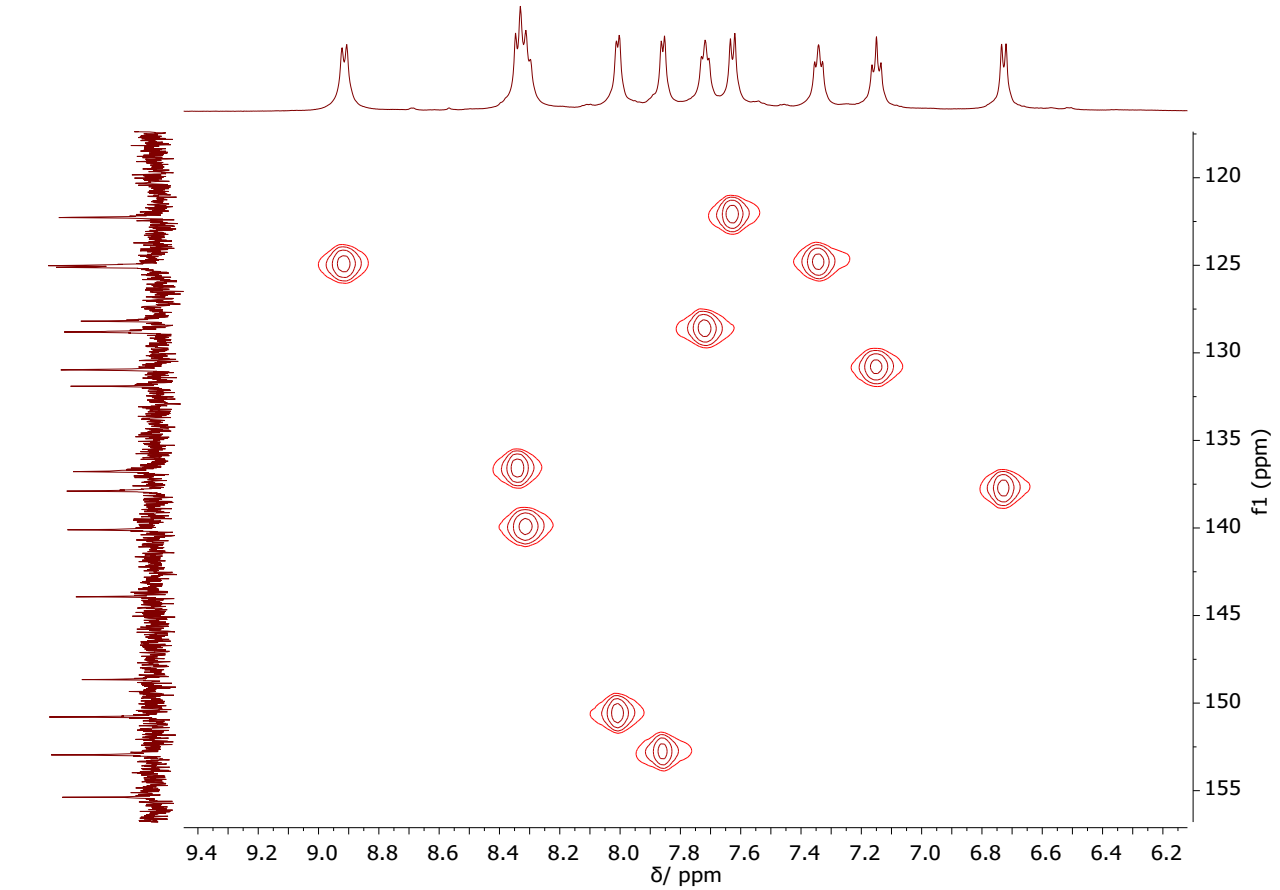

Figure S15. ^{1}H-^{13}C HSQC (DMSO-d_6, 298 K) spectrum of **2** in the aromatic region.

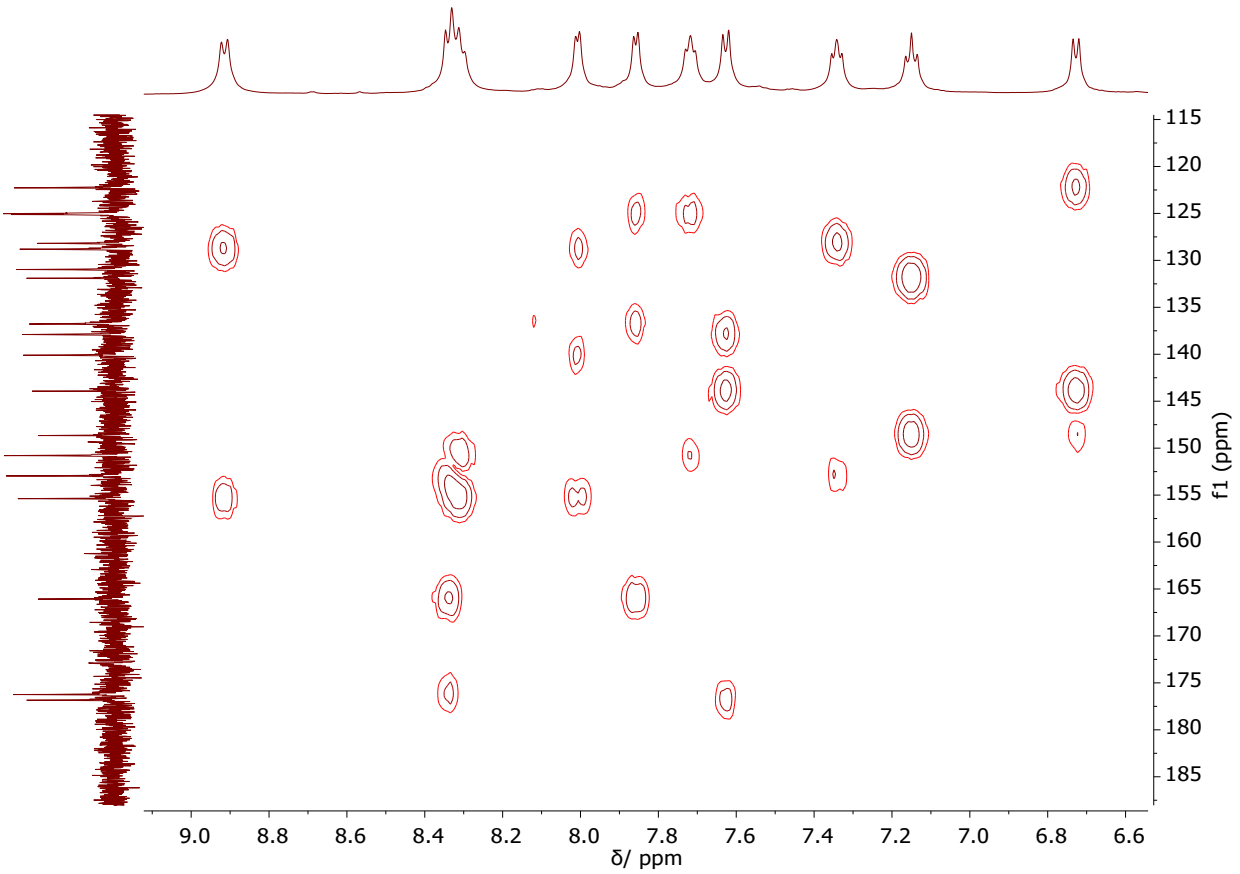

Figure S16. ^{1}H-^{13}C HMBC (DMSO-d_6, 298 K) spectrum of **2** in the aromatic region.

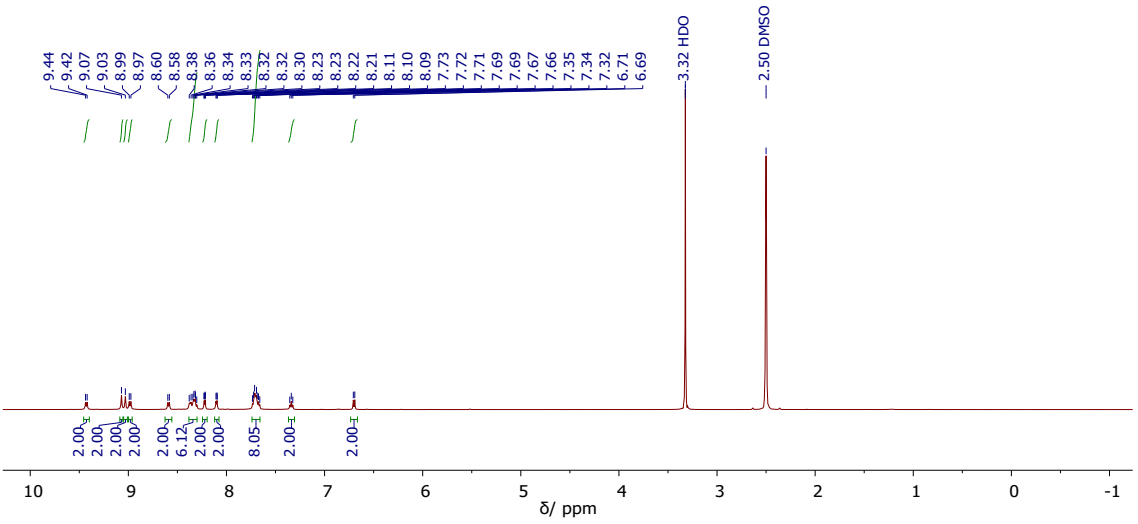

Figure S17. ^{1}H NMR (500 MHz, DMSO-d_6, 298 K) spectrum of **3**.

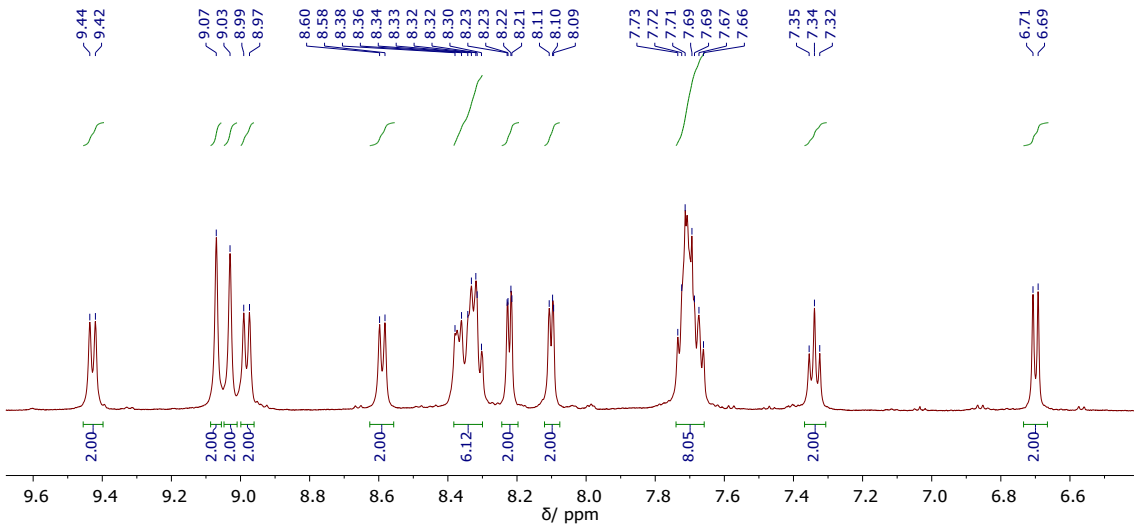

Figure S18. ^{1}H NMR (500 MHz, DMSO-d_6, 298 K) spectrum of **3** in the aromatic region.

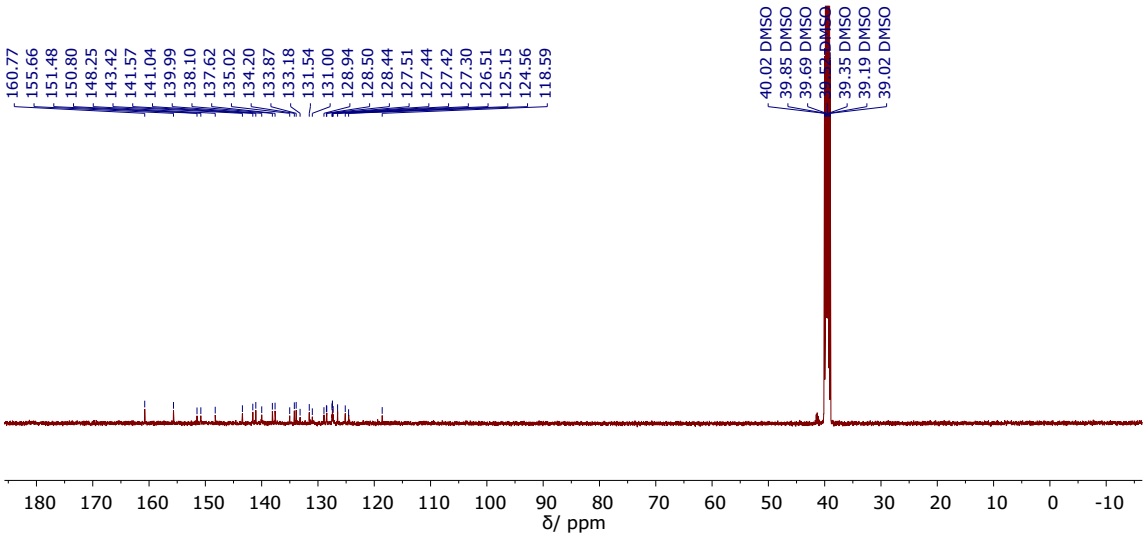

Figure S19. ^{13}C{^{1}H} NMR (126 MHz, DMSO-d_6, 298 K) spectrum of **3**.

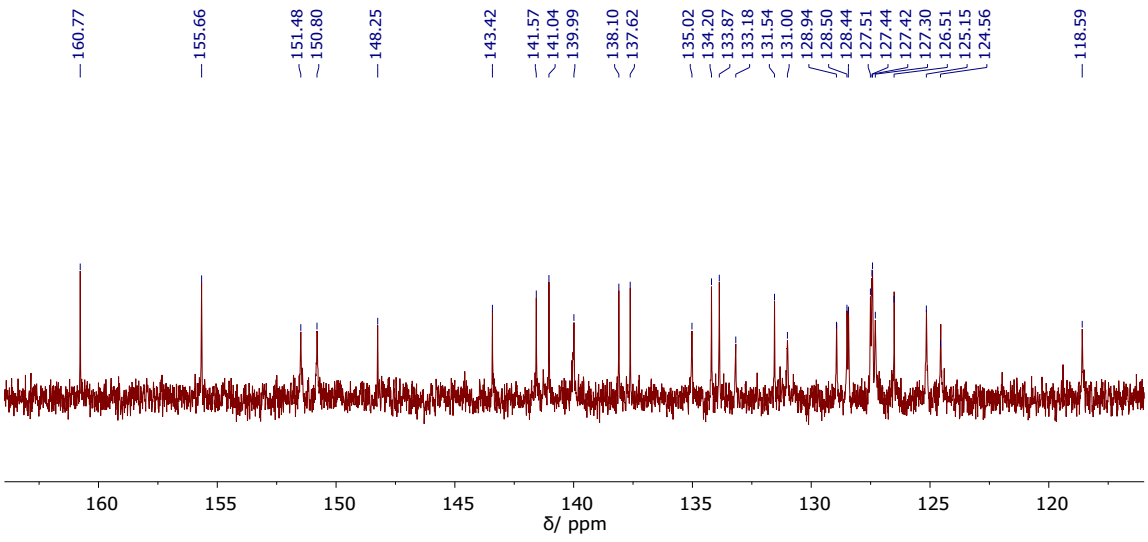

Figure S20. ^{13}C{^{1}H} NMR (126 MHz, DMSO-d_6, 298 K) spectrum of **3** in the aromatic region.

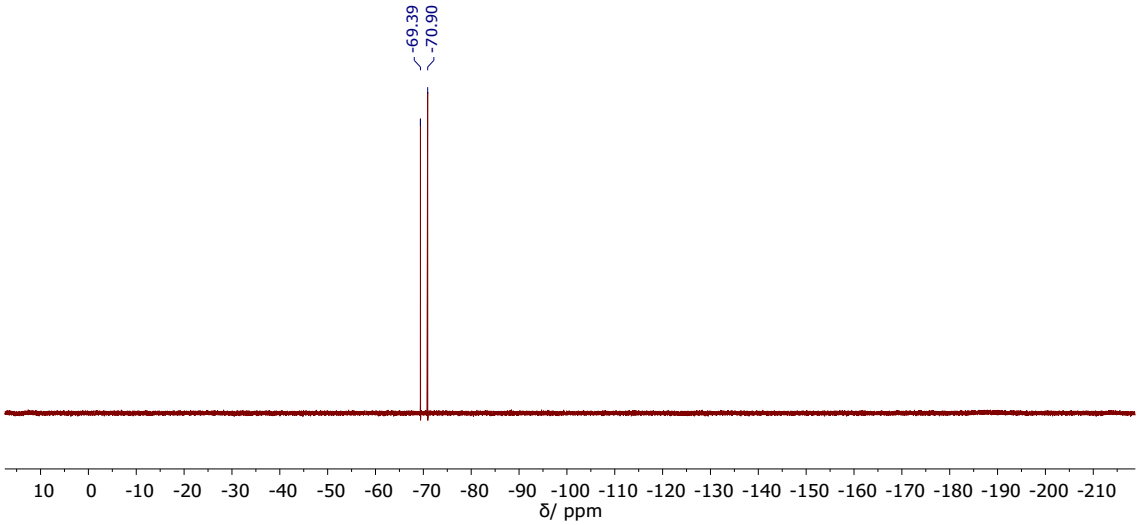

Figure S21. $^{19}F\{^{1}H\}$ NMR (471 MHz, DMSO-d_6, 298 K) spectrum of **3**.

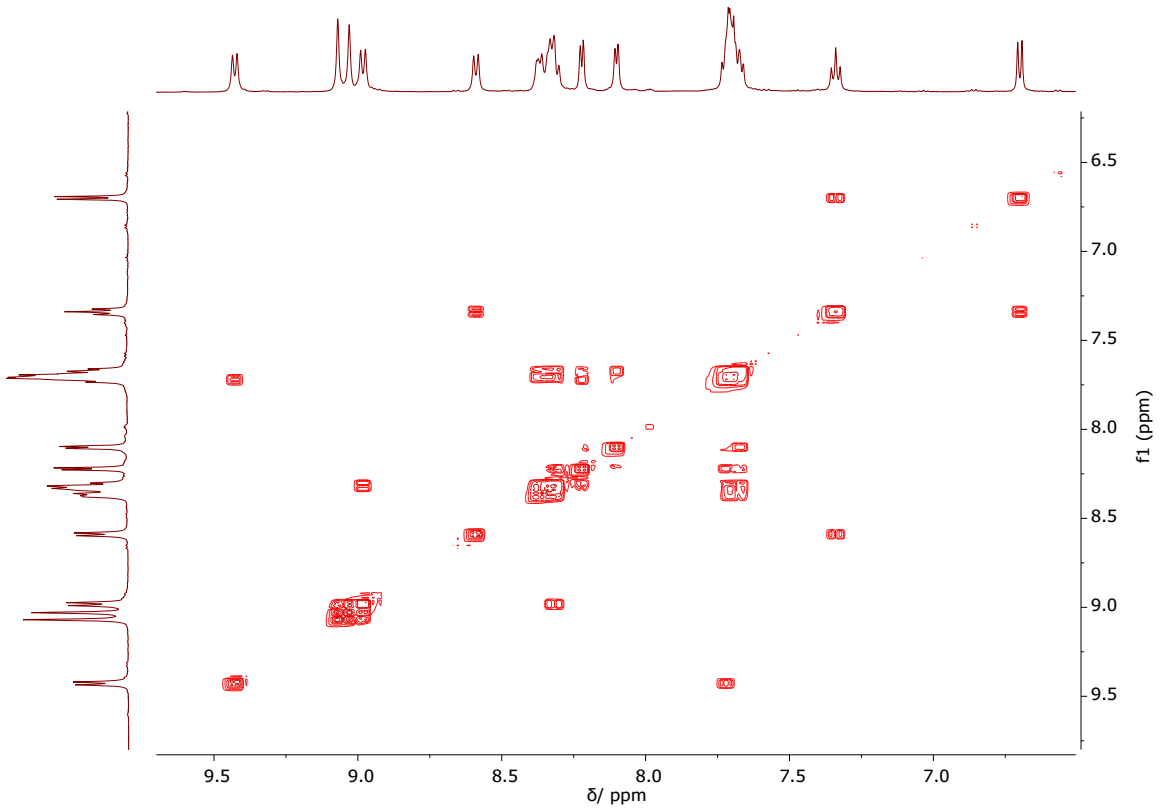

Figure S22. ^{1}H-^{1}H COSY (500 MHz, DMSO-d_6, 298 K) spectrum of **3** in the aromatic region.

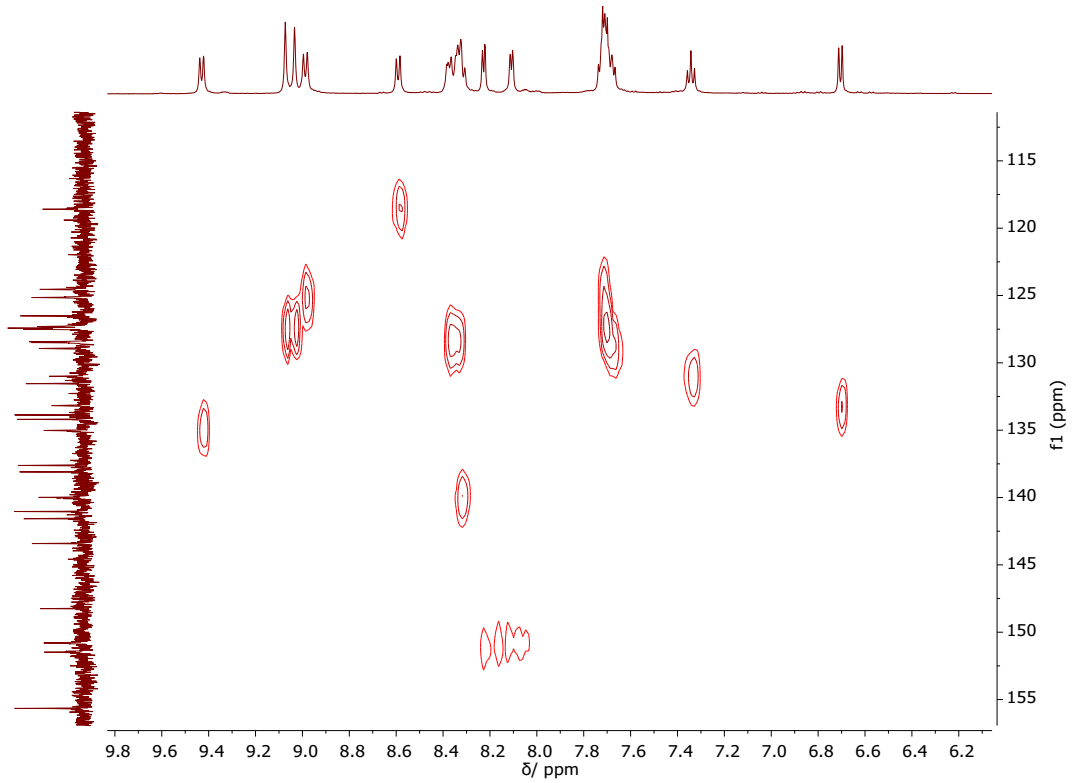

Figure S23. ^{1}H-^{13}C HSQC (DMSO-d_6, 298 K) spectrum of **3** in the aromatic region.

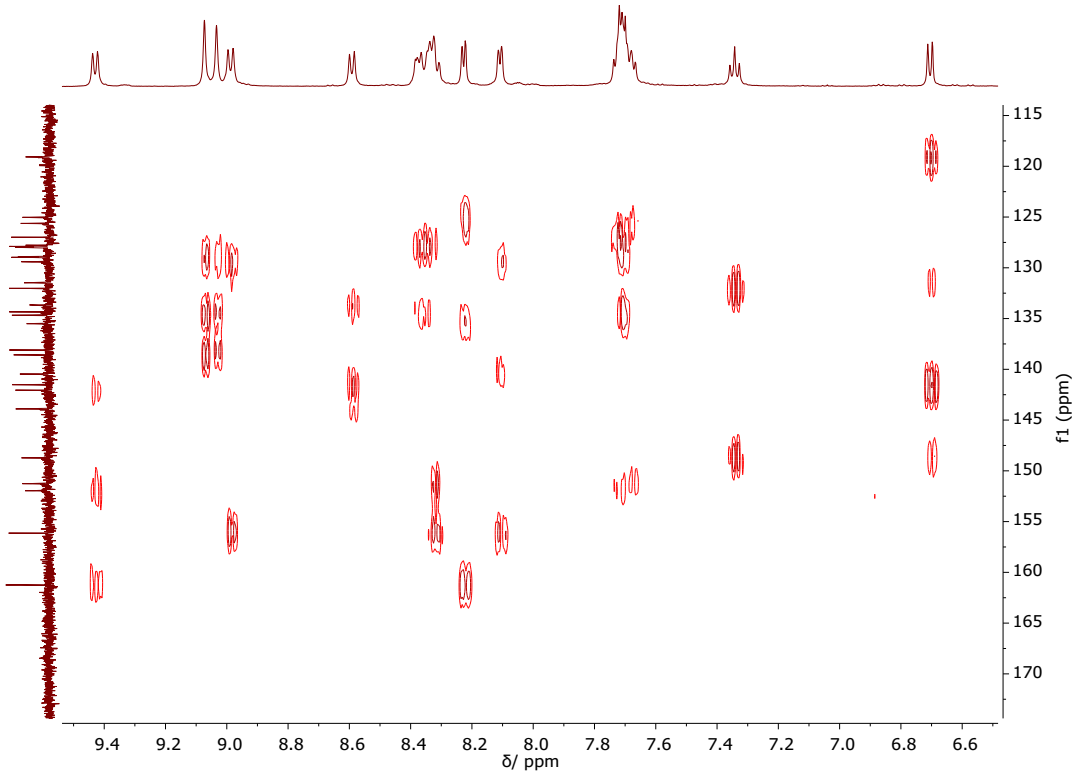

Figure S24. ^{1}H-^{13}C HMBC (DMSO-d_6, 298 K) spectrum of **3** in the aromatic region.

ESI-MS spectra

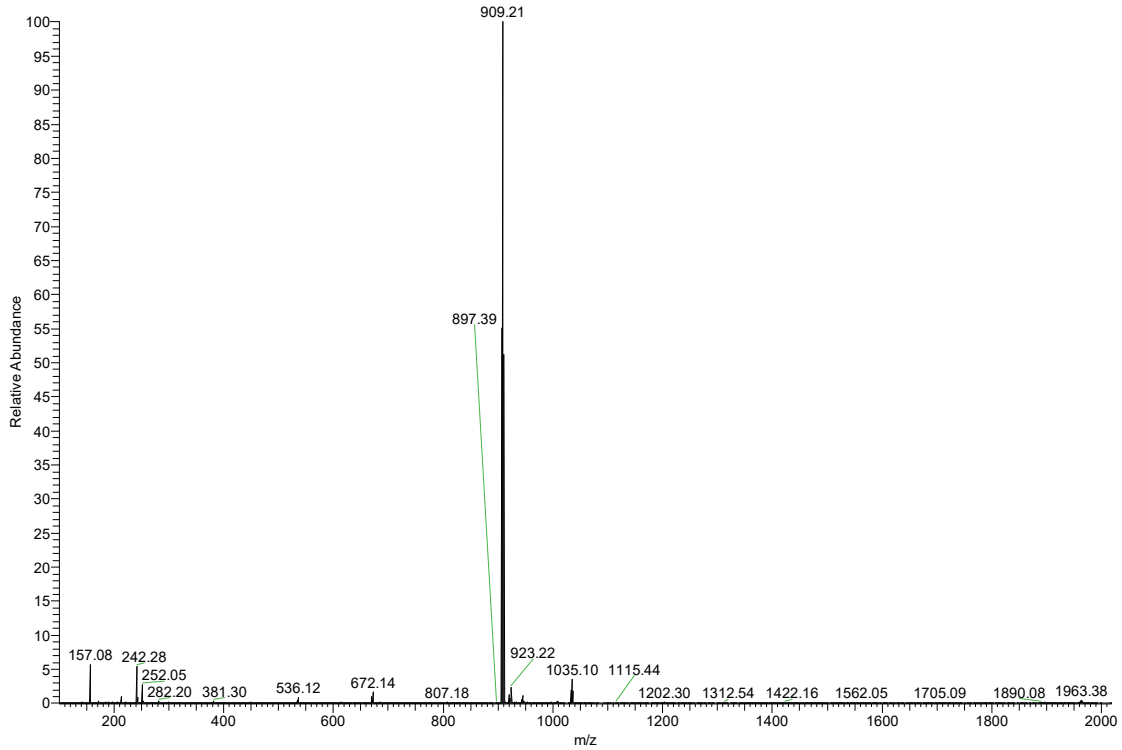

Figure S25. ESI+ mass of complex **1**.

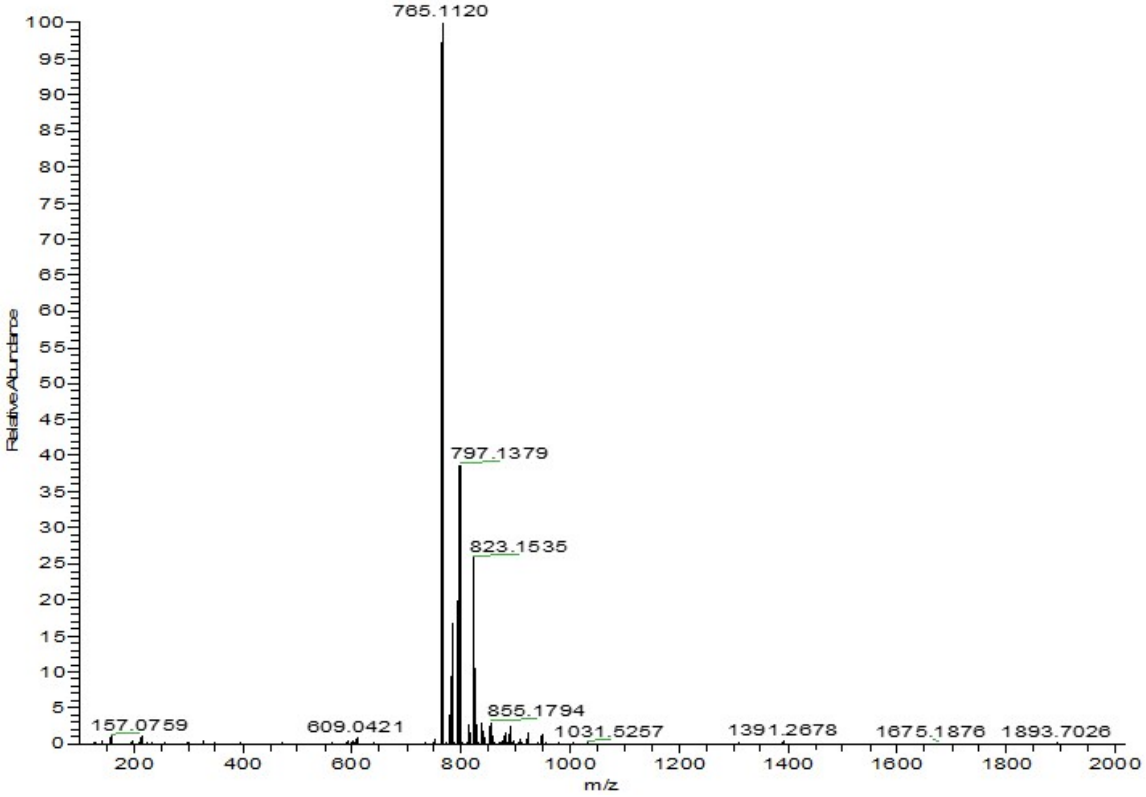

Figure S26. ESI+ mass of complex **2**.

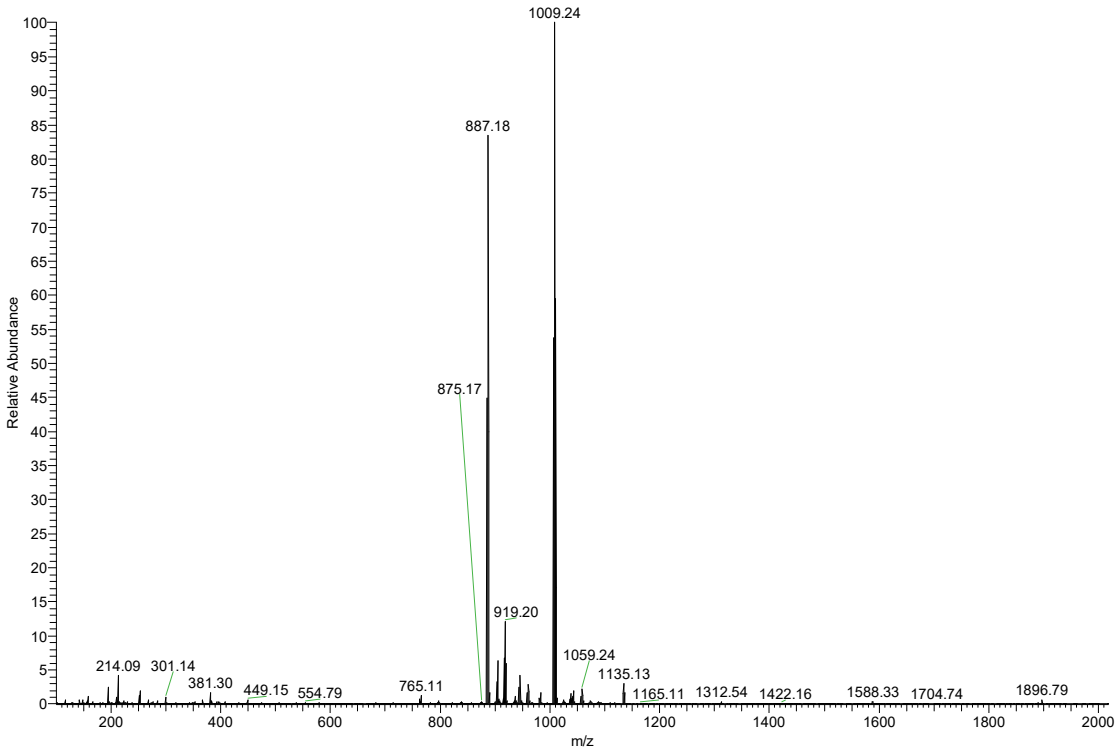

Figure S27. ESI+ mass of complex **3**.

HPLC traces

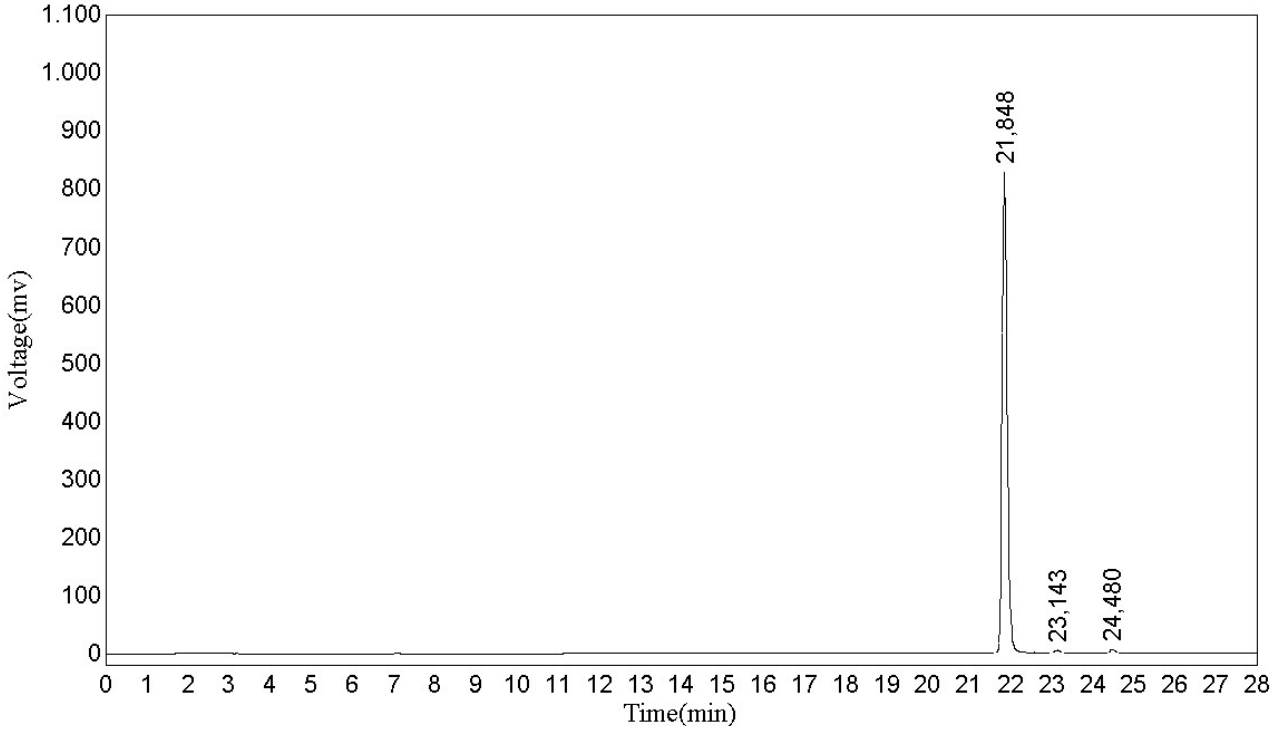

Figure S28. HPLC-UV chromatogram of complex **1**.

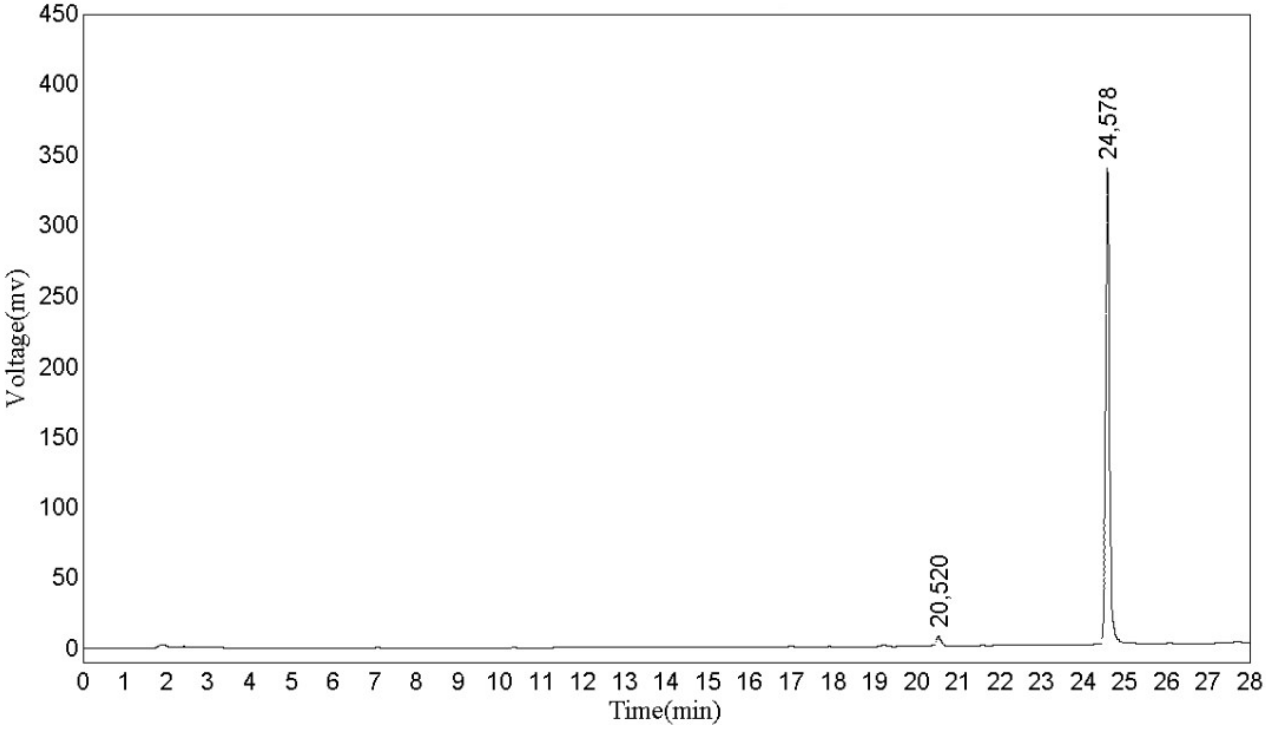

Figure S29. HPLC-UV chromatogram of complex **3**.

X-ray diffraction

Table S1. Selected bond distances (Å) and angles (°) for complexes **1**, **[2][OSO$_2$CF$_3$]** and **4**.

Comp.	C^N				N^N or Z		Bite angle (C-Ir-N)		Bite angle (N-Ir-N)
1	Ir(1)-C(17)	2.04(1)	Ir(1)-N(3)	2.06(1)	Ir(1)-N(1)	2.158(9)	C(36)-Ir(1)-N(6)	80.8(5)	75.8(4)
	Ir(1)-C(36)	2.02(2)	Ir(1)-N(6)	2.05(1)	Ir(1)-N(2)	2.17(1)	C(17)-Ir(1)-N(3)	81.0(5)	
[2][OSO$_2$CF$_3$]	Ir(1)-C(21)	2.06(2)	Ir(1)-N(3)	2.07(1)	Ir(1)-N(1)	2.15(2)	C(21)-Ir(1)-N(3)	80.6(7)	76.3(6)
	Ir(1)-C(34)	2.03(2)	Ir(1)-N(4)	2.05(1)	Ir(1)-N(2)	2.14(2)	C(34)-Ir(1)-N(4)	79.1(7)	
4	Ir(1)-C(10)	2.01(1)	Ir(1)-N(1)	2.05(1)	Ir(1)-Cl(1)	2.456(3)	C(10)-Ir(1)-N(1)	80.8(4)	-
	Ir(1)-C(23)	2.01(1)	Ir(1)-N(2)	2.035(9)	Ir(1)-S(1)	2.388(3)	C(23)-Ir(1)-N(2)	81.1(4)	

Table S2. Crystal data and structure refinement for complexes **1**, **[2][OSO_2CF_3]** and **4**.

	1	**2[OSO_2CF_3]**	**4**
Asymmetric unit	3($C_{48}H_{28}IrN_8$), 3(PF_6), 0.25(CH_2Cl_2), 0.25(C_2H_6O), H_2O	$C_{36}H_{20}IrN_4O_4$, CF_3SO_3, C_3H_6O	$C_{28}H_{18}ClIrN_2O_5S$, C_2H_6OS
Formula weight	3255.08	971.91	800.28
Temperature/K	100.15	100(2)	293(2)
Crystal system	Triclinic	Monoclinic	Monoclinic
Space group	Pī	$P2_1/c$	$P2_1/c$
a/Å	19.672(14)	8.853(16)	8.8665(19)
b/Å	20.536(12)	22.71(4)	14.973(3)
c/Å	21.434(15)	20.71(4)	20.940(5)
α/°	103.13(2)	90	90
β/°	105.29(2)	98.96(3)	91.731(3)
γ/°	113.322(19)	90	90
Volume/Å^3	7112(8)	4112(13)	2778.6(10)
Z	2	4	4
ρ_{calc}g/cm^3	1.520	1.570	1.913
μ/mm^{-1}	2.945	3.366	5.101
F(000)	3204.0	1912	1568.0
Crystal size/mm^3	0.23 × 0.13 × 0.04	0.09 × 0.05 × 0.02	0.08 × 0.06 × 0.03
Wavelength (Å)	0.71073	0.71073	0.71073
Index ranges	-23 ≤ h ≤ 23 -24 ≤ k ≤ 19 -25 ≤ l ≤ 25	-8 ≤ h ≤ 8 -20 ≤ k ≤ 20 -19 ≤ l ≤ 19	-10 ≤ h ≤ 10 -17 ≤ k ≤ 17 -19 ≤ l ≤ 24
Independent reflections	24178 [R_{int} = 0.1436]	3831 [R_{int} = 0.2042]	4805 [R_{int} = 0.0888]
Data/restraints/parameters	24178/2364/1958	3831 / 544 / 521	4805/0/383
Goodness-of-fit on F^2	1.004	0.935	1.029
Final R indexes [I≥2σ (I)]	R_1 = 0.0713 wR_2 = 0.1549	R_1 = 0.0700 wR_2 = 0.1664	R_1 = 0.0575 wR_2 = 0.0970
Largest diff. peak/hole, e Å^{-3}	1.28/-0.77	0.58/-0.68	0.93/-1.04

[a] $R = \Sigma||F_o|-|F_c||/\Sigma|F_o|$. [b] $wR = \{\Sigma w(F_o^2-F_c^2)^2/\Sigma w(F_o^2)^2\}^{1/2}$. [c] GOF = $\{\Sigma [w((F_o^2-F_c^2)^2)/(n-p)\}^{1/2}$, where n = number of reflections and p = total number of parameters refined.

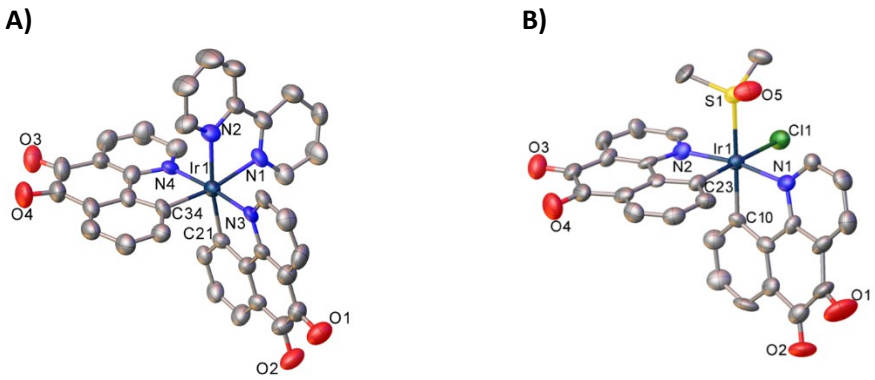

Figure S30. ORTEP diagram of cation of complex **Δ 2** (B) and **Δ 4** (C). Ellipsoids are at the 30% probability level. Hydrogen atoms and PF_6^- and $OSO_2CF_3^-$ anions have been omitted for clarity.

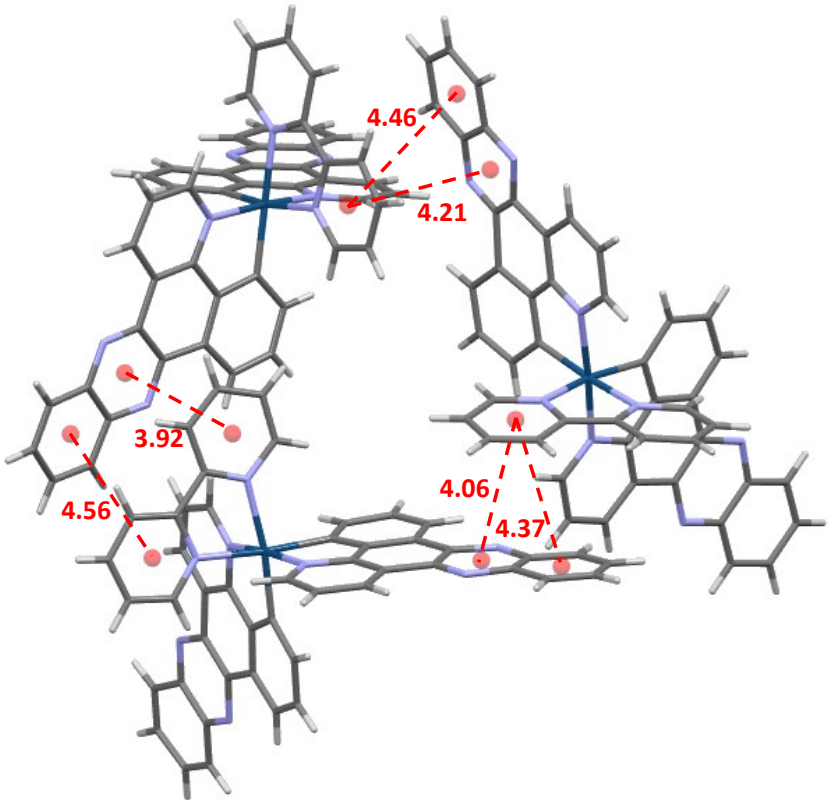

Figure S31. Trimer-Δ of complex **1** formed through π–π interactions (red, centroid–centroid distances indicated, Å).

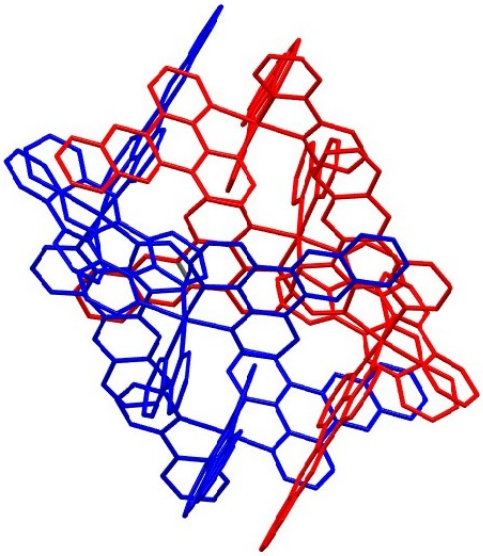

Figure S32. Complex **1**. Two trimers present in the unit cell, one coloured in blue (Δ enantiomers, trimer-Δ) and the other in red (Λ enantiomers, trimer-Λ), *c* axis perpendicular.

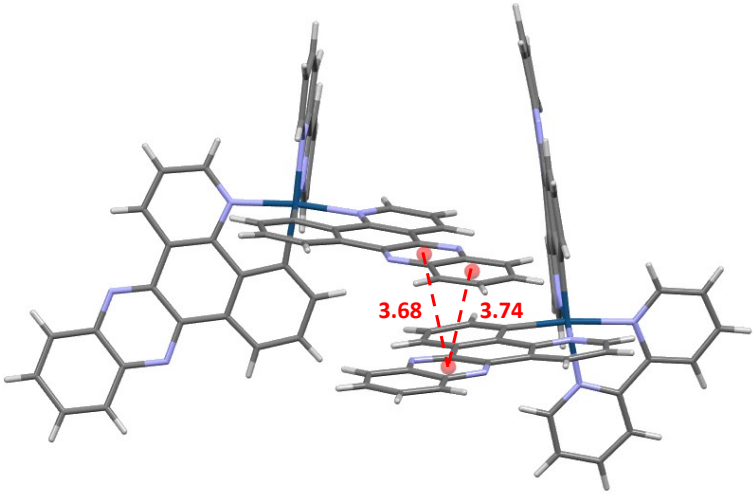

Figure S33. π–π interactions (red, centroid–centroid distances indicated, Å) between two pbpz ligands of two different molecules of **1**, one of trimer-Δ and the other of trimer-Λ.

Analysis of π-π stacking by ^{1}H NMR spectroscopy

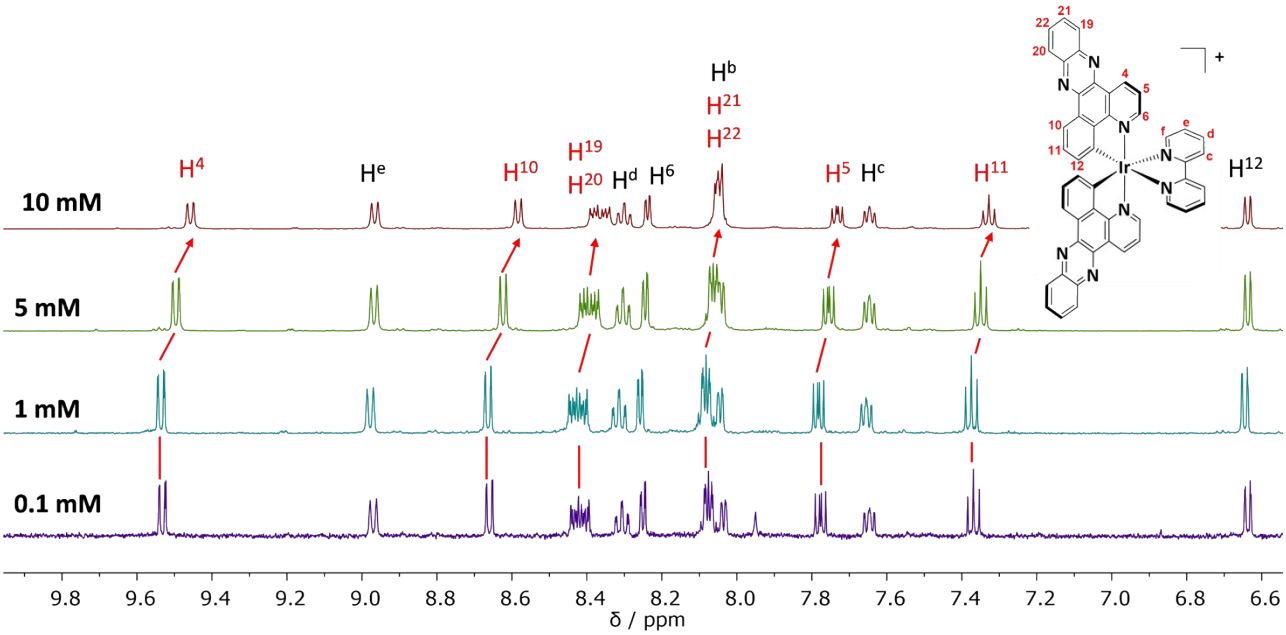

Figure S34. ^{1}H NMR spectra of **1** in DMSO-d_6 at different concentrations. The protons that suffer higher shifting to lower frequency when the concentration is increased are indicated in red and the arrows reflect this shifting.

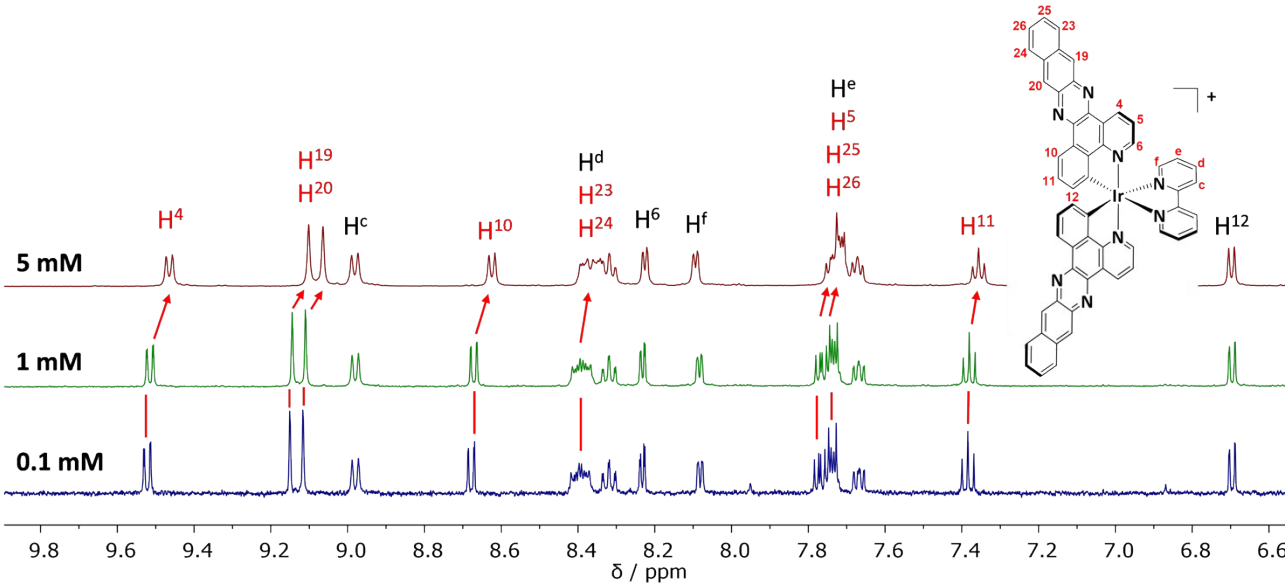

Figure S35. ^{1}H NMR spectra of **3** in DMSO-d_6 at different concentrations. The protons that suffer higher shifting to lower frequency when the concentration is increased are indicated in red and the arrows reflect this shifting.

Table S3. Effect of the concentration on the ^{1}H NMR resonances, $\Delta(\delta_{conc} - \delta_{dil})$, for **1** and **3** in DMSO-d_6 from 0.1 to 5 mM. [$\Delta\delta$] values ≥ 0.04 are marked in bold.

Comp. $\Delta\delta$ (ppm)	H^4	H^5	H^6	H^{12}	H^{11}	H^{10}	H^{19}/ H^{20}	H^{21}/ H^{22}	H^{23}/ H^{24}	H^{25}/ H^{26}
1	**-0.04**	-0.02	-0.01	0.00	-0.02	**-0.04**	**-0.04**	-0.03	--	--

3	**-0.06**	**-0.05**	0.00	0.00	-0.03	**-0.06**	**-0.05**	--	**-0.04**	-0.03

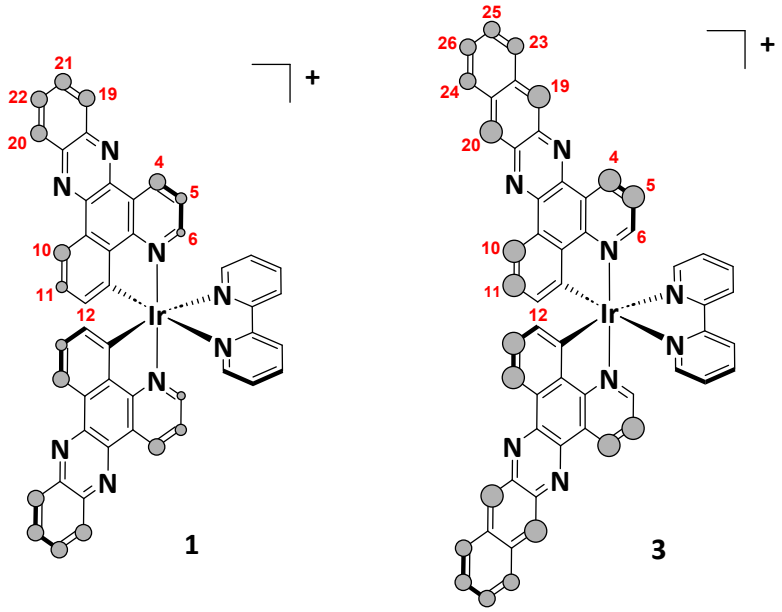

Figure S36. Concentration effect on the protons of complexes **1** and **3** in DMSO-d_6. The size of the circles shows how much the chemical shift of the proton varies. The greater the variation of the chemical shift, the larger the circle.

Stability and photostability.

^{1}H NMR.

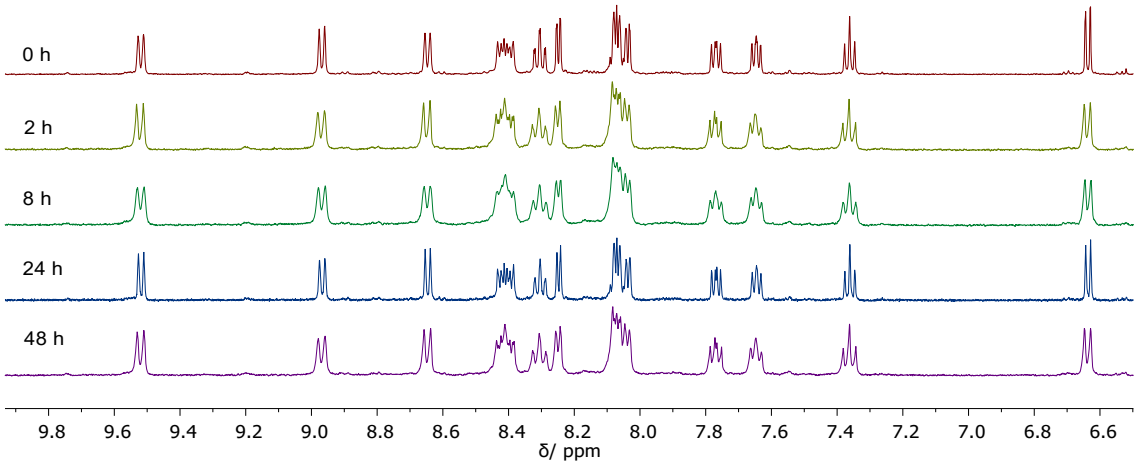

Figure S37. ^{1}H NMR of complex **1** in DMSO-d_6 at different times in the dark.

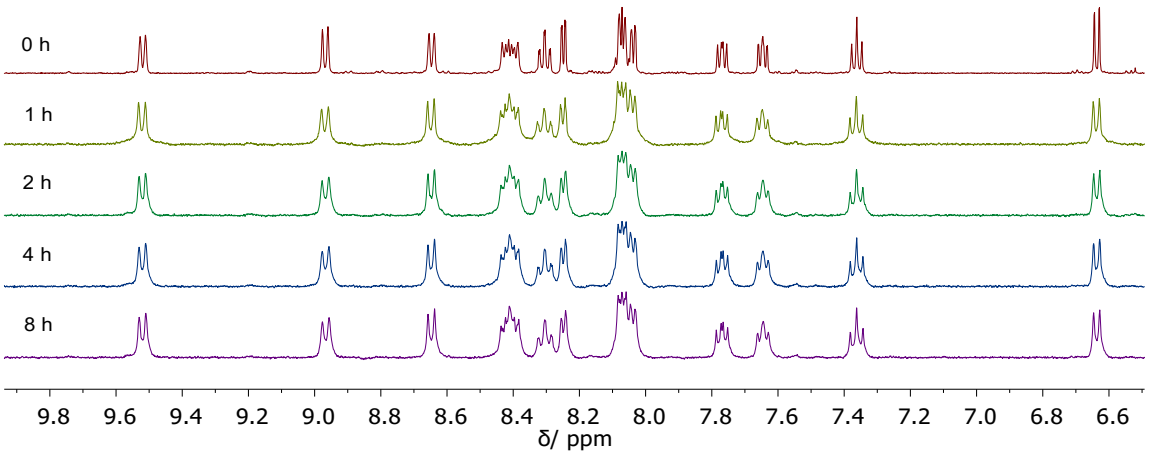

Figure S38. ^{1}H NMR of complex **1** in DMSO-d_6 at different times under blue light irradiation (470 nm, 51.4 mW cm^{-2}).

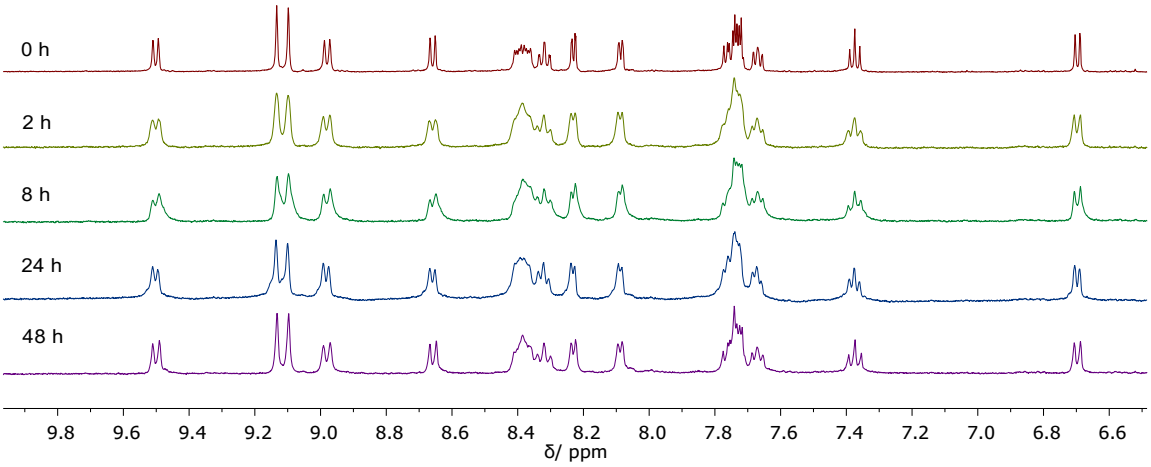

Figure S39. ^{1}H NMR of complex **3** in DMSO-d_6 at different times in the dark.

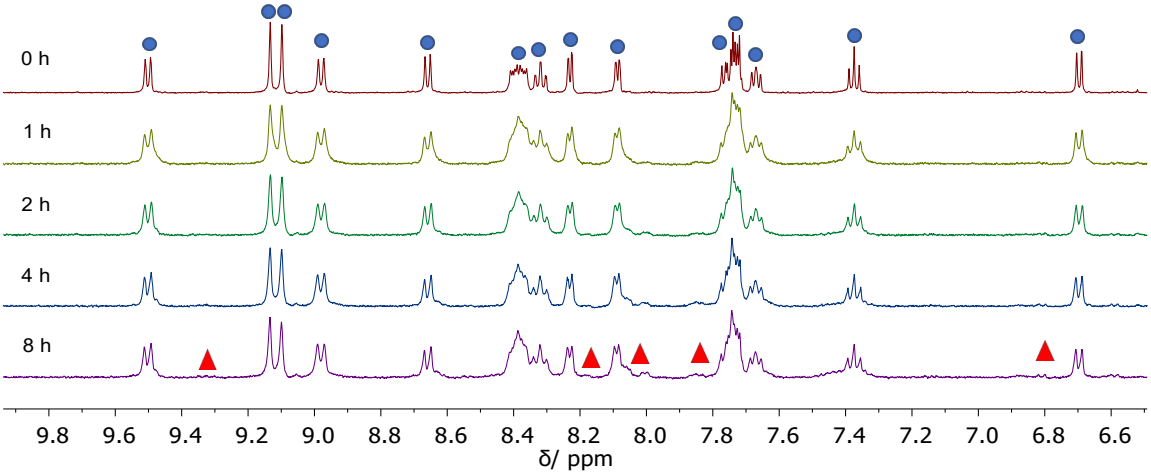

Figure S40. ^{1}H NMR of complex **3** in DMSO-d_6 at different times under blue light irradiation (470 nm, 51.4 mW cm^{-2}). Blue signals (•) correspond to complex **3**. Red triangles correspond to the photodegradation

product (▲).

Table S4. Photoevolution (%) of complexes **1** and **3** in DMSO-d_6.

	Photoevolution (%)			
	1		3	
Time (h)	Dark	470 nm	Dark	470 nm
0	0	0	0	0
1	0	0	0	0
2	0	0	0	4
4	0	0	0	6
8	0	0	0	11
24	0	-	0	-
48	0	-	0	-

UV-vis spectroscopy.

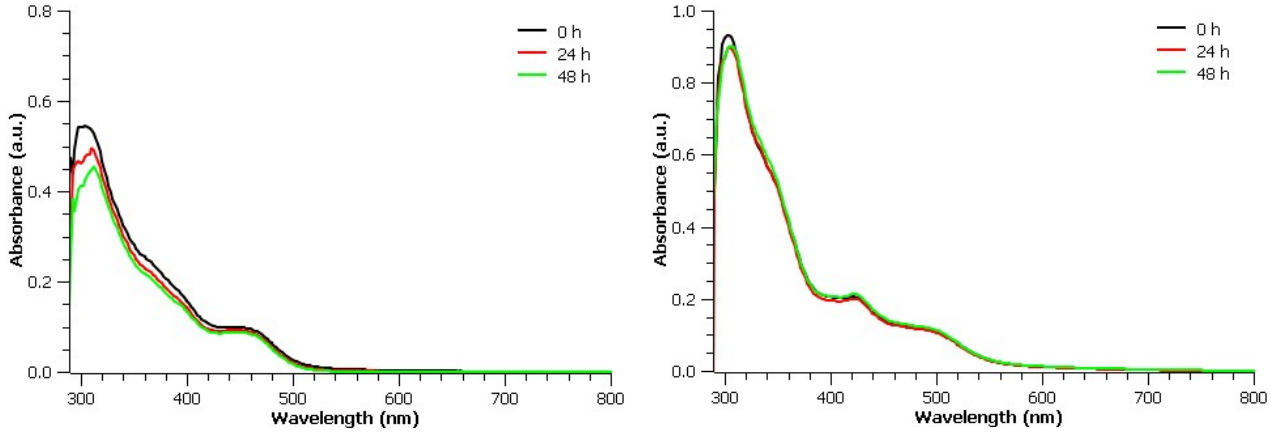

Figure S41. UV-vis spectra of complexes **1** (left) and **3** (right) in DMEM (1% DMSO) at different times at 1.0 × 10^{-5} M in the dark.

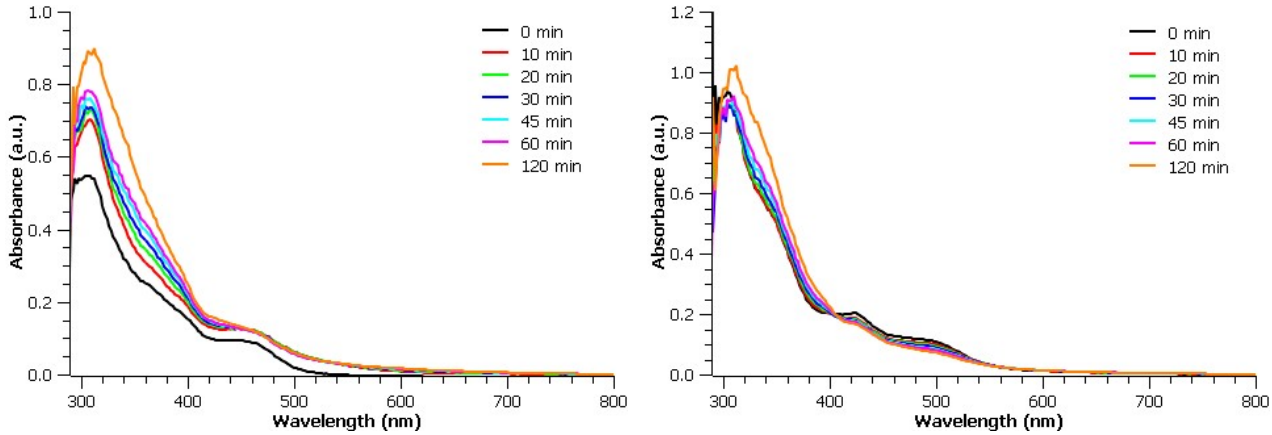

Figure S42. UV-vis spectra of complexes **1** (left) and **3** (right) in DMEM (1% DMSO) at different times under blue light irradiation (470 nm, 51.4 mW cm^{-2}) at 1.0 × 10^{-5} M.

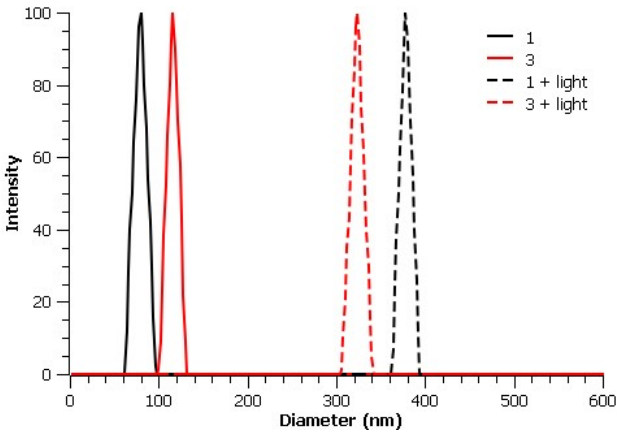

Figure S43. DLS of complexes **1** and **3** in water (10% DMSO) before and after 1 h of blue light irradiation (470 nm, 51.4 mW cm^{-2}).

Photophysical properties

Table S5. Molar extinction coefficients (ε) of the UV-vis bands and emission and excitation wavelengths of complexes **1** and **3** at 1.0×10^{-5} M in degassed acetonitrile and aerated water (1% DMSO).

Compound	λ / nm (ε / M^{-1} cm^{-1})		λ_{em} (λ_{exc}) /nm	
	MeCN	Water (1% DMSO)	MeCN	Water (1% DMSO)
1	272 (159000), 302 (65000), 358 (28000), 390 (20000), 438 (12000)	266 (85000), 302 (44000), 400 (12000), 470 (5700)	596 (440)	632 (470)
3	246 (82000), 300 (132000), 320 (87000), 340 (71000), 394 (22000), 414 (25000), 478 (15000)	246 (78000), 300 (77000), 336 (44000), 422 (14000), 502 (7000)	550 (420)	576 (422)

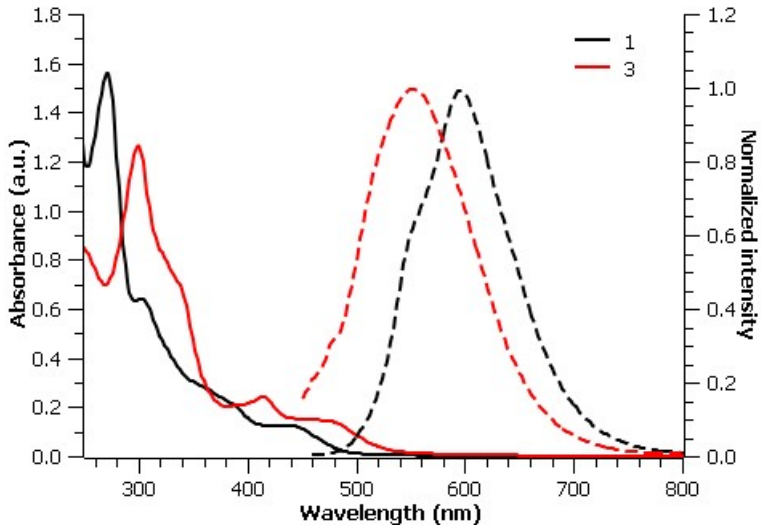

Figure S44. UV-vis absorption and emission spectra of complexes **1** and **3** in degassed acetonitrile.

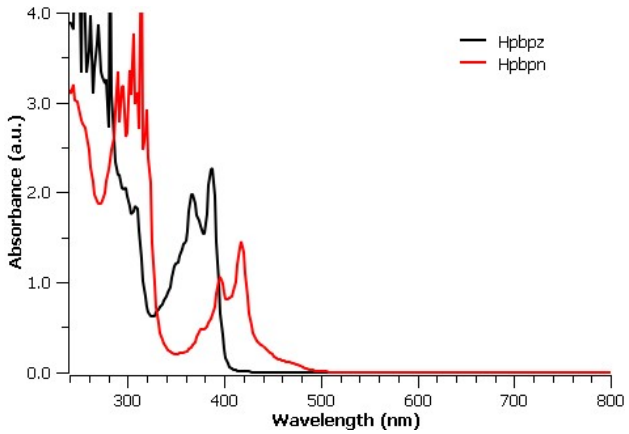

Figure S45. UV-vis absorption spectra of Hpbpz and Hpbpn in degassed acetonitrile (1.0×10^{-5} M).

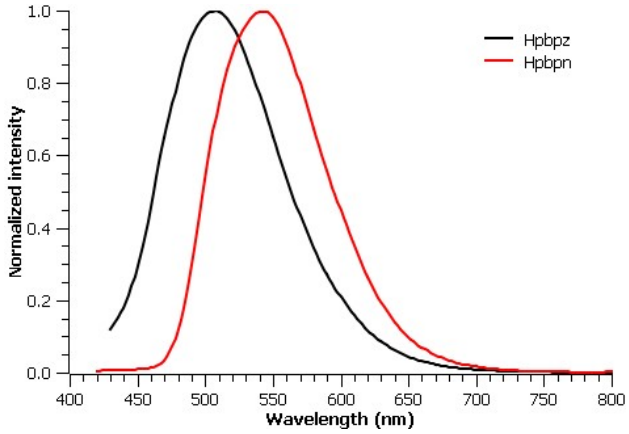

Figure S46. Normalized emission spectra of Hpbpz and Hpbpn in degassed acetonitrile (1.0×10^{-5} M).

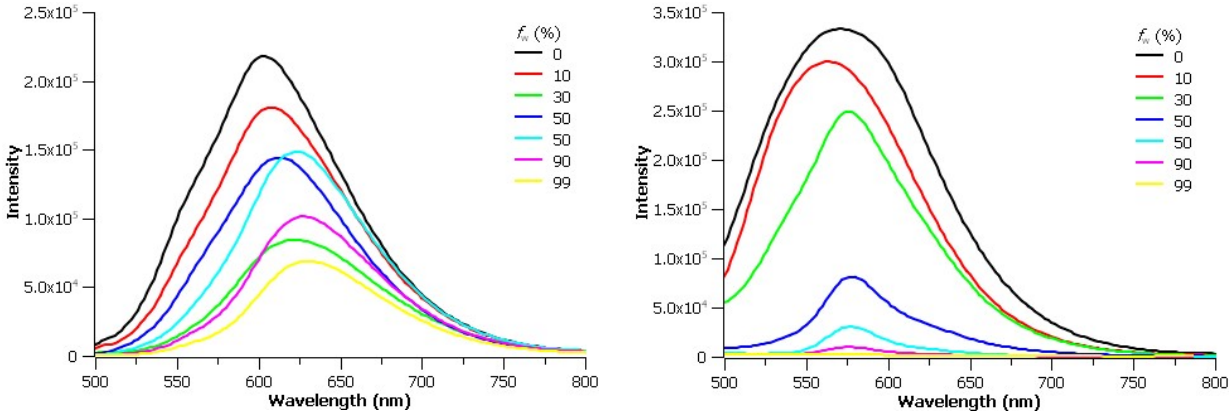

Figure S47. Emission spectra of complexes **1** (left) and **3** (right) in H_2O:DMSO mixtures with different water fractions (f_w) at 1.0×10^{-5} M.

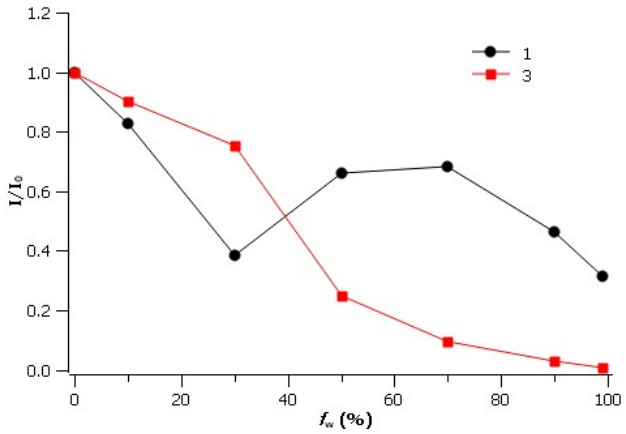

Figure S48. Representation of I/I_0 vs. water fraction (f_w) for **1** and **3**. I_0 corresponds to the emission intensity of the solution in 100% DMSO.

Emission lifetime measurements.

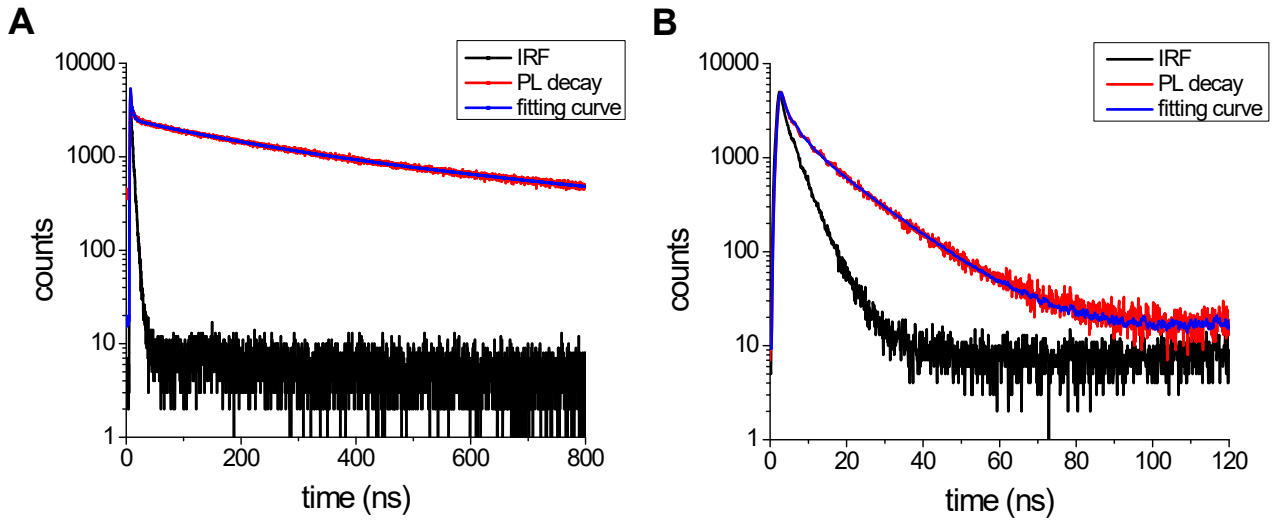

Figure S49. Photoluminescence decay curves of complexes **1** (**A**) and **3** (**B**) in acetonitrile (λ_{exc} = 370 nm). Corresponding instrument response curves are shown in black.

Transient Absorption Spectroscopy (TAS) measurements.

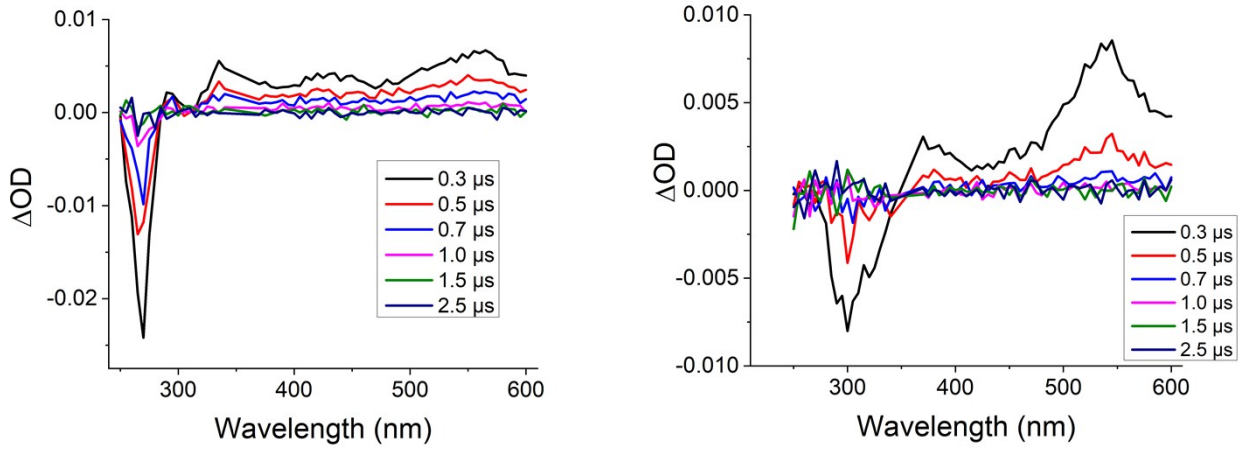

Figure S50. Transient absorption spectra for complexes **1** (left) and **3** (right) in acetonitrile (λ_{exc} = 355 nm).

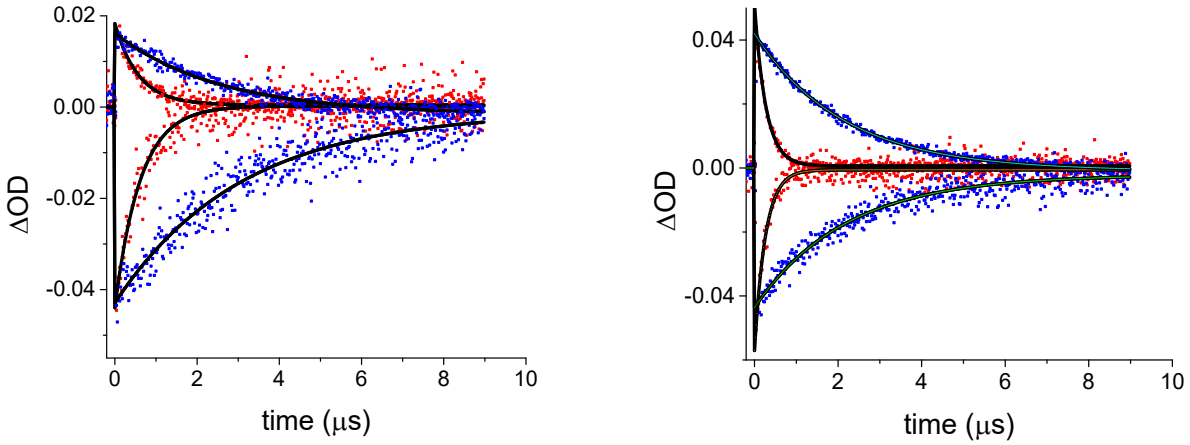

Figure S51. Transients of **1** (left) and **3** (right) at selected wavelengths corresponding to ground state bleaching (270 nm for **1**; 300 nm for **3**) and excited state absorption (560 nm for **1**; 545 nm for **3**), in aerated (red) and degassed (blue) conditions. Black lines represent the best fit for each transient.

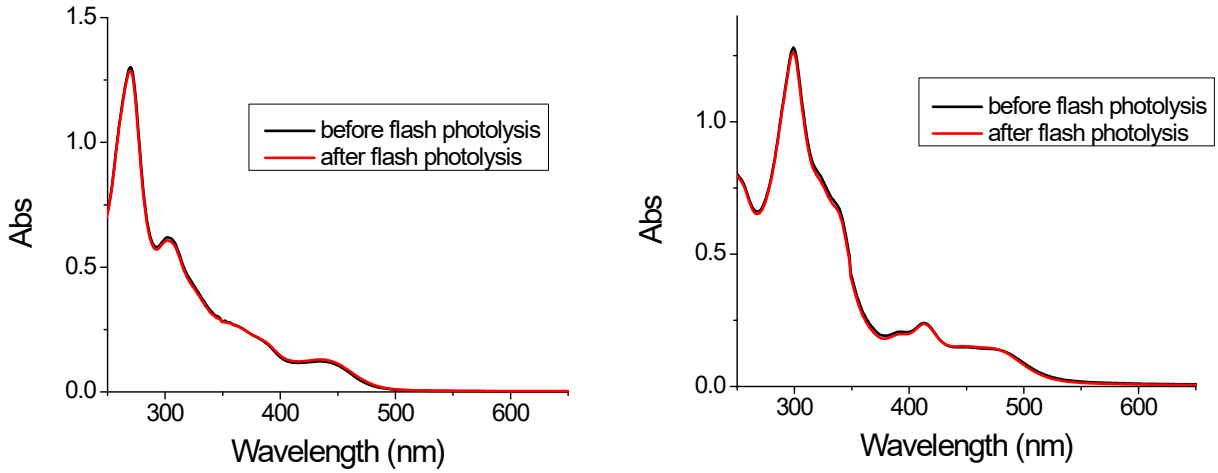

Figure S52. UV-vis absorption spectra of **1** (left) and **3** (right) before (black) and after (red) laser flash photolysis experiments, in acetonitrile.

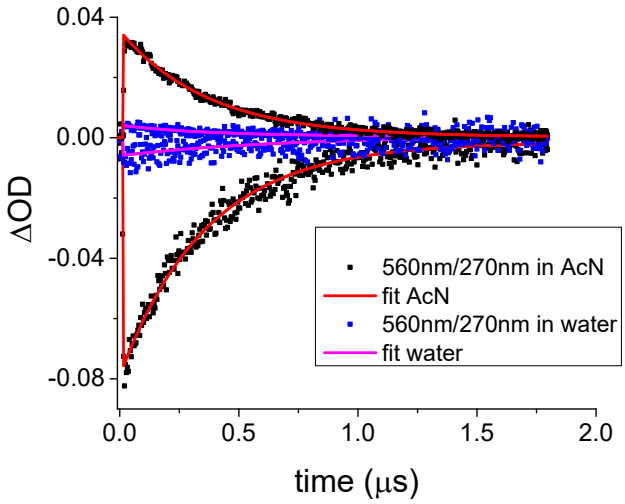

Figure S53. Transients at selected wavelengths (points) and corresponding single-exponential fitting curve (lines) for **1**, in water (1% DMSO) and acetonitrile. Absorbance of both solutions was matched at 355 nm.

ROS Generation

Triplet state quenching.

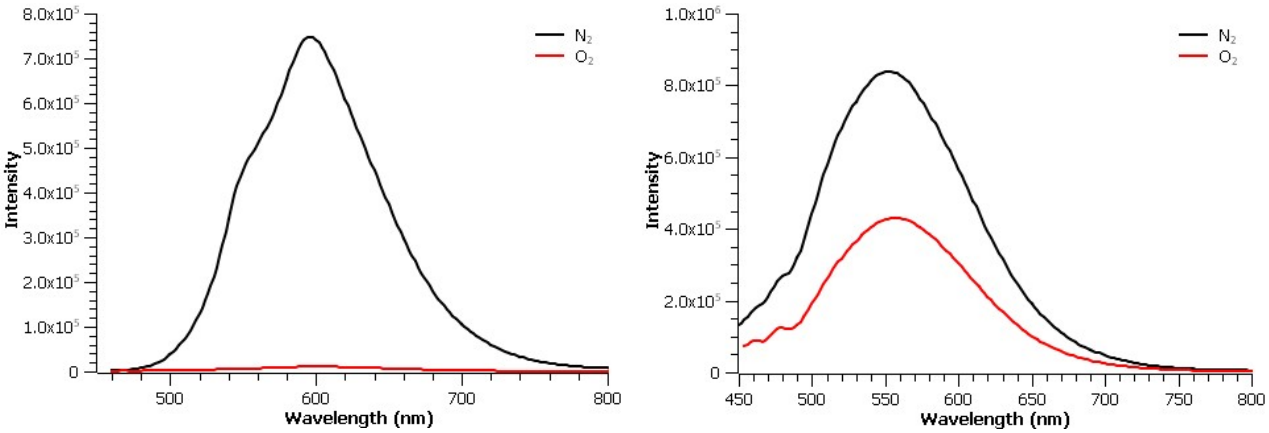

Figure S54. Triplet state quenching by O_2 bubbling for **1** (left) and **3** (right) in acetonitrile at 1.0×10^{-5} M.

Singlet oxygen ($^1O_2$) generation.

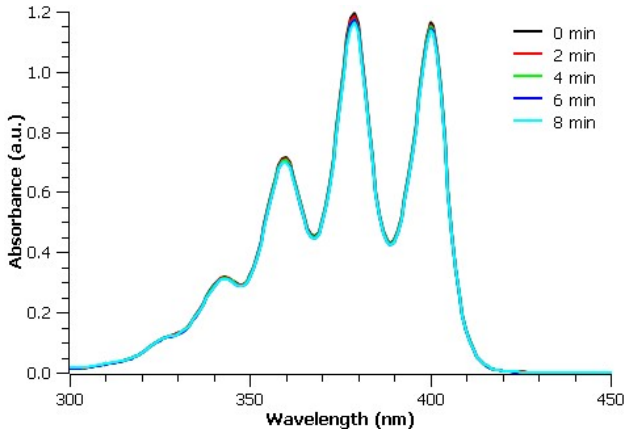

Figure S55. Evolution of the UV-vis spectra of ABDA without photosensitizer under blue light irradiation in water (10% DMSO).

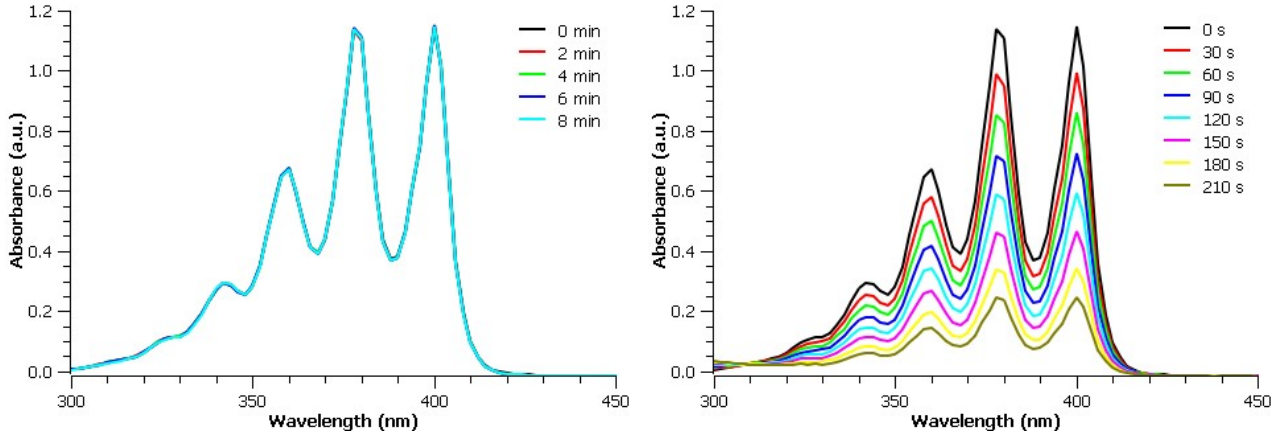

Figure S56. Evolution of the UV-vis spectra of ABDA in the presence of complex **1** in dark (left) and under blue light irradiation (right) in water (10% DMSO). The peaks at 400, 378 and 360 nm (characteristics of ABDA) decreased steadily with time.

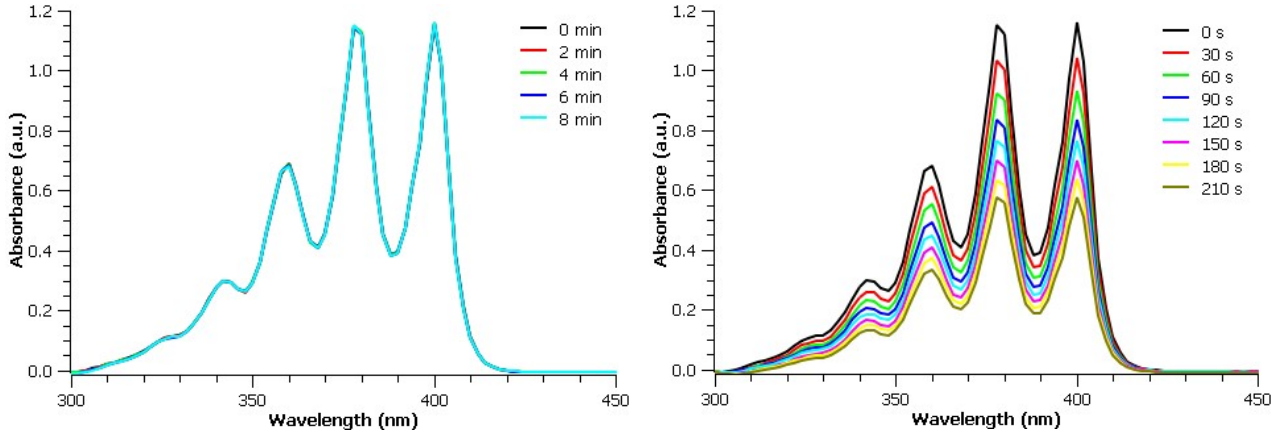

Figure S57. Evolution of the UV-vis spectra of ABDA in the presence of complex **3** in dark (left) and under blue light irradiation (right) in water (10% DMSO). The peaks at 400, 378 and 360 nm (characteristics of ABDA) decreased steadily with time.

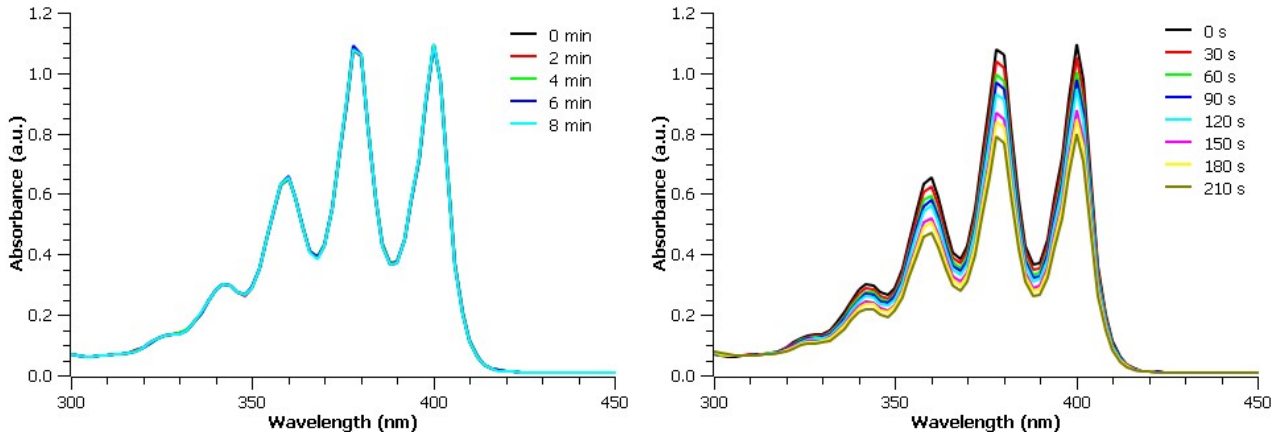

Figure S58. Evolution of the UV-vis spectra of ABDA in the presence of complex $[Ru(bpy)_3]^{2+}$ in dark (left) and under blue light irradiation (right) in water (10% DMSO). The peaks at 400, 378 and 360 nm (characteristics of ABDA) decreased steadily with time.

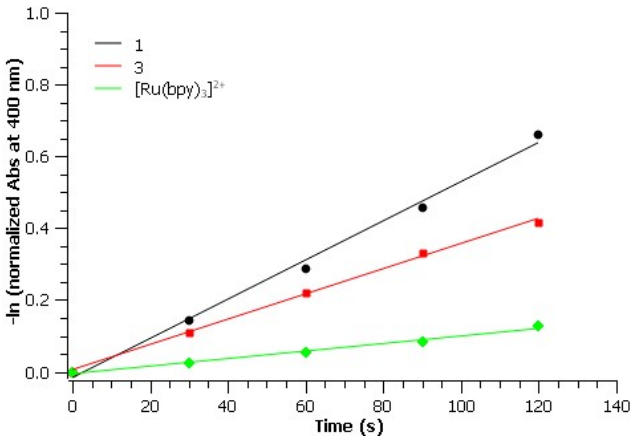

Figure S59. Comparative plots of -ln(normalized Abs at 400 nm) as a function of time for the experiment of photooxidation of ABDA in the presence of complexes **1**, **3** and $[Ru(bpy)_3]^{2+}$ under blue light irradiation.

Superoxide anion radical ($O_2^{\bullet-}$) generation.

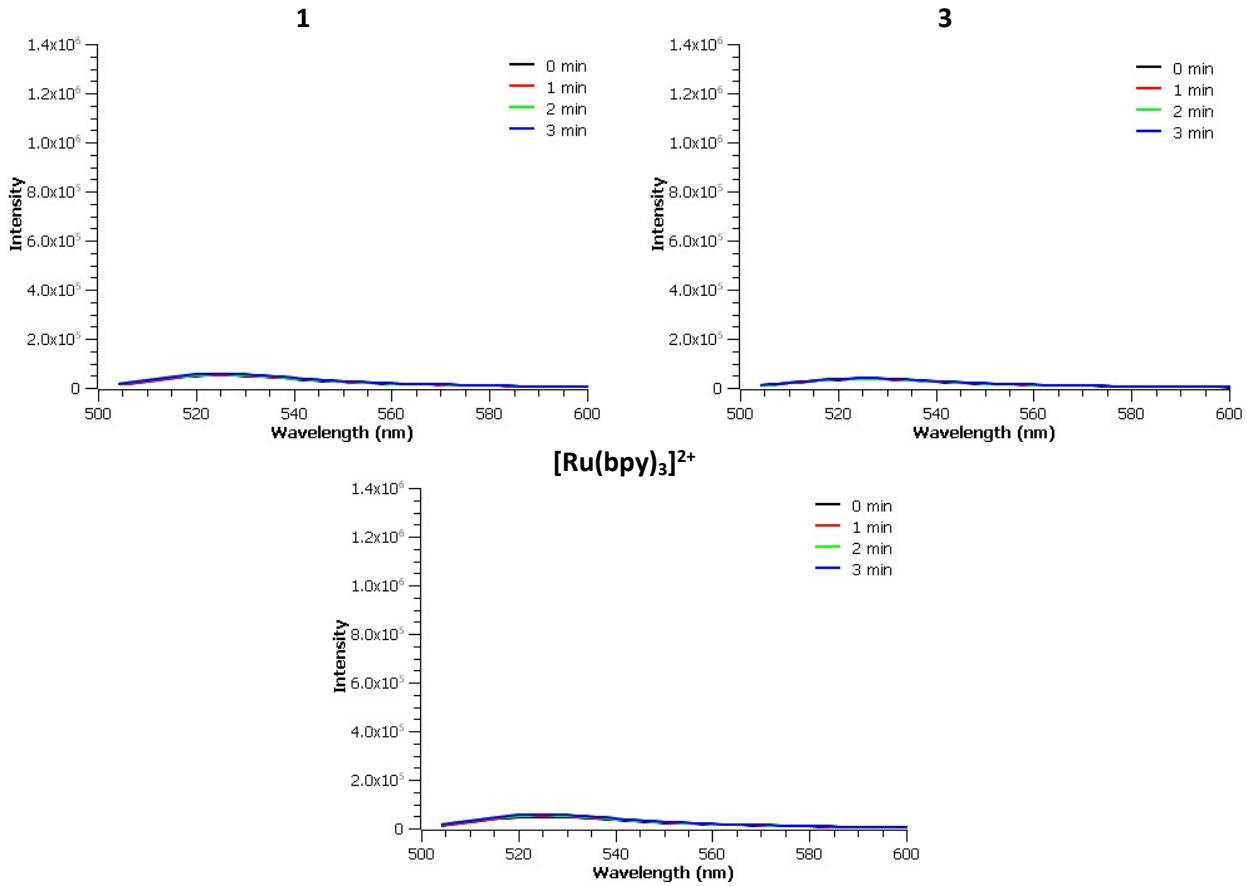

Figure S60. Evolution of the fluorescence emission spectra of DHR123 in dark conditions with **1**, **3** and $[Ru(bpy)_3]^{2+}$ in water (0.2% DMSO).

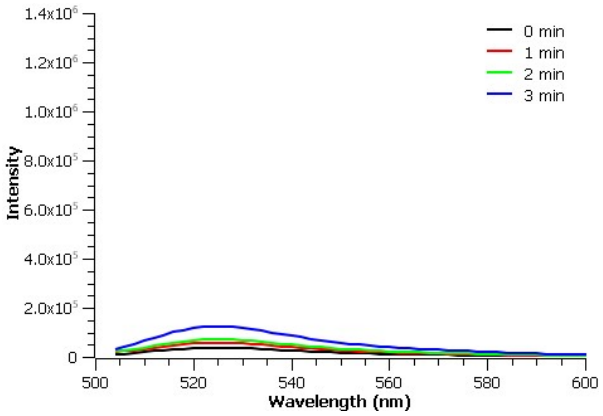

Figure S61. Evolution of the fluorescence emission spectra of DHR123 upon blue light irradiation (470 nm, 51.4 mW cm^{-2}) without any photosensitizer in water (0.2% DMSO).

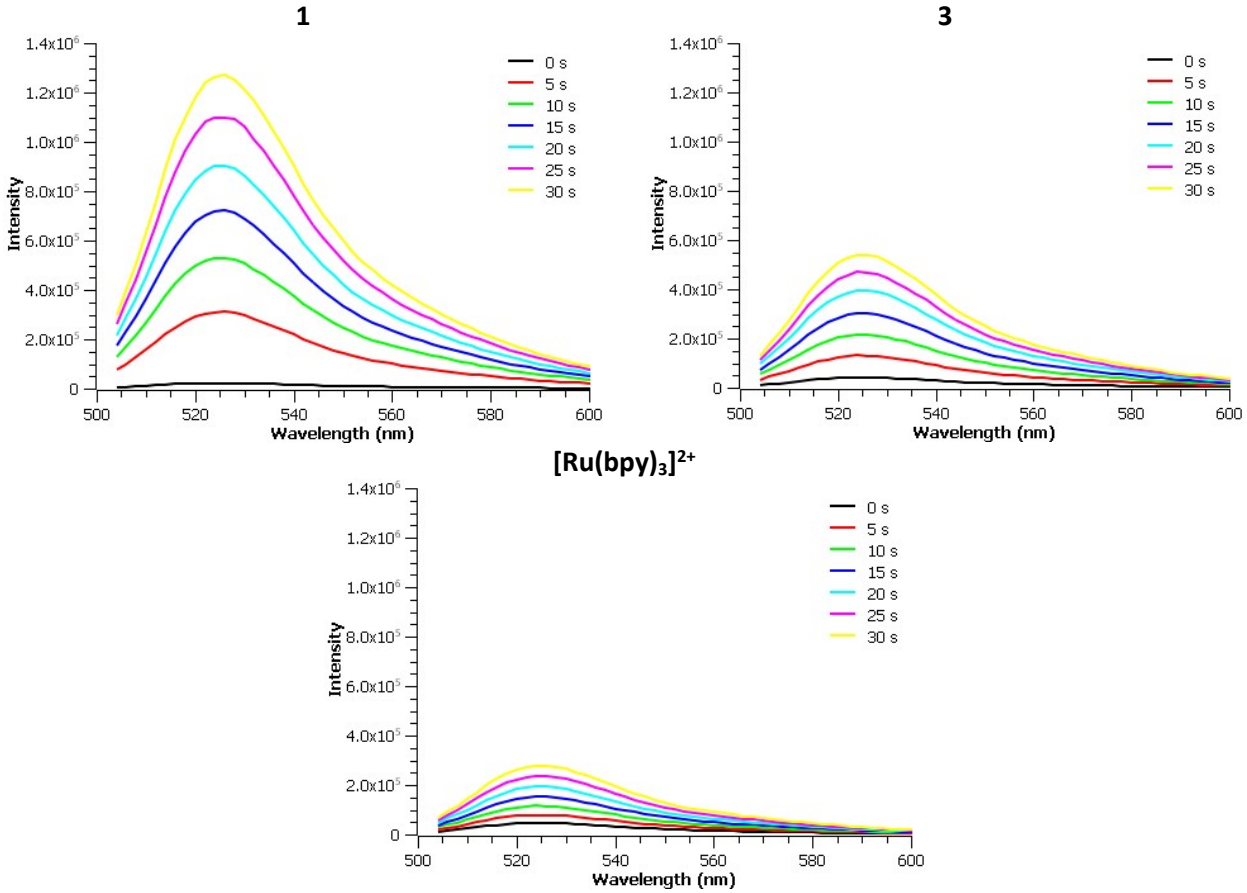

Figure S62. Evolution of the fluorescence emission spectra of DHR123 upon blue light irradiation (470 nm, 51.4 mW cm^{-2}) with **1**, **3** and $[Ru(bpy)_3]^{2+}$ in water (0.2% DMSO).

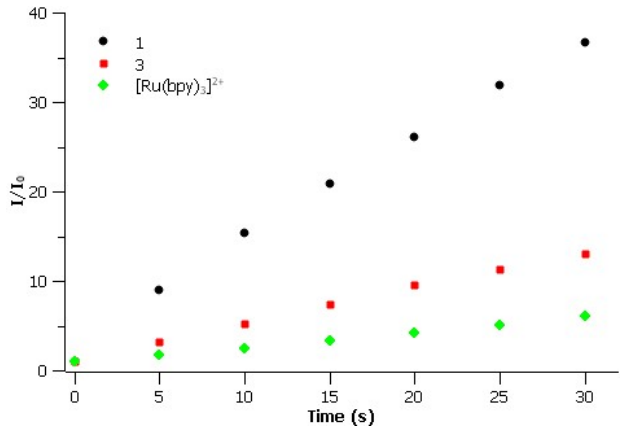

Figure S63. Comparative plots of I/I_0 as a function of time for the experiment of photooxidation of DHR123 with PSs under blue light irradiation (470 nm, 51.4 mW cm^{-2}) in water (0.2% DMSO).

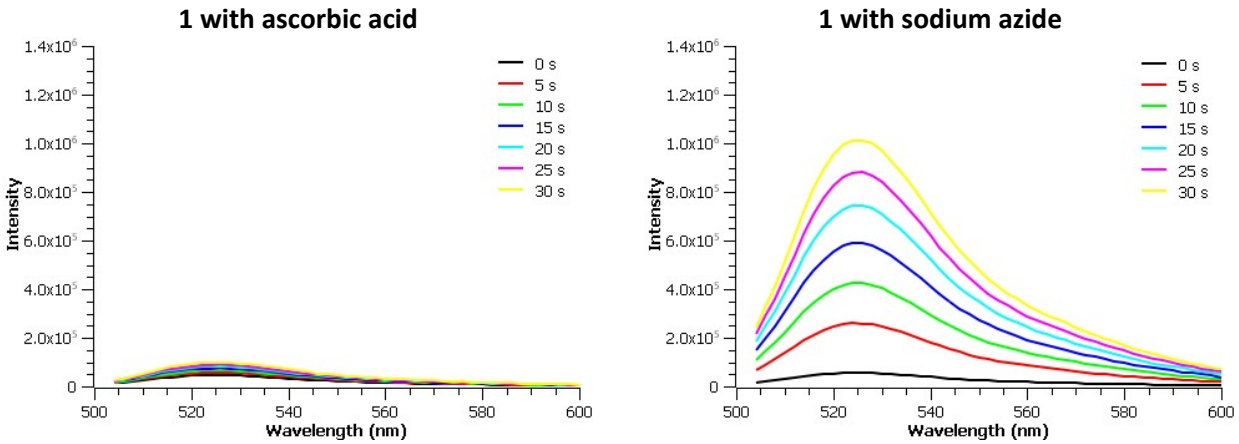

Figure S64. Evolution of the fluorescence emission spectra of DHR123 upon blue light irradiation (470 nm, 51.4 mW cm^{-2}) with **1** and 1,000 equiv. of scavenger (ascorbic acid or sodium azide) in water (0.2% DMSO).

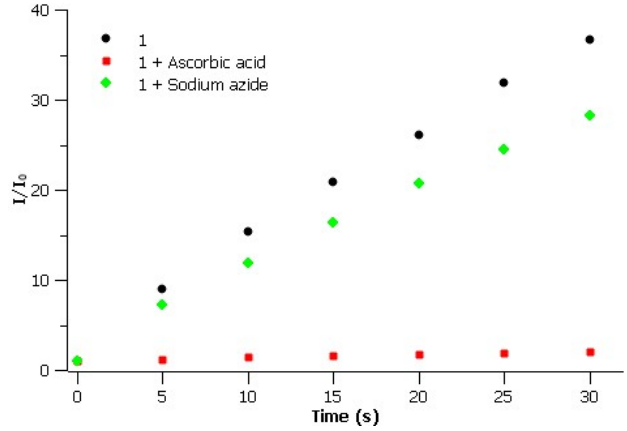

Figure S65. Comparative plots of I/I_0 as a function of time for the experiment of photooxidation of DHR123 with **1** under blue light irradiation (470 nm, 51.4 mW cm^{-2}) in water (0.2% DMSO) in the presence of scavengers.

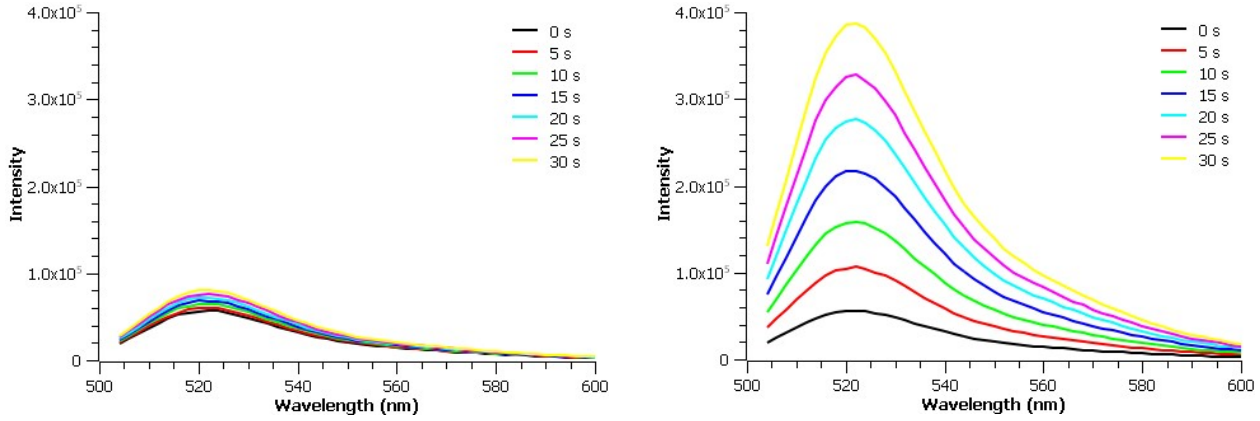

Figure S66. Evolution of the fluorescence emission spectra of DHR123 upon blue light irradiation (470 nm, 51.4 mW cm^{-2}) in the absence (left) or in the presence of **1** (right) in acetonitrile.

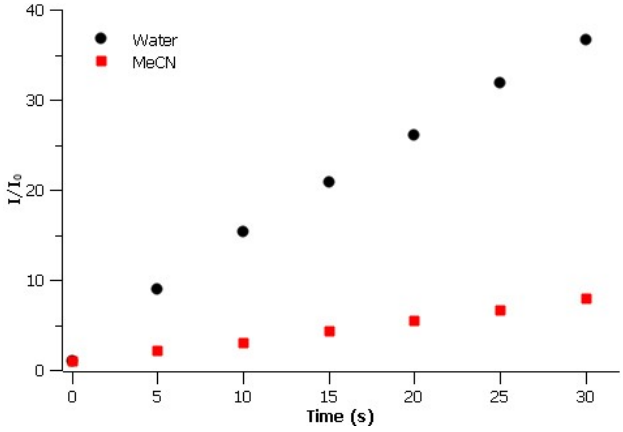

Figure S67. Comparative plots of I/I_0 as a function of time for the experiment of photooxidation of DHR123 with **1** under blue light irradiation (470 nm, 51.4 mW cm^{-2}) in water (0.2% DMSO) and acetonitrile.

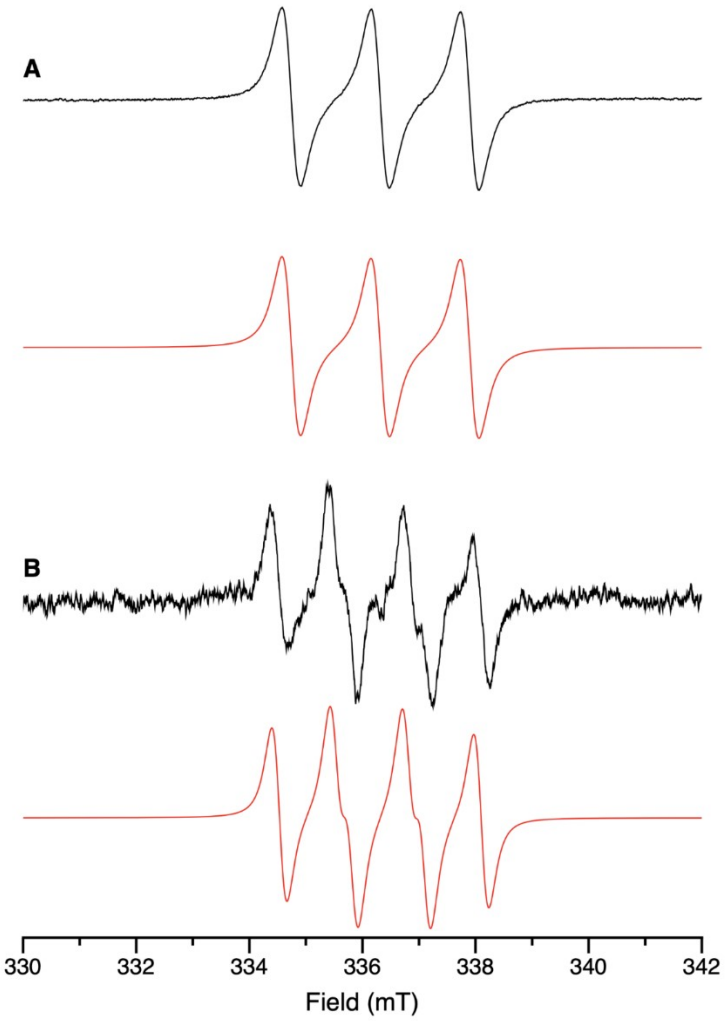

Figure S68. EPR spectra of irradiated samples of compound **1** in acetonitrile in the presence of TEMP (A) or DMPO (B). (black experimental data, red EPR simulation).

Synthesis and characterization of nanoparticles

Synthesis of copolymers

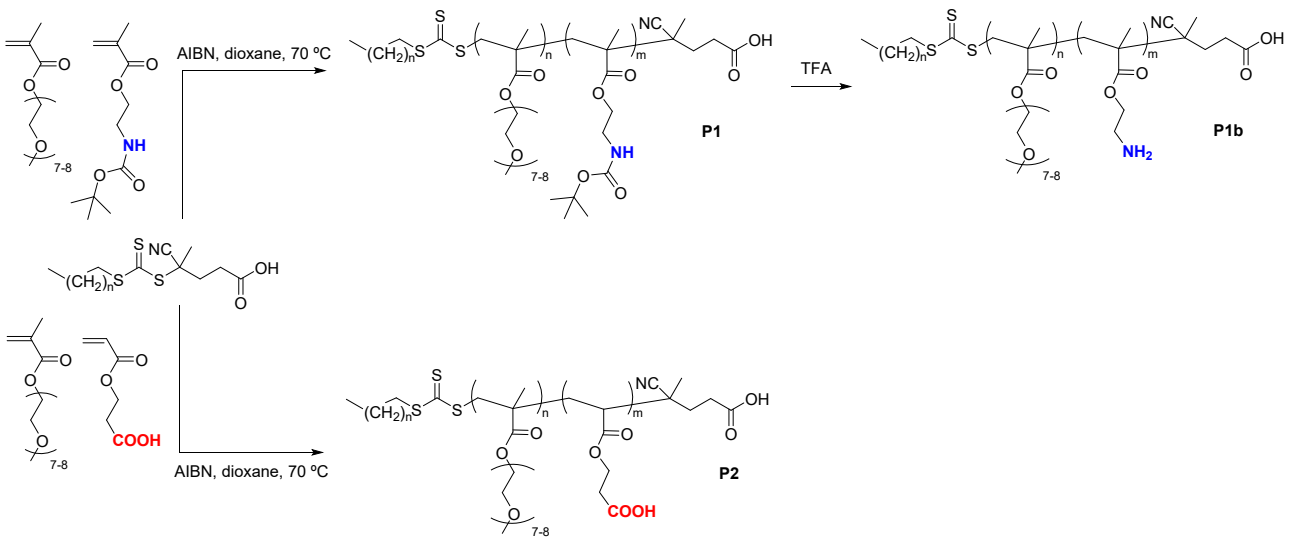

Scheme S1. Synthesis of random copolymers to produce polymeric nanoparticles.

Table S6. Table of equivalents used in RAFT polymerizations.

Polymer	CTA	AIBN	PEGMA	BOC-aminoethylMA	CEA	Conversion (%)
P1	1 eq	0.5 eq	40 eq	40 eq	-	87
P2	1 eq	0.5 eq	40 eq	-	80 eq	90

Synthesis of nanoparticles

Table S7. Content of polymers used to form the nanoparticles presented in this work.

Nanoparticle	P1b	P2	Crosslink agent	Drug	DLS (PDI)	Ir content (μM)
NP	Polymer-NH_2 1.5 mL (20 mg/mL)	Polymer-COOH 1.5 mL (20 mg/mL)	EDC (5%) 0.5 mL	-	146 nm (0.26)	
NP1	Polymer-NH_2 1.5 mL (20 mg/mL)	Polymer-COOH 1.5 mL (20 mg/mL)	EDC (5%) 0.5 mL	**1** 0.25 mL (7 mg/mL DMF)	150 nm (0.29)	23.319
NP3	Polymer-NH_2 1.5 mL (20 mg/mL)	Polymer-COOH 1.5 mL (20 mg/mL)	EDC (5%) 0.5 mL	**3** 0.25 mL (7 mg/mL DMF)	194 nm (0.21)	27.560

NMR of copolymers

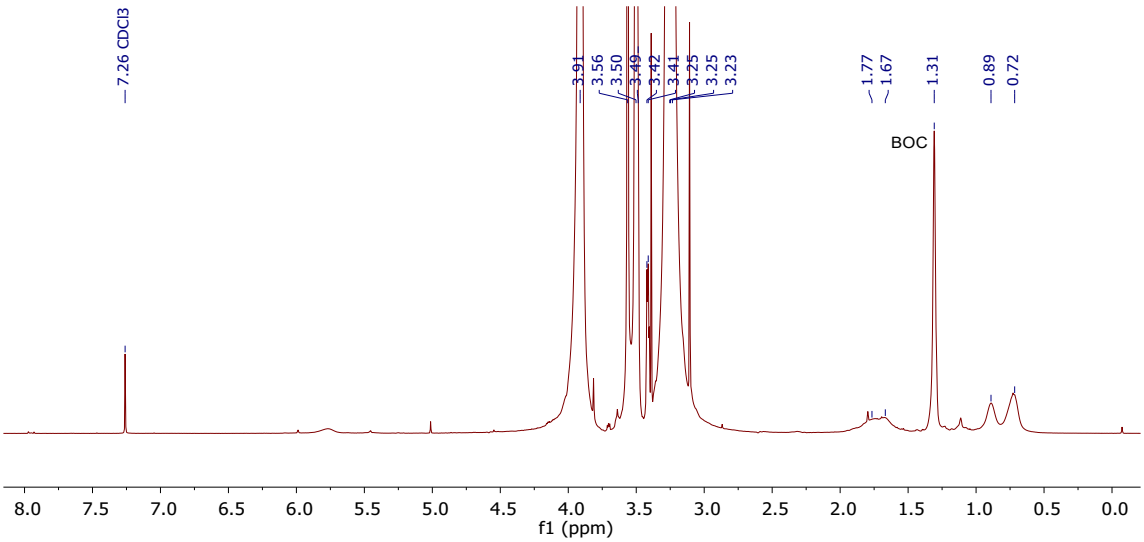

Figure S69. ^{1}H NMR (500 MHz, $CDCl_3$, 298 K) spectrum of copolymer **P1**.

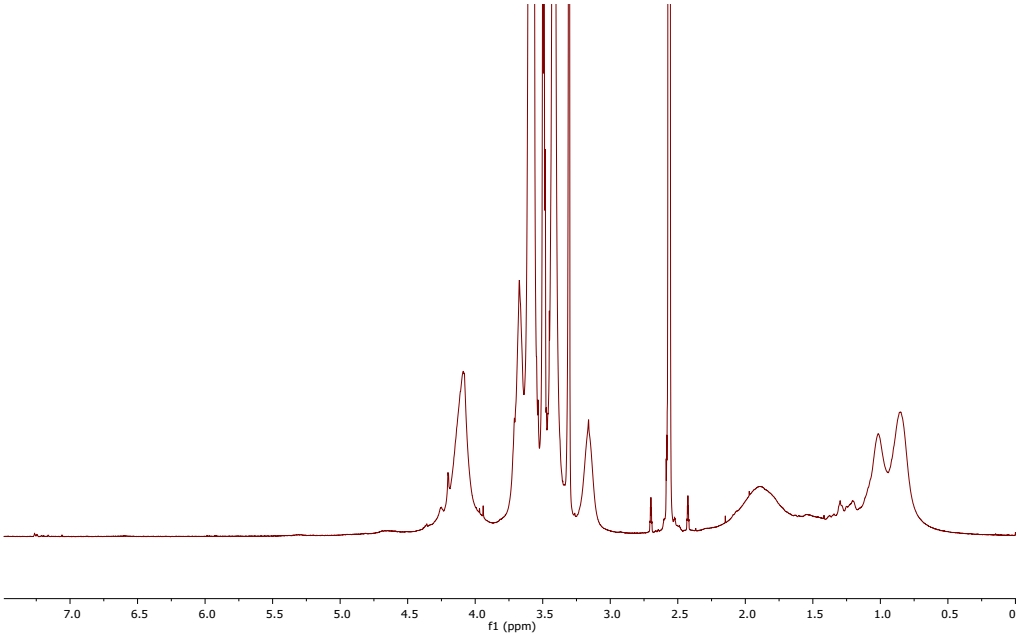

Figure S70. ^{1}H NMR (500 MHz, DMSO-d_6, 298 K) spectrum of copolymer **P1b** after removing the BOC protecting group.

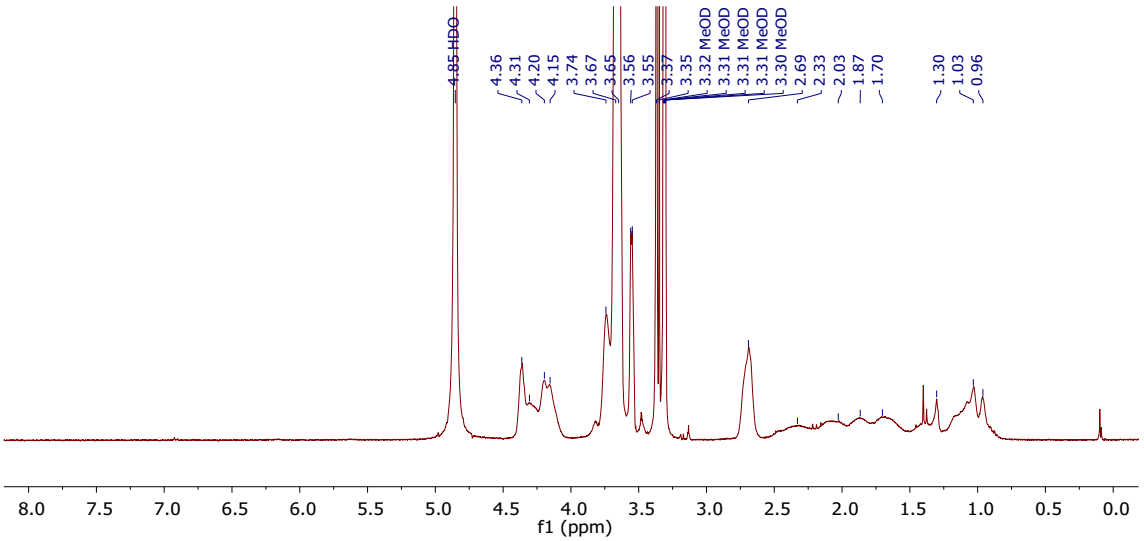

Figure S71. ^{1}H NMR (400 MHz, CD_3OD, 298 K) spectrum of copolymer **P2**.

DLS

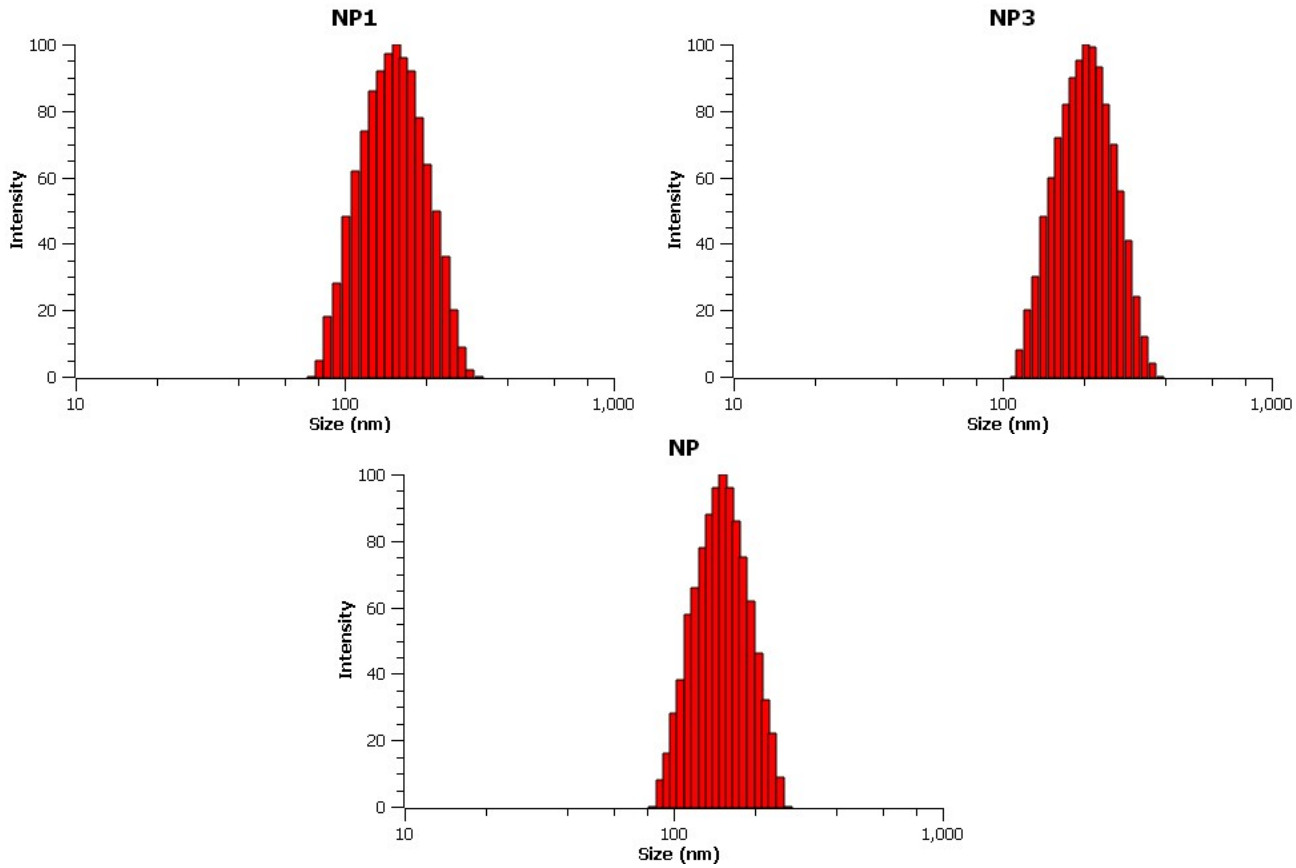

Figure S72. Dynamic light scattering spectra of nanoparticles **NP1**, **NP3** and NP without drug.

SEM

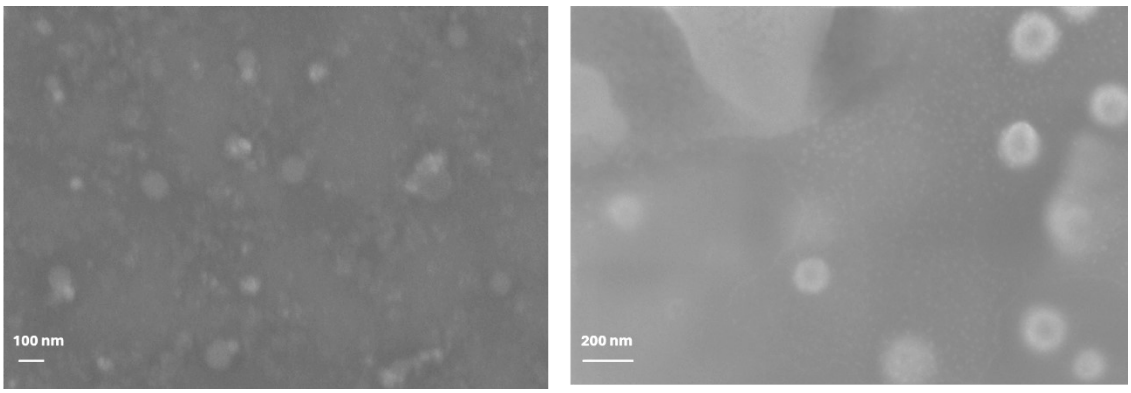

Figure S73. SEM images of **NP1** (left) and **NP3** (right).

UV-vis and luminescence of nanoparticles

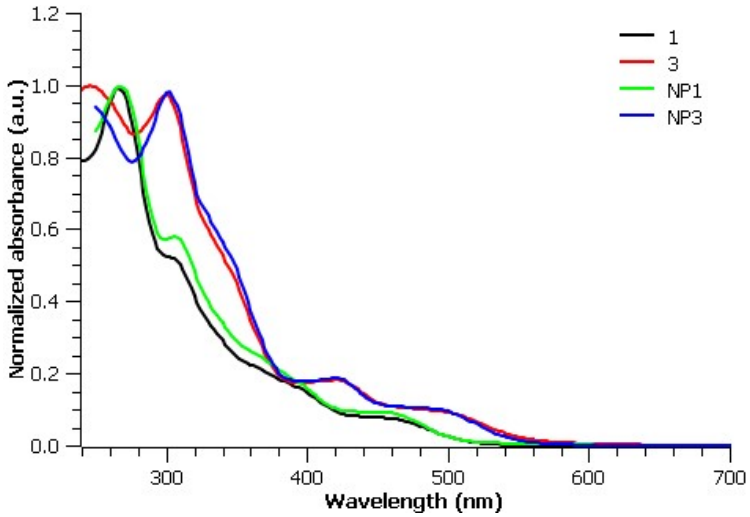

Figure S74. UV-vis absorbance of **NP1** and **NP3**, and complexes **1** and **3**, in aqueous solution.

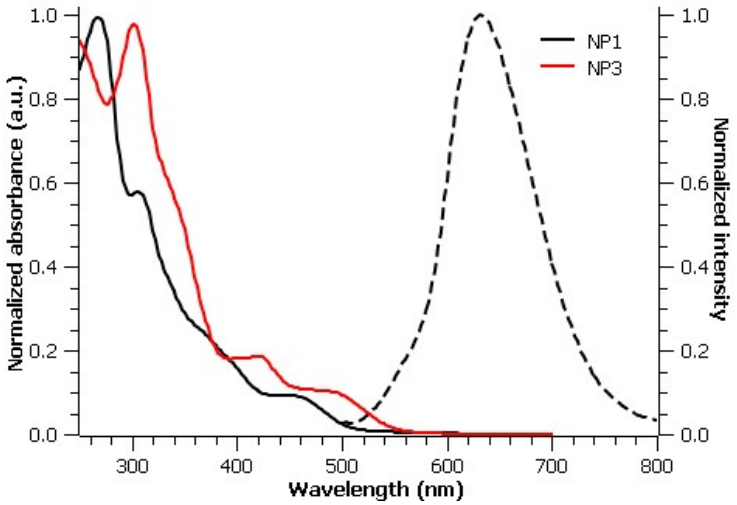

Figure S75. UV-vis absorption and emission spectra of nanoparticles **NP1** and **NP3** in aqueous solution.

Computational studies

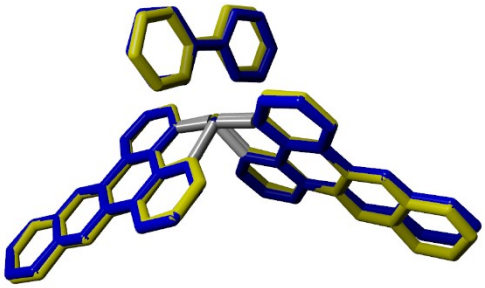

Figure S76. Superposition of the X-ray structure (blue) and DFT equilibrium structures (yellow) of compound **1**. For the sake of clarity the hydrogen atoms are hidden.

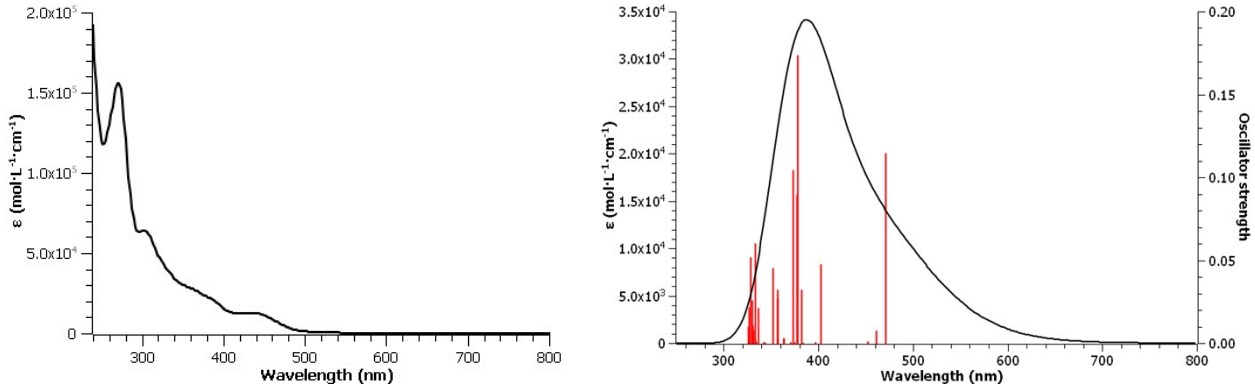

Figure S77. Experimental UV-vis spectrum of complex **1** in degassed acetonitrile (left) and calculated TD-DFT(SMD, acetonitrile)/6-31G(d,p)//SDD level (right).

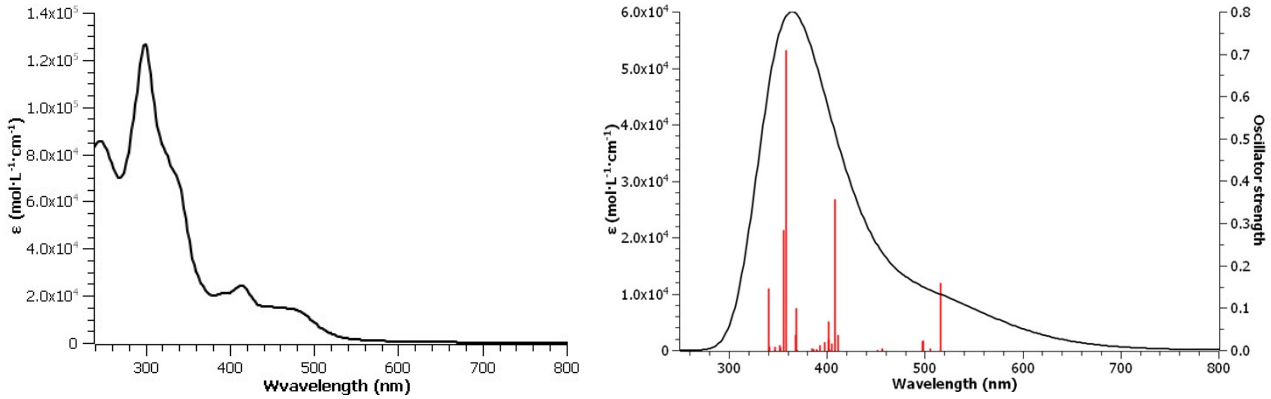

Figure S78. Experimental UV-vis spectrum of complex **3** in degassed acetonitrile (left) and calculated TD-DFT(SMD, acetonitrile)/6-31G(d,p)//SDD level (right).

Compound 1 **Compound 3**

Figure S79. Top

Table S8. Adiabatic excitation energies (eV) calculated at the optimized lowest-lying singlet and triplet excited states of **1** and **3** at the TD-DFT (SMD, acetonitrile)/6-31G(d,p)//SDD level.

State	S_1	S_2	T_1	T_2	T_3	T_4
1	2.46	2.54	2.01	2.01	2.31	2.38
3	2.23	2.30	0.67	0.67	2.16	2.07

A) B)

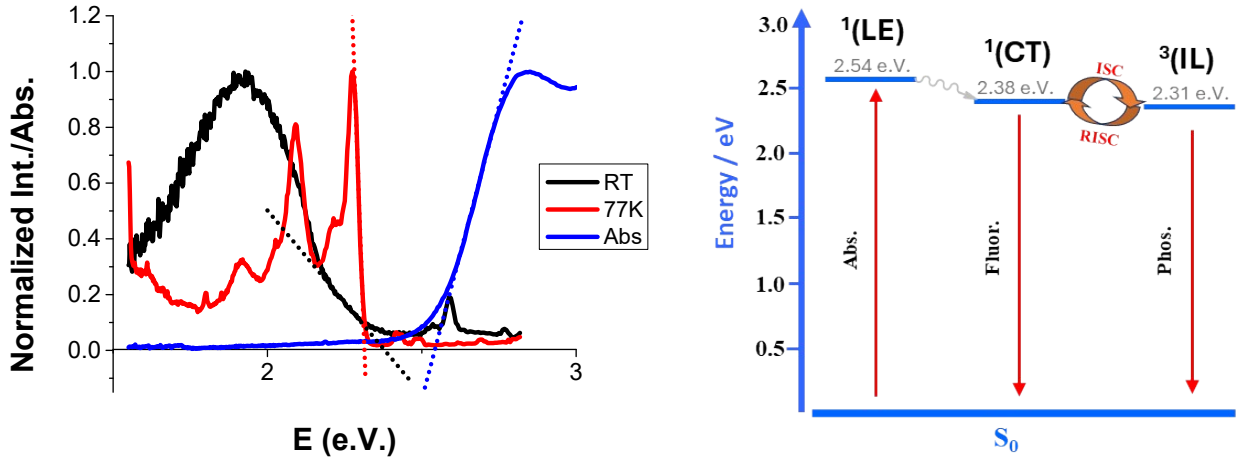

Figure S80. A) Absorption (blue) and emission at RT (black) and 77K (red) spectra of **1**. The dashed lines were used to estimate the energy of the local excited state (^{1}LE) initially populated by the absorption of light (blue dashed line), the energy of the emissive state after initial relaxation (^{1}CT, black dashed line) and the energy of the lowest triplet state (^{3}IL) otained at 77 K (red dashed line); the assinments as charge transfer (CT) and intraligand (IL) are based on the spectral shapes (broad ^{1}CT band and vibrational resolution in the ^{3}IL band; **B**) summarized scheme of the electronic transitions in **1** upon photon excitation; the presence of RISC is infered from the small energy difference between ^{1}CT and ^{3}IL and also due to the long lifetime of the ^{1}CT emission (delayed fluorescence).

Hemolytic activity

Table S9. Hemolytic activity of complexes **1** and **3**.

Complex	Treatment	% Hemolysis*
1	Dark (1 μM)	2.8
	Light (0.2 μM)	3.0
	Light (0.02 μM)	0.0
3	Dark (1 μM)	1.9
	Light (0.2 μM)	5.0
	Light (0.02 μM)	0.0

* Porcine red blood cells were exposed to complexes **1** and **3** at the indicated concentrations for 1 h at 37 °C, in the dark or under blue light. The % of hemolysis was determined in each condition by measuring hemoglobin release into the supernatant. Experiments were conducted in triplicate.

NADH oxidation

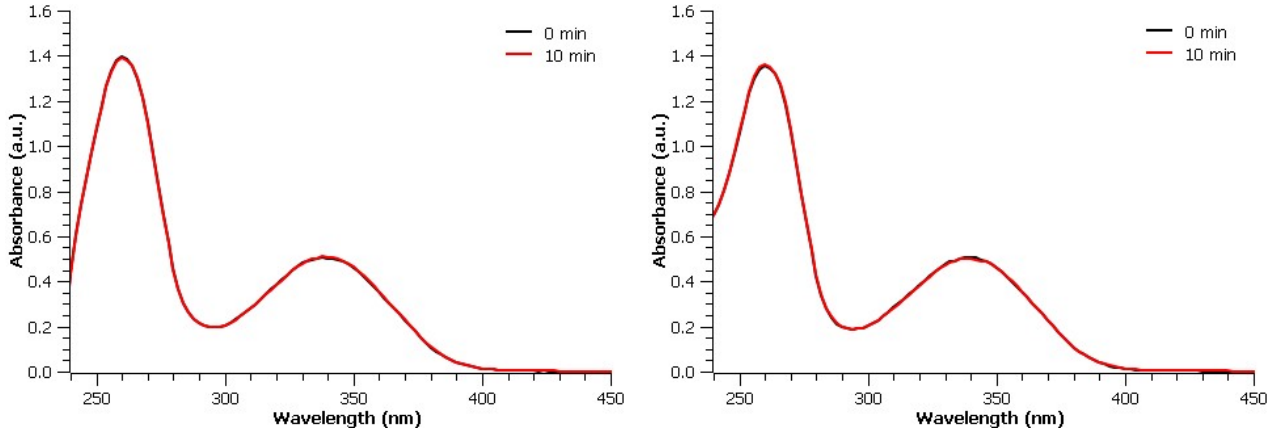

Figure S81. UV−vis spectra for the catalytic oxidation of NADH (100 μM) to NAD^+ in the presence of complexes **1** (left) and **3** (right) at 1.0 μM over a period of 10 minutes in water (0.1% DMSO) at room temperature in the dark.

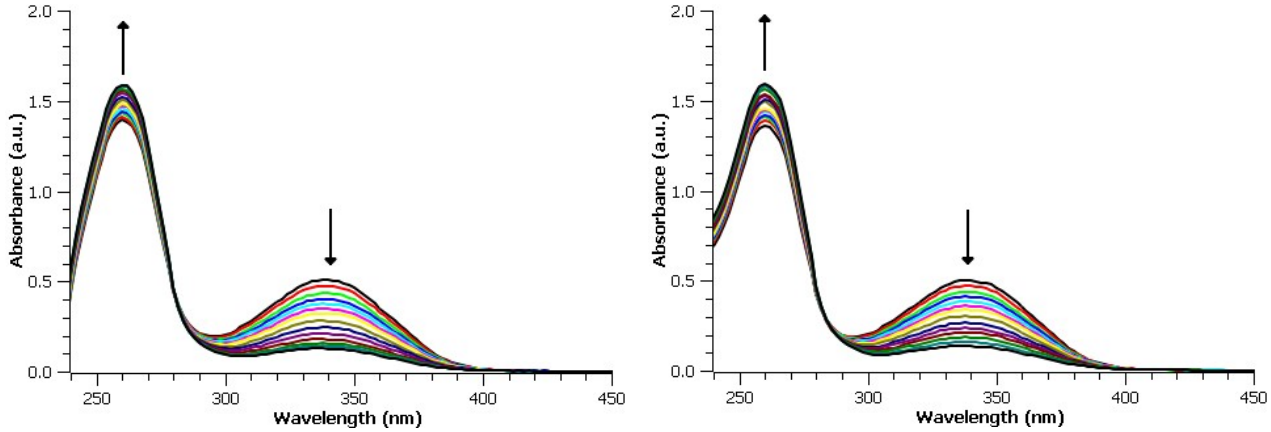

Figure S82. UV−vis spectra for the catalytic oxidation of NADH (100 μM) to NAD^+ in the presence of complexes **1** (left) and **3** (right) at 1.0 μM over a period of 10 minutes in water (0.1% DMSO) at room temperature under blue light irradiation.

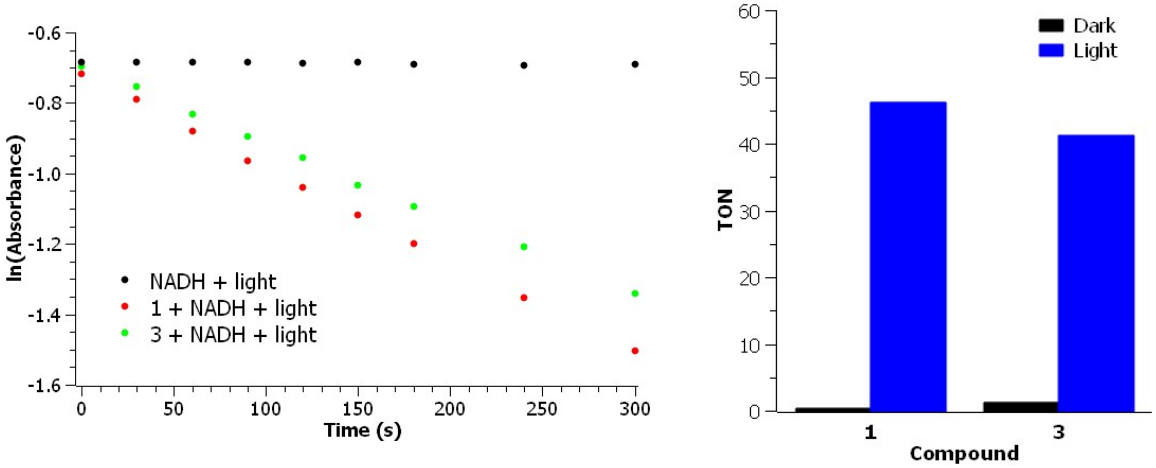

Figure 83. First-order kinetic plot of the photooxidation of NADH with complexes **1** and **3** (left) and TON values for complexes in the dark and under blue light irradiation (470 nm) after 5 min of reaction (right).

Table S10. TON and TOF values for the photooxidation of NADH with **1** and **3** under blue light irradiation after 5 minutes of reaction.

	1	**3**
TON	46	41
TOF (h^{-1})	555	495

Table S11. Photocytotoxic activity of empty **NP**, **NP1** and **NP3**, and the polymers **P1b** and **P2**, in 2D cell cultures.

2D-cultures	**A549**			**HeLa**		
	IC_{50} (μg/mL)		**PI**	**IC_{50} (μg/mL)**		**PI**
	Dark	**Light**		**Dark**	**Light**	
NP1	2.596 ± 0.009	0.37 ± 0.017	70	2.961 ± 0.69	0.105 ± 0.049	28
NP3	103.3 ± 33	1.505 ± 0.31	69	70.701 ± 7.4	1.097 ± 0.16	65
Empty NP	>200	>200	-	>200	>200	-
P1b	>200	>200	-	>200	>200	-
P2	>200	>200	-	>200	>200	-

Table S12. Iridium derivatives with values of $IC_{50} \leq 10$ nM.

Product	**Cells**	**IC_{50} (nM)**	**λ (nm)**	**Dose**	**Ref**
NP1	A549	0.86	460	24.1 J cm^{-2}	This work
NP1	HeLa	2.4	"	"	This work
[Cp*Ir(C^N)Cl]	A549	4	460	24.1 J cm^{-2}	a
$[Cp^*Ir(C^N)L]^+$	"	1	"	"	a
"	"	0.4	"	"	a
"	"	0.4	"	"	a
"	HeLa	4.2	"	"	a
"	"	0.7	"	"	a
"	"	0.8	"	"	a

“	PC-3	1.1	“	“	a
“	“	1.2	“	“	a
“	“	0.5	“	“	a
$[Ir(C^N)_2(NHC^NHC)]^+$	A549R	0.86	365	20 mW cm^{-2}	b
“	“	2.8	“	“	b
“	A549	3.4	450	10 mW cm^{-2}	c
“	A549R	1.9	“	“	c
“	“	3.6	“	“	c
$[Ir(C^N)_2(N^N)]^+$	SK-MEL-28	4	Visible	100 J cm^{-2}	d
“	“	3	“	“	d
[Ir(por)(NHC)Cl]	NCI-H460	9	Visible	2.8 mW cm^{-2}	e
“	“	6	“	“	e
“	“	5	“	“	e
$[Ir(C^N)_2(N^N)]^+$	A549	8	425	36 J cm^{-2}	f
“	NCI-H460	5.05	--	--	g

Por = porphyrin

a Carlos Gonzalo-Navarro, Elisenda Zafon, Juan Angel Organero, Félix A. Jalón, Joao Carlos Lima, Gustavo Espino, Ana María Rodríguez, Lucía Santos, Artur J. Moro, Sílvia Barrabés, Jessica Castro, Javier Camacho-Aguayo, Anna Massaguer, Blanca R. Manzano, Gema Dura *J. Med. Chem*. **2024**, *67*, 1783–1811.

b Yi Li, Cai-Ping Tan, Wei Zhang, Liang He, Liang-Nian Ji, Zong-Wan Mao, *Biomaterials* **2015**, *39*, 95–104.

c Yi Li, Bing Liu, Xin-Ran Lu, Meng-Feng Li, Liang-Nian Jia, Zong-Wan Mao, *Dalton Trans.* **2017**, *46*, 11363–11371.

d Chengzhe Wang, Levi Lystrom, Huimin Yin, Marc Hetu, Svetlana Kilina, Sherri A. McFarland, Wenfang Sun, *Dalton Trans*. **2016**, *45*, 16366–16378.

e Tsz-Lung Lam, Ka-Chung Tong, Chen Yang, Wai-Lun Kwong, Xiangguo Guan, Ming-De Li, Vanessa Kar-Yan Lo, Sharon Lai-Fung Chan, David Lee Phillips, Chun-Nam Lok, Chi-Ming Che, *Chem. Sci.* **2019**, *10*, 293–309.

f Wei-Wei Qin, Zheng-Yin Pan, Dai-Hong Cai, Yi Li, Liang He, *Dalton Trans*. **2020**, 49, 3562–3569.

g Yan Yang, Yi-Dong Bin, Qi-Pin Qin, Xu-Jian Luo, Bi-Qun Zou, Hua-Xin Zhang, *ACS Med. Chem. Lett.* **2019**, *10*, 1614–1619.

Internalization Analysis

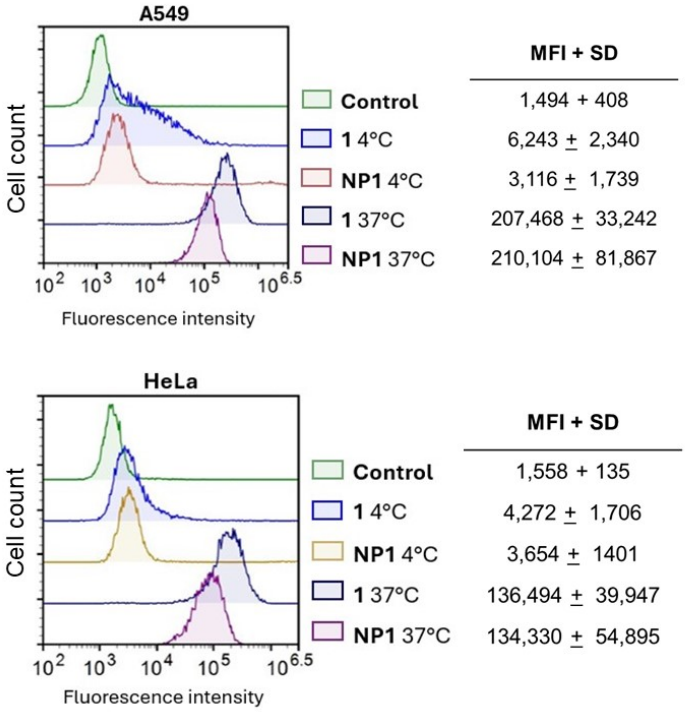

Figure S84. Cellular internalization at 4 °C and 37 °C. Representative flow cytometry histograms of A549 and HeLa cells incubated for 4 h with complex **1** at 5 µM or **NP1** at 50 µg/mL (1.17 µM) at 4 °C or at 37 °C. Untreated control cells were used as a reference. The fluorescence intensity of 10,000 cells is represented in the histograms. The mean fluorescence intensity (MFI) ± SD of three independent experiments is indicated.

Microscopy for Subcellular Distribution.

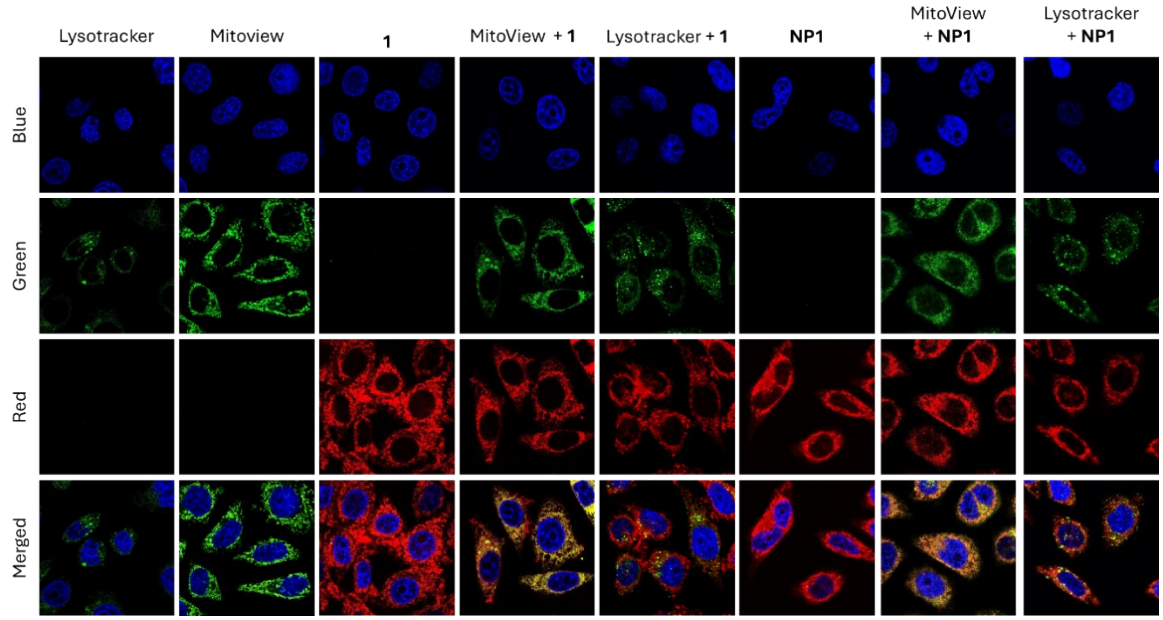

Figure S85. Confocal microscopy imaging of the subcellular distribution of **1** and **NP1**. HeLa cells were incubated with **1** or **NP1** ($\lambda_{ex}/\lambda_{em}$: 440/596 nm) at 50 μg/mL for 1 h at 37 °C. The commercial dyes MitoView™ Green (Biotium) ($\lambda_{ex}/\lambda_{em}$: 490/523 nm) and LysoTracker™ Green DND-26 (ThermoFisher Scientific) ($\lambda_{ex}/\lambda_{em}$: 504/511 nm) and Hoechst ($\lambda_{ex}/\lambda_{em}$: 352/454 nm) were used to localize the mitochondria, lysosomes, and cell nuclei, respectively. Images were captured using a Nikon A1R confocal microscope using the following acquisition settings: blue channel: $\lambda_{ex}/\lambda_{em}$: 400/450 nm 33258, green channel: $\lambda_{ex}/\lambda_{em}$: 488/525 nm and red channel: $\lambda_{ex}/\lambda_{em}$: 488/595 nm. Merged images show the green and red fluorescence overlapping in orange.

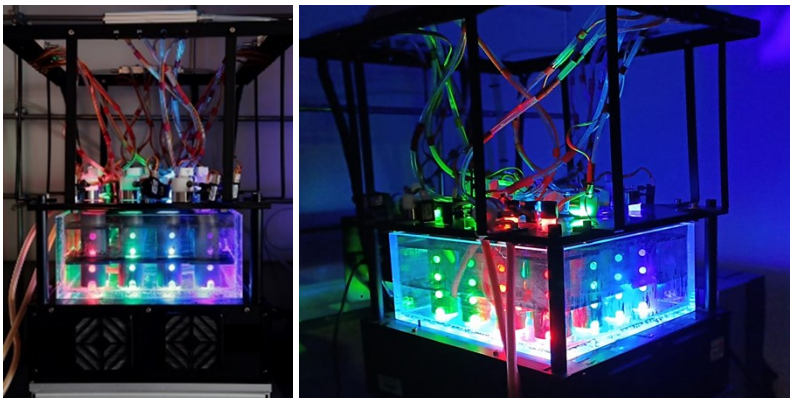

Figure S86. 'Medusa' photoreactor used for the photochemical experiments.

Biological Studies Raw Data.

ROS generation.

A549 cells replicates 1 - 3:

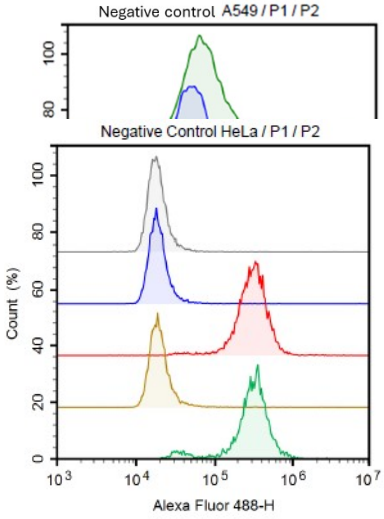

#	Sample	Gate	Median X
1	Negative Control HeLa	P2	18,347
2	1 Dark	P2*	18,786
3	1 Light	P2*	312,068
4	3 Dark	P2*	19,273
5	3 Light	P2*	318,831

HeLa cells replicates 1 – 3:

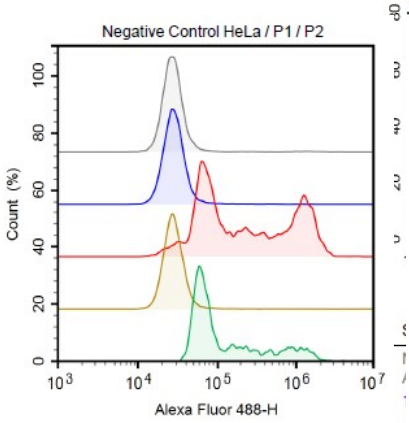

#	Sample	Gate	Median X
1	Negative Control HeLa	P2	27,621
2	1 Dark	P2*	28,346
3	1 Light	P2*	170,251
4	3 Dark	P2*	28,049
5	3 Light	P2*	78,355

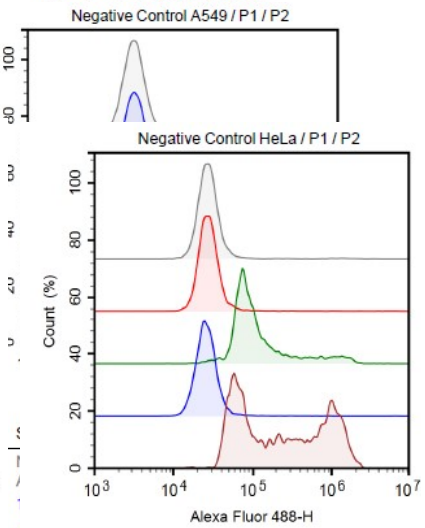

#	Sample	Gate	Median X
1	Negative Control HeLa	P2	27,621
2	1 Dark.	P2*	27,754
3	1 Light.	P2*	91,215
4	3 Dark.	P2*	25,971
5	3 Light.	P2*	212,573

Superoxide anion production.

A549 cells replicates 1 – 3:

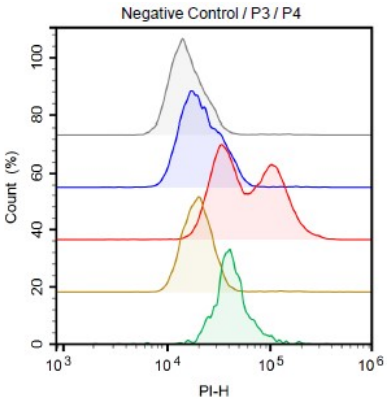

#	Sample	Gate	Median X
1	Negative Control	P4	15,195
2	1 Dark	P4*	20,516
3	1 Light	P4*	55,805
4	3 Dark	P4*	19,935
5	3 Light	P4*	41,260

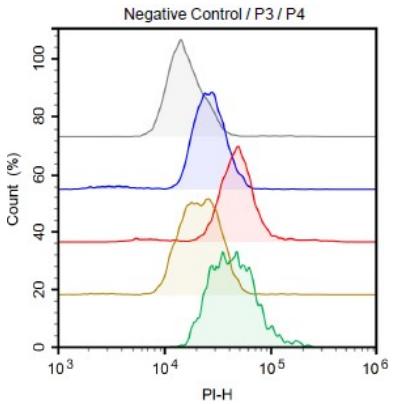

#	Sample	Gate	Median X
1	Negative Control	P4	15,280
2	1 Dark	P4*	26,215
3	1 Light	P4*	47,960
4	3 Dark	P4*	21,714
5	3 Light	P4*	43,193

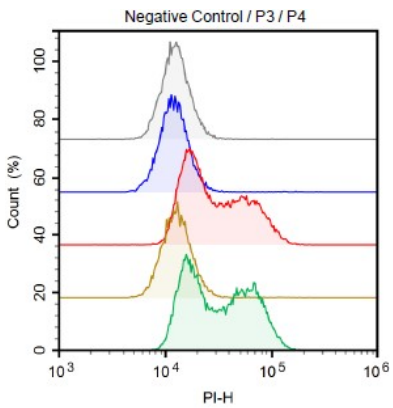

#	Sample	Gate	Median X
1	Negative Control	P4	12,509
2	1 Dark	P4*	12,017
3	1 Light	P4*	25,376
4	3 Dark	P4*	12,824
5	3 Light	P4*	29,840

HeLa cells replicates 1 – 3:

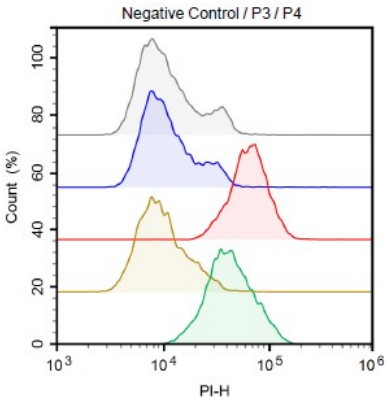

#	Sample	Gate	Median X
1	Negative Control	P4	9,583
2	1 Dark	P4*	9,973
3	1 Light	P4*	65,667
4	3 Dark	P4*	9,218
5	3 Light	P4*	42,165

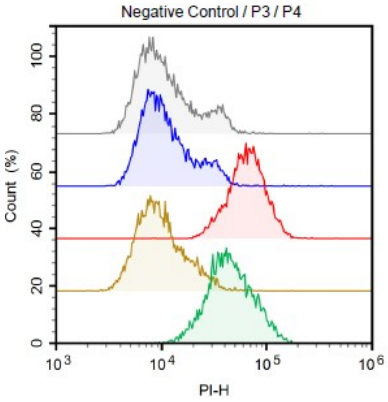

#	Sample	Gate	Median X
1	Negative Control	P4	9,583
2	1 Dark	P4*	9,973
3	1 Light	P4*	65,667
4	3 Dark	P4*	9,218
5	3 Light	P4*	44,353

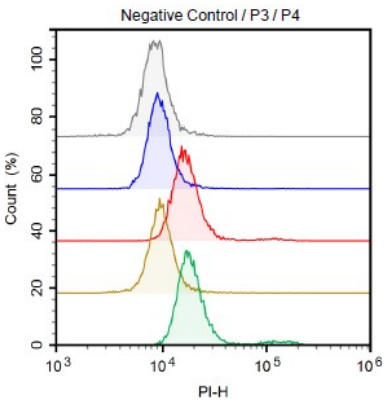

#	Sample	Gate	Median X
1	Negative Control	P4	8,732
2	1 Dark	P4*	9,494
3	1 Light	P4*	16,971
4	3 Dark	P4*	9,887
5	3 Light	P4*	18,871

Mitochondrial Membrane Depolarization (JC1 probe).

Replicate 1:

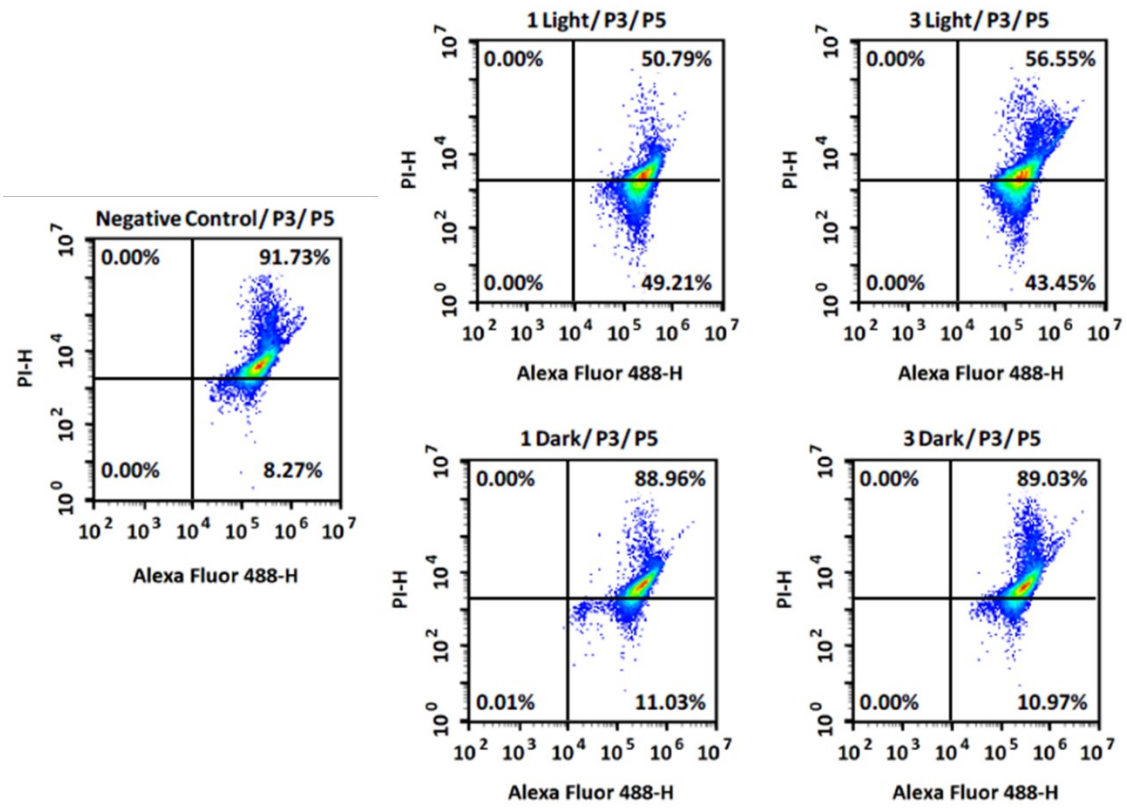

Replicate 2:

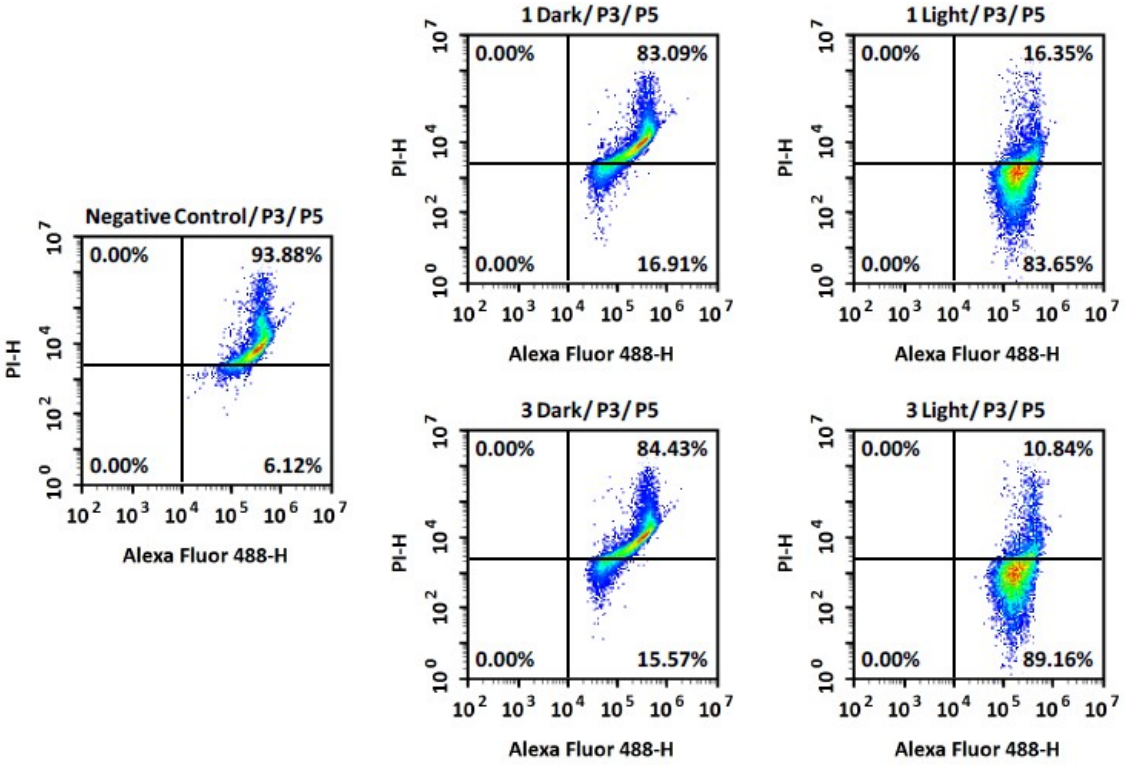

Repliate 3:

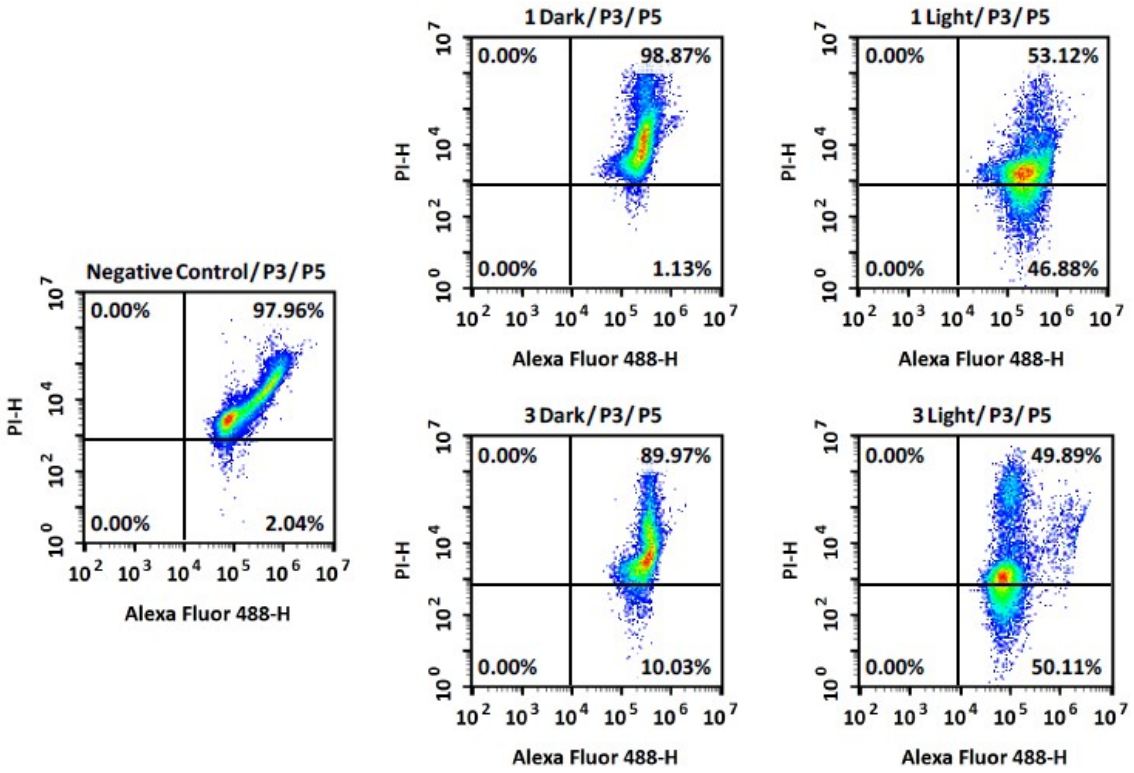
Negative Control / P3 / P5
0.00%
97.96%
0.00%
2.04%
1 Dark / P3 / P5
0.00%
98.87%
0.00%
1.13%
1 Light / P3 / P5
0.00%
53.12%
0.00%
46.88%
3 Dark / P3 / P5
0.00%
89.97%
0.00%
10.03%
3 Light / P3 / P5
0.00%
49.89%
0.00%
50.11%
PI-H
Alexa Fluor 488-H

Replicate 4:

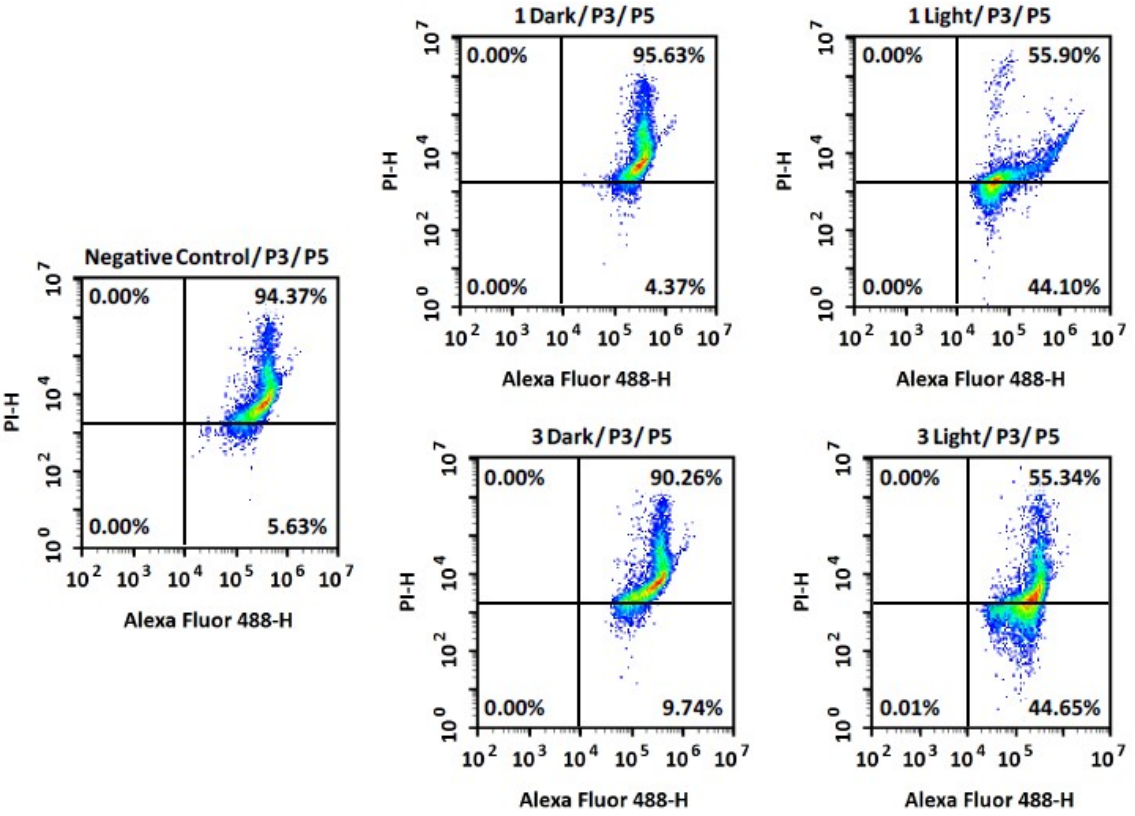
Negative Control / P3 / P5
0.00%
94.37%
0.00%
5.63%
1 Dark / P3 / P5
0.00%
95.63%
0.00%
4.37%
1 Light / P3 / P5
0.00%
55.90%
0.00%
44.10%
3 Dark / P3 / P5
0.00%
90.26%
0.00%
9.74%
3 Light / P3 / P5
0.00%
55.34%
0.01%
44.65%
PI-H
Alexa Fluor 488-H

Cell death mechanism (Annexin/propidium iodide).

Replicate 1:

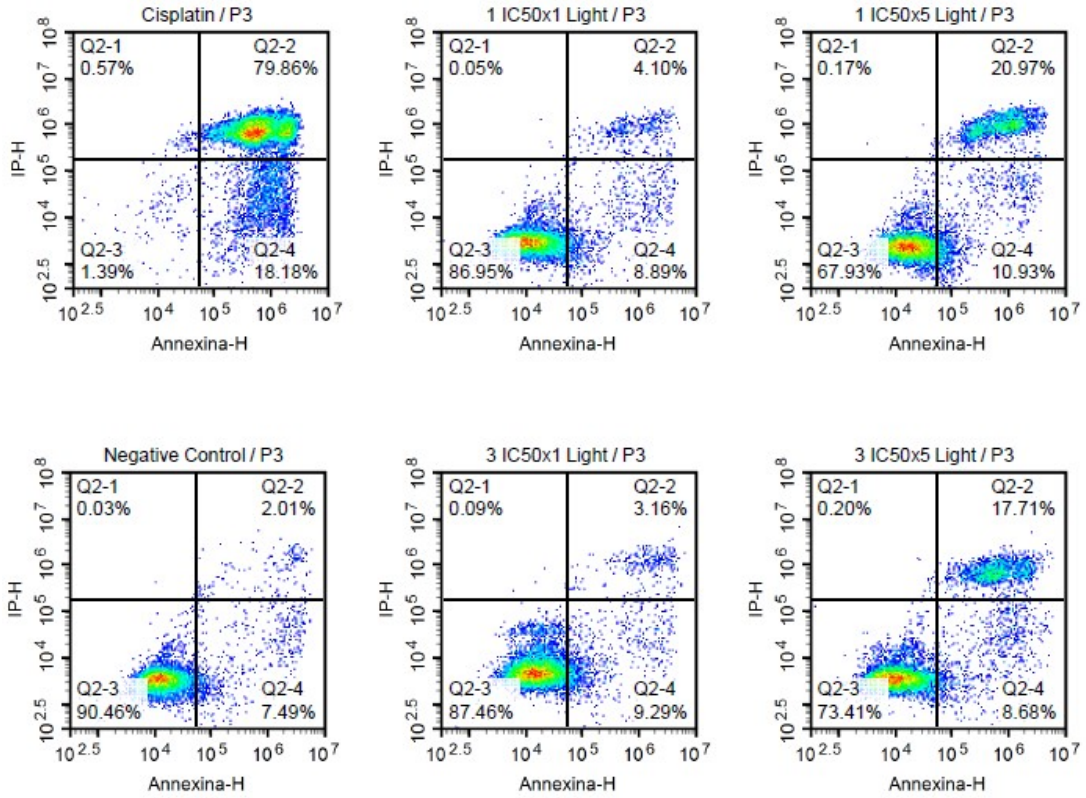

Replicate 2:

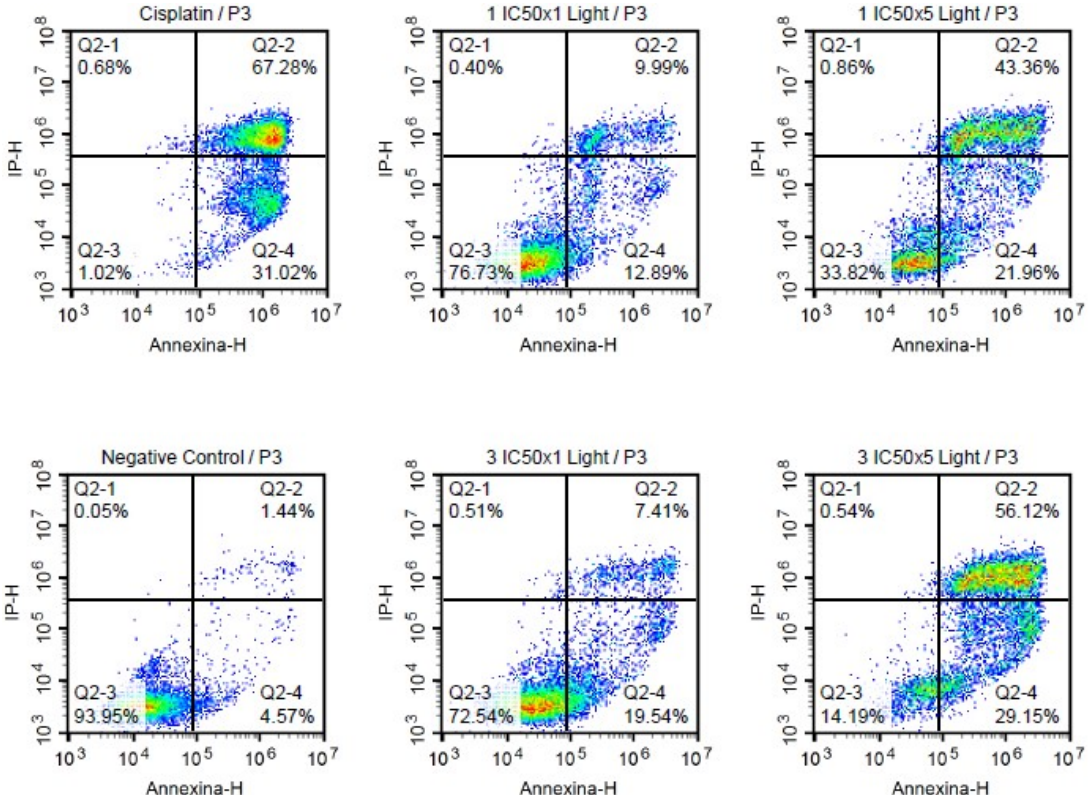

Replicate 3:

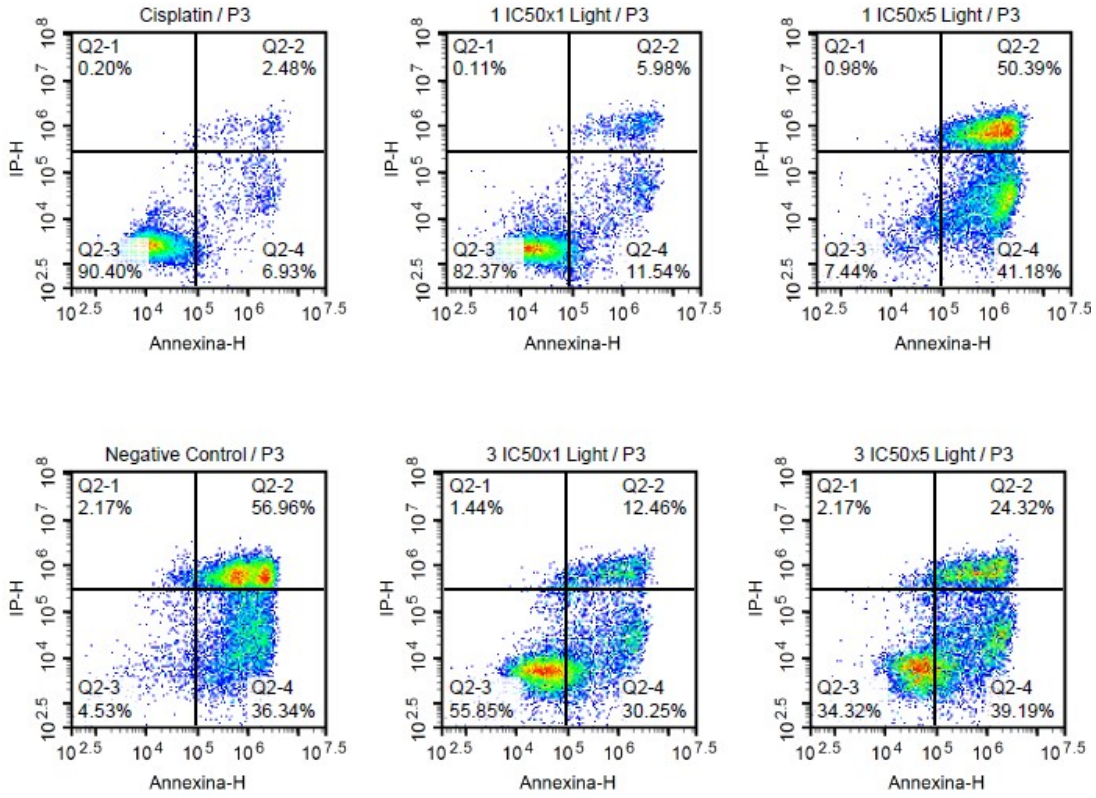

Celullar internalization.

A549 cells replicates 1 – 3:

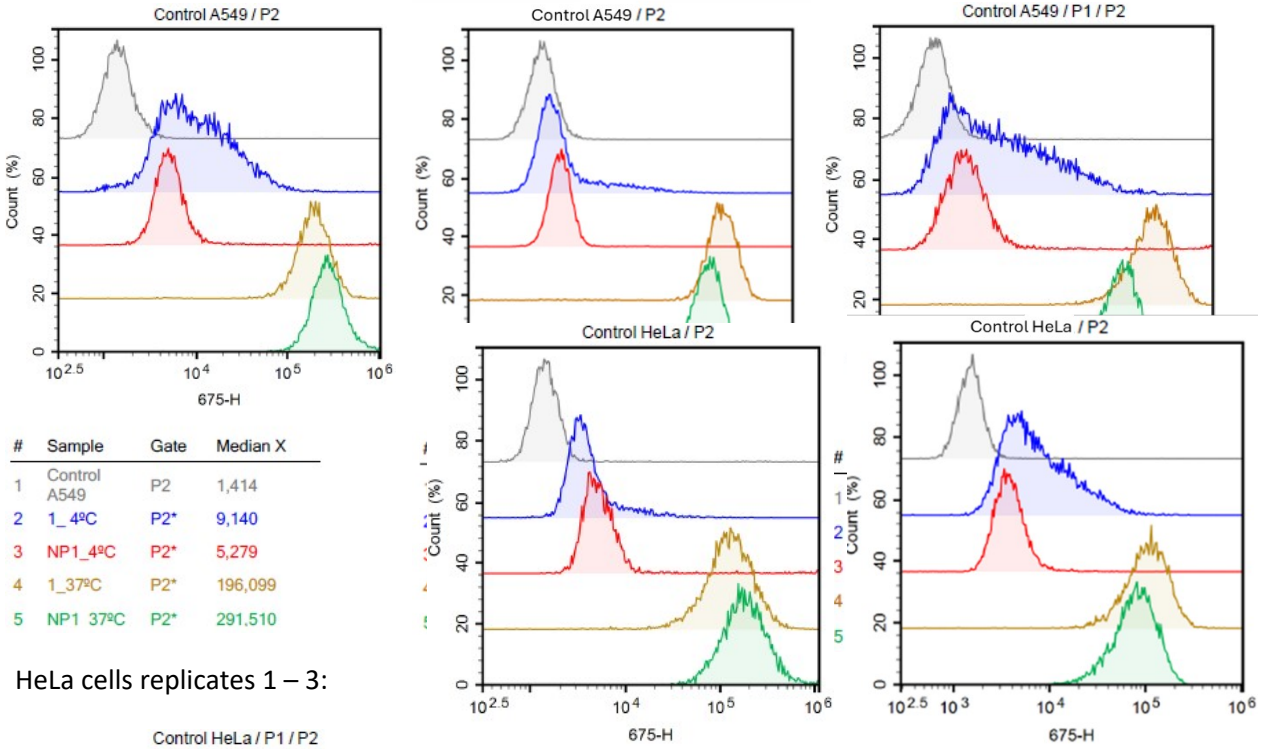

#	Sample	Gate	Median X
1	Control A549	P2	1,414
2	1_ 4ºC	P2*	9,140
3	NP1_4ºC	P2*	5,279
4	1_37ºC	P2*	196,099
5	NP1 37ºC	P2*	291,510

HeLa cells replicates 1 – 3:

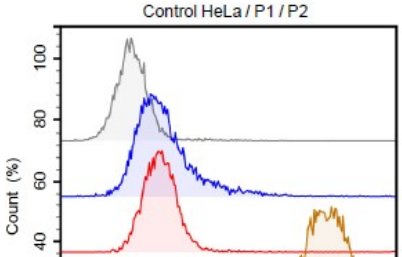

#	Sample	Gate	Median X
1	Control HeLa	P2	1,457
2	1_4ºC	P2*	3,660
3	NP1_4ºC	P2*	5,271
4	1_37ºC	P2*	128,008
5	NP1 37ºC	P2*	185,498

#	Sample	Gate	Median X
1	Control HeLa	P2	1,516
2	1_4ºC	P2*	6,428
3	NP1_4ºC	P2*	3,745
4	1_37ºC	P2*	107,571
5	NP1 37ºC	P2*	80,790

REFERENCES

1 T. Sainuddin, J. McCain, M. Pinto, H. Yin, J. Gibson, M. Hetu and S. A. McFarland, *Inorganic Chemistry*, 2016, **55**, 83–95.

2 L. Fu, L. Liu, Z. Ruan, H. Zhang and L. Yan, *RSC Advances*, 2016, **6**, 40312–40322.

3 *SAINT+ v7.12a. Area-Detector Integration Program. Bruker-Nonius AXS. Madison. Wisconsin, USA, 2004*.

4 *G. M. Sheldrick, SADABS version 2004/1. A Program for Empirical Absorption Correction.*, University of Göttingen, Göttingen, Germany, 2004.

5 *SHELXTL-NT version 6.12. Structure Determination Package. Bruker-Nonius AXS.*, Madison, Wisconsin, USA, 2001.

6 M. S. Lowry, W. R. Hudson, R. A. Pascal and S. Bernhard, *Journal of the American Chemical Society*, 2004, **126**, 14129–14135.

7 T. Entradas, S. Waldron and M. Volk, *Journal of Photochemistry & Photobiology, B: Biology*, 2020, **204**, 111787.

8 J. M. Wessels, C. S. Foote, W. E. Ford and M. A. J. Rodgers, *Photochem Photobiol*, 1997, **65**, 96–102.

9 J. S. Nam, M. G. Kang, J. Kang, S. Y. Park, S. J. C. Lee, H. T. Kim, J. K. Seo, O. H. Kwon, M. H. Lim, H. W. Rhee and T. H. Kwon, *J Am Chem Soc*, 2016, **138**, 10968–10977.

10 Z. Liu, I. Romero-canelón, B. Qamar, J. M. Hearn, A. Habtemariam, N. P. E. Barry, A. M. Pizarro, G. J. Clarkson and P. J. Sadler, *Angew. Chem. Int. Ed. Engl.*, 2014, **53**, 3941–3946.

11 C. Gonzalo-Navarro, E. Zafon, J. A. Organero, F. A. Jalón, J. C. Lima, G. Espino, A. M. Rodríguez, L. Santos, A. J. Moro, S. Barrabés, J. Castro, J. Camacho-Aguayo, A. Massaguer, B. R. Manzano and G. Durá, *Journal of Medicinal Chemistry*, 2024, **67**, 1783–1811.

12 S. Stoll and A. Schweiger, *Journal of Magnetic Resonance*, 2006, **178**, 42–55.